

Thesis for the degree of Master in Mechanical  
Engineering

# Parameter identification in the dynamics of a flexible circular cylinder in Vortex-Induced Vibration

The usage of equivalent parameters and its implications

Cintia Monreal Jiménez

July 2015



Universidad Autónoma de San Luis Potosí  
Facultad de Ingeniería  
Centro de Investigación y Estudios de Posgrado

**Committee**

Dr. Francisco Oviedo Tolentino

Dra. Geydy Luz Gutiérrez Urueta

Dr. Francisco Gerardo Pérez Gutiérrez

Dr. Emilio Jorge González Galván

**Date of graduation**

31.08.2015

A mis padres, por ser mi más grande motivación. A mi mami por enseñarme que la tenacidad es lo único que se necesita para llegar a cualquier lugar, y a mi papi por mostrarme que no hay problema que con ingenio y creatividad no se pueda resolver. A mi hermano por hacerme la vida entretenida y siempre estar ahí para mí. A mi hermana y sobrina por compartir su tiempo conmigo. A mis abuelitas, por educarme y ser un ejemplo en mi vida. Y a toda mi familia, y amigos, por hacerme sonreír.

A mis profesores por sus conocimientos. Al Dr. Fidencio por exigirme siempre lo mejor. Al Dr. Oviedo por su ayuda para hacer mi tesis. Y a la Dra. Geydy por su tiempo.

A mis compañeras de fútbol por su amistad dentro y fuera de la cancha, y por hacerme querer a esta universidad.

Para todos ustedes, que forman parte importante de mi día a día.



# Abstract

Despite several investigations on vortex-induced vibrations (VIV), many fundamental questions still exist. Some of these interrogations are directly related to the parameters involved in the mathematical model, namely: mass, spring and damping coefficients. In this work, a standard method to identify these parameters of a *cantilevered uniform flexible circular cylinder* in a steady current along the entire lock-in region is proposed. To achieve this, an experimental apparatus of a flexible circular cylinder mounted on an acrylic plate was built. The dynamic response of the cylinder was recorded using a high speed video camera and a Matlab® code was developed to determine it using the PTV technique. At the same time, the hydrodynamic response downstream the cylinder was known using a customized system to seed the fluid and the PIV technique.

Results obtained in this work suggest that the use of equivalent parameters in the motion equation,  $m\ddot{y} + c\dot{y} + ky = F$ , can explain in a better way the behavior of the cylinder. The variation in the total phase angle,  $\phi_{total}$ , is consistent with the maximum amplitude of the cylinder. The behavior of the added mass,  $m'$ , is consistent with the frequency of the cylinder. The constant value of the vortex phase angle,  $\phi_{vortex}$ , is consistent with the fact that the hydrodynamic response of the cylinder is the same across the synchronization regime. Regarding comparison between actual results and the ones available in the literature, there is no evidence of two distinctly different jumps between modes as stated by Govardhan & Williamson (2000). Furthermore, PIV technique clearly proved that the entire synchronization region is associated with the 2S mode, contrary to what was observed by Govardhan & Williamson (2000) and Evangelinos & Karniadakis (1999).



# Contents

<b>List of symbols</b>	<b>7</b>
<b>Introduction</b>	<b>11</b>
<b>1 Background on Vortex-Induced Vibration</b>	<b>15</b>
1.1 Mechanical Vibrations . . . . .	15
1.2 Vortex-Induced Vibration . . . . .	16
1.2.1 Types of experimental apparatus . . . . .	16
1.2.2 Mathematical model . . . . .	19
1.2.3 Types of dynamic response in vortex-induced vibrations . . . . .	21
1.2.4 Types of hydrodynamic response in vortex-induced vibrations . . . . .	22
<b>2 Flow around a circular cylinder in steady and oscillatory currents</b>	<b>25</b>
2.1 Flow around a cylinder in steady current . . . . .	25
2.1.1 Regimes of flow around a smooth circular cylinder . . . . .	25
2.1.2 Vortex shedding . . . . .	27
2.2 Forces on a cylinder in steady current . . . . .	30
2.2.1 Drag and lift . . . . .	31
2.3 Forces on a cylinder in oscillatory flows . . . . .	35
2.3.1 Drag force in oscillatory flow . . . . .	35
2.3.2 Lift force in oscillatory flow . . . . .	39
2.4 Circular cylinders in Vortex-Induced Vibration . . . . .	41
2.4.1 Solutions to vibration equation . . . . .	41
2.4.2 Damping . . . . .	45
2.4.3 Cross-flow vortex-induced vibrations . . . . .	49
<b>3 Dynamic and hydrodynamic analysis of a circular cylinder in Vortex-Induced Vibration</b>	<b>53</b>
3.1 Experimental setup . . . . .	53
3.2 Testing materials . . . . .	54
3.3 Obtaining parameters . . . . .	58
3.3.1 Stiffness of the cylinder ( $k$ ) . . . . .	58
3.3.2 Free vibration with viscous damping ( $\zeta$ ) . . . . .	59
3.3.3 Discretized model: Results . . . . .	61
3.4 Dynamic response . . . . .	62
3.4.1 Test 1 . . . . .	62

3.4.2	Test 2 . . . . .	64
3.4.3	Results in the synchronization regime . . . . .	68
3.5	Hydrodynamic response . . . . .	72
3.5.1	Particle Image Velocimetry . . . . .	72
3.5.2	Vortex shedding pattern . . . . .	73
<b>4</b>	<b>The usage of equivalent parameters and its implications</b>	<b>77</b>
4.1	Equivalent parameters vs real parameters . . . . .	77
4.1.1	Phase angle ( $\phi_{total}$ ) . . . . .	78
4.1.2	Phase angle ( $\phi_{vortex}$ ) . . . . .	78
4.1.3	Added mass . . . . .	80
4.2	Comparing actual results with literature . . . . .	80
4.2.1	Phase angle . . . . .	80
4.2.2	Hydrodynamic mass coefficient . . . . .	82
	<b>Conclusions</b>	<b>83</b>
	<b>Acknowledgments</b>	<b>87</b>
	<b>Bibliography</b>	<b>89</b>
	<b>Appendix</b>	<b>93</b>



# List of Figures

- 0.1 The Seattle Post-Intelligencer’s front page, Nov. 8, 1940. . . . . 13
- 1.1 Rigid and flexible cylinders. . . . . 17
- 1.2 Different systems to study VIV. . . . . 18
- 1.3 Tapered and uniform cylinders. . . . . 18
- 1.4 Converting a real problem to a mathematical model. . . . . 19
- 1.5 Sketches of the two different types of dynamic response. **H** means an hysteretic transition and **I** means an intermittent switching of modes. Based on Govardhan & Williamson (2000). . . . . 22
- 1.6 Sketches of the vortex shedding patterns founded in Vortex-Induced Vibrations. **S** means a single vortex and **P** means a vortex pair, each pattern is defined by the number of pairs and single vortices formed per cycle. Gray lines encircles the vortices shed in one complete cycle. Based on Williamson & Roshko (1988). . . . . 24
- 2.1 Regimes of flow around a smooth circular cylinder in steady current. **A**: laminar boundary layer separation; **B**: turbulent boundary layer separation; and **C**: turbulent boundary layer separation with boundary layer completely turbulent. . . . . 26
- 2.2 The shear layer. The shear layer roll up to form a vortex, one for each side of the cylinder. Based on Sumer & Fredsøe (1997). . . . . 28
- 2.3 Vortex shedding mechanism. In the first scheme, the vortex **A** is larger and throws the vortex **B** across the wake. In the second scheme, the vortex **B** has grown enough to throw the vortex **C** across the wake. This mechanism is repeated in an alternate manner at each side of the cylinder to form the “vortex street”. Based on Sumer & Fredsøe (1997). . . . . 28
- 2.4 Sketch of the Strouhal number for a smooth circular cylinder. Based on experimental data from: Williamson (1989), Roshko (1961), and Schewe (1983). . . . . 29
- 2.5 Sketch of the separation points. Based on Sumer & Fredsøe (1997). . . . . 30
- 2.6 Definition sketch. . . . . 31
- 2.7 Sketch of time development of pressure distribution at different moments of the vortex shedding process. Based on Drescher (1956). . . . . 32
- 2.8 Sketch of pressure distributions, potential flow theory and  $Re = 10^5$ . Bsaed on Achenbach (1968). . . . . 33

2.9	Drag coefficient for a smooth circular cylinder as function of the $Re$ number. Based on data from: Schewe (1983) and Schlichting (1979).	34
2.10	Pressure distributions. $S$ denotes the separation points. a) Circular cylinder in the subcritical regime, and b) Circular cylinder in the supercritical regime. Based on Achenbach (1968).	34
2.11	Movement of a plate in a still fluid; a) horizontal plate, and b) vertical plate. Based on Sumer & Fredsøe (1997).	36
2.12	Sketch of potential flow around an accelerated cylinder moving in the $x$ axis at $U$ velocity in otherwise still fluid.	36
2.13	Sketch of the lift force coefficient (RMS) as function of $KC$ number. Based on Williamson (1985).	40
2.14	Sketch of a flexibly-mounted system vibrating in $y$ direction.	41
2.15	Free vibrations with viscous damping. a) over-damped case with no vibration, and b) underdamped case the oscillations decrease with time.	43
2.16	Forced vibrations with viscous damping.	44
2.17	Phase delay ( $\phi$ ) illustration.	45
2.18	Free vibrations in vacuum without damping.	46
2.19	Free vibrations in vacuum with damping.	47
2.20	Free vibrations in still fluid with damping.	48
2.21	Recorded response of the structure in a free decay experiment.	49
2.22	Different type of oscillations.	50
2.23	Hydrodynamic mass in still fluid and in current.	51
2.24	Sketch of the hydrodynamic mass coefficient for a circular cylinder vibrating in the cross-flow direction (forced oscillations) and subject to a current. $V_r$ is the reduced velocity, where $U$ is the velocity of the main flow, $D$ is the diameter of the cylinder and $f$ is the frequency of the forced vibrations. Based on Sarpkaya (1978)	51
3.1	Experimental model scheme.	54
3.2	PTV technique in the tip of the cylinder.	55
3.3	Schematic diagram: experimental procedure for the estimation of stiffness of the cylinder.	58
3.4	Actual photos of the stiffness experiment. a) equilibrium position, b) displacement $x_1$ with a force applied $F_1$ , c) displacement $x_2$ with a force applied $F_2$ .	59
3.5	Response of the bronze cylinder in free vibration.	61
3.6	Discretized model. a) In air the equations only include the mass due to the structure, b) in water the equations include the mass due to the structure and the hydrodynamic mass.	62
3.7	Maximum amplitude in the transverse direction vs Reynolds number.	63
3.8	Maximum amplitude in the transverse direction vs Reynolds number from Oviedo et al. (2014).	63
3.9	Maximum amplitude in the transverse direction vs Reynolds number.	64

3.10	The three tests vs Reynolds number. . . . .	65
3.11	Error lines of the average maximum amplitude. . . . .	65
3.12	Path of the tip of the cylinder. a) initial @ $Re=182$ , b) upper @ $Re=209$ and c) lower @ $Re=263$ . . . . .	66
3.13	Orbits of the free-end of the cylinder and cylinder displacements over time in both axes. Both columns show the three branches of the lock-in region: a) initial @ $Re=182$ , b) upper @ $Re=209$ and c) lower @ $Re=263$ . . . . .	67
3.14	Maximum amplitude in the cross-flow direction vs Reynolds number.	68
3.15	Frequency of the cylinder vs Reynolds number. . . . .	69
3.16	Maximum amplitude in the cross-flow direction and total phase angle vs Reynolds number. . . . .	70
3.17	Maximum amplitude in the cross-flow direction and added mass vs Reynolds number. . . . .	71
3.18	Phase angles vs Reynolds number. . . . .	72
3.19	Experimental model with the laser. . . . .	73
3.20	PIV technique. . . . .	73
3.21	Vorticity in the three branches of the synchronization regime. All the images were taken when the cylinder was in its maximum amplitude. a) initial @ $Re=182$ , b) upper @ $Re=209$ and c) lower @ $Re=256$ . . .	74
3.22	1mm Mitutoyo® calibration pattern. . . . .	75
4.1	Comparison of $\phi_{total}$ using equivalent and real parameters. . . . .	79
4.2	Comparison of $\phi_{vortex}$ using equivalent and real parameters. . . . .	79
4.3	Comparison of $m'$ using equivalent and real parameters. . . . .	80
4.4	Schematic diagram of the low ( $m*\zeta$ ) type of response showing the two jump phenomena (free vibration). Based on Govardhan & Williamson (2000). . . . .	81
4.5	Comparison of the hydrodynamic mass coefficient: in gray, cross-flow forced vibrations (Sarpkaya, 1978); and in red, cross-flow free oscillations. . . . .	82



# List of Tables

- 3.1 Impulse response of the different materials in still air. a)Stainless steel, b)Silver steel, c)Aluminum, d)Bronze, and e)Iron . . . . . 56
- 3.2 Impulse response of the different materials in still water. a)Stainless steel, b)Silver steel, c)Aluminum, d)Bronze, and e)Iron . . . . . 57
- 3.3 Parameters obtained for the experimental model.<sup>(1)</sup> . . . . . 61
- 4.1 Parameters obtained for the mathematical model. . . . . 78



# List of symbols

$a$	acceleration
$A^*$	normalized maximum amplitude, $A/D$
$A$	cross-sectional area of the cylinder
$c$	structural damping, viscous damping coefficient
$C_D$	drag coefficient
$C_M$	inertia coefficient
$C_L$	lift coefficient
$C_m$	hydrodynamic mass coefficient
$C_{mc}$	hydrodynamic mass coefficient in current
$C_p$	pressure coefficient
$\delta$	logarithmic decrement
$D$	diameter of the cylinder
$f$	body oscillation frequency, frequency of vibrations
$f_n$	natural frequency
$f_v$	vortex shedding frequency
$F$	fluid force in the transverse direction
$F_D$	drag, total in-line force
$F_f$	resultant force due to friction per unit length
$F_L$	lift, total cross-flow force
$F_{potential}$	potential force
$F_p$	resultant force due to pressure per unit length

$F_{total}$	total fluid force
$F_{vortex}$	vortex force
$k$	spring constant
$KC$	Keulegan-Carpenter number
$m'$	hydrodynamic mass
$m$	total mass of the system
$m'_c$	hydrodynamic mass in current
$m^*\zeta$	mass-damping parameter
$\mu$	dynamic viscosity
$p$	pressure
$p_0$	hydrostatic pressure
$\phi$	phase angle, represents the offset between the fluid force and the body displacement
$\phi$	angular coordinate
$\phi_{total}$	total phase angle
$\phi_{vortex}$	vortex phase angle
$\varphi$	phase delay
$r, \theta$	polar coordinates
$r_0$	cylindre radius
$Re$	Reynolds number
$\rho$	fluid density
$\zeta$	total damping
$\zeta_f$	fluid damping
$\zeta_s$	structural damping
$St$	Strouhal number
$T$	period of the vibration



$t$	time
$\tau_0$	wall shear stress
$U_b$	body velocity in the in-line direction
$U_m$	maximum value of oscillatory-flow velocity
$U$	main flow velocity
$\nu$	kinematic viscosity
$V_r$	reduced velocity
$v$	speed
$\omega$	angular oscillation frequency
$\omega_d$	damped natural angular frequency
$\omega_{dv}$	angular frequency of damped free vibrations
$\omega_n$	undamped natural angular frequency
$\omega_v$	angular frequency of undamped free vibrations
$x, y$	x- and y-displacements of structure
<i>overbar</i>	time average
<i>overdot</i>	differentiation with respect to time



# Introduction

Mechanical vibrations are one of the most important topics in mechanical engineering. Depending on the situation, vibrations can be desired or not. For example, in a vehicle suspension vibrations are necessary in order to allow wheels to remain always in contact to the ground and not lose stability, as well as to dissipate energy and bring a comfortable trip. In energy harvesting, the piezoelectric effect (the ability of certain materials to generate an electric charge as a response to mechanical vibrations) is being used to produce environmentally friendly energy. On the other hand, undesired vibrations must be avoided and considered in the design of mechanical devices. For example, vibrations in machines, such as an unbalanced helicopter motor, may lead to failure and therefore to catastrophic events. Vibrations caused by earthquakes may also cause catastrophic events, but due to structural failure (creeping or stress peak).

A specific type of mechanical vibrations is the one caused by fluid-structural coupling. The most famous example of this kind of vibrations is the Tacoma Narrows Bridge (see Fig. 0.1). The bridge collapsed at 64 km/h, a much lower wind speed for which this structure was designed. The cause of failure is related to vortex-induced vibrations. Without speaking strictly, vortex-induced vibrations (VIV) occurs when the structure become coupled in an unstable oscillation driven by a fluid (wind in the case of the Tacoma Bridge). The oscillations increase their amplitude in each cycle because the structure is unable to dissipate energy at the same rate at which the fluid inserts energy into it. Finally the oscillations are so large that cause failure due to excessive deflection and stress.

The Tacoma bridge event marked the necessity to consider VIV effects in civil and structural engineering. Since then, several fundamental studies were carried out by different researches, many of them discussed in the reviews of Sarpkaya (1979), Griffin & Ramberg (1982), Bearman (1984), Parkinson (1989) and Williamson & Govardhan (2004).

Despite several works on VIV, many fundamental questions still exist. Some of these interrogations are directly related to the parameters involved in the mathematical model, namely: mass, spring and damping coefficients. This thesis is an effort to propose a standard method to identify the parameters which will allow to explain these questions.

The following 4 chapters will be a broader explanation on this brief introduction. In Chapter 1, the fundamentals of mechanical vibrations as well as those of VIV

---

are settled down. Basic concepts and simple explanations based on the state of art are developed here. Chapter 2, treats the theory of flow around a circular cylinder in steady and oscillatory currents. This is a comprehensive explanation of what is established in the literature for circular cylinders submitted to a current, including VIV. In Chapter 3 the experimental details and the results of the experiments are shown. Some of the main results included are the mass coefficient, the phase angle between the fluid force and the body displacement, the dynamic response of the tip of the cylinder, and the vortex shedding pattern; all along the lock-in region. Chapter 4 is a comparison between the results using equivalent parameters and the 'real' parameters. Here an explanation is offered for the differences obtained in Chapter 3 and those available in the literature.

# First Picture of Narrows Bridge Falling LANGLIE LEADING BY 2,045



## Seattle Post-Intelligencer

WEATHER FORECAST	
High	50
Low	35
Wind	Light
Clouds	Partly
Moisture	60%
Barometer	30.2

VOL. CXIX, NO. 47

Published by Harold G. Lunt  
Director of Seattle, Wash.

5

SEATTLE, FRIDAY, NOVEMBER 8, 1940

THIRTY-TWO PAGES

DAILY 5c, SUNDAY 10c

### Going Down



**AWESOME SPECTACLE**—Caught by the camera in the very act of falling apart, the mammoth \$4,600,000 Tacoma Narrows bridge, one of the structural showpieces of the Pacific Northwest, is shown in its death throes in this remarkable photograph.

Lashed by a forty-two-mile-an-hour wind, the roofed-off of the 2,500-foot center suspension span away, buckled, and at last twisted under shortly before noon yesterday. In this picture a 100-foot section

of the roofed, first portion of the bridge is shown, in one hurrying speed down into the water 155 feet below while huge concrete blocks and other debris shower like falling leaves around it. Arrow indicates auto whose

driver was forced to flee for his life. He reached safety just before this section gave way and plunged into the water with the car. The dramatic picture was taken by James Bushford, Tacoma photographer.

### Mayor Holds Onto His Slim Advantage

By Dan B. Markel  
The mayor held onto his slim advantage last Thursday at precinct polls when Arthur B. Langlie and his opponent, Charles C. Dill, reported results of the election. The mayor's slim lead was maintained in the election, which was held by a majority of only 512.

### Bandits Slay Two U. Engineer Describes Close Escape on Span

KIDNING, China, Nov. 7.—(AP)—The Chinese magistrate at Chang-shu, about seventy-five miles north of Kiating, reported to the United States consulate today that two members of a Soedann, Wash. mob slaying party were slain and two wounded in an attack by robbers Tuesday night on the newly built mainline railway near Chong-ching. The magistrate identified the dead as Mrs. Emily Bertram, Chicago, and her son, David.

### U. Engineer Describes Close Escape on Span

By F. E. Farquharson  
Associate Professor of Engineering at the University of Washington, who directed rescue team to narrow the span's uppermost "apple" (As Told in a Post-Intelligencer Report)  
It wasn't bravery on my part; I didn't believe it would happen, and besides, I was anxious to see motion pictures of the natural way

### Narrows Span Lies At Bottom of Sound

By Doug Welch  
Tacoma Narrows Suspension Bridge lay in 120 feet of water at the bottom of Puget Sound tonight. Engineers say it is the greatest bridge failure in history.

**TODAY'S**

Assessments	16, 17
Classified Ads	26, 27, 28, 29
Deaths	3
Crossword Puzzle	4
James Murray	5
Dr. Burdette	6
Spring's On The Slide	7
Editorial Page	8
Financial	24, 25
Pink's Lines	26
Personal Announcements	27
Memorabilia Section	31 to 32

Figure 0.1: The Seattle Post-Intelligencer's front page, Nov. 8, 1940.



# 1 Background on Vortex-Induced Vibration

This chapter is a review of basic concepts. A brief explanation about mechanical vibrations, its definition and their different types, is given. The definition of VIV is also given, when can be observed and different apparatus that exist in the literature to study it. At the end of the chapter, the basic equations to study VIV and the different dynamic and hydrodynamic responses reported in the literature are established.

## 1.1 Mechanical Vibrations

Vibration is a term normally used to describe oscillations in a mechanical system. Each vibration has its own magnitude, frequency and phase angle. Magnitude refers to the maximum variation of the displacement, namely is the distance between the equilibrium point and the farthest point in the oscillation. The equilibrium point is a certain point in the space where if the system is released with zero velocity and no forces are applied, the system would remain at rest. Frequency means the number of cycles per time unit. The phase angle is helpful because it can be used to know the offset between two waves or oscillations.

It is important to note that strictly speaking vibration and oscillation are not the same. Both last in time converting energy from one type to another. For example, a pendulum converts kinetic energy into potential energy, it oscillates but it does not vibrate. To declare that vibrations are occurring, a special type of energy, namely deformation or elastic potential energy, must appear. However, several authors have proposed different definitions and not always the elastic potential energy is involved. For purposes of this research, the classical definition given at the beginning of this section is sufficient.

In general terms, there are two kinds of mechanical vibrations: free vibrations and forced vibrations. Free vibrations occurs when the body is kept in movement by restoring gravitatory or elastic forces. Forced vibrations, on the other hand, are provided by an external periodic or intermittent force. Both types of vibrations can be damped or undamped. The damped vibrations decrease with time until the system reaches the equilibrium position again. Opposite to that, the undamped vibrations may continue infinitely if the frictional effects are neglected. This is

only possible mathematically, being that friction is always present and it acts as a damping force. An extensive explanation of vibration systems and its responses is given in sec. 2.4.1.

## 1.2 Vortex-Induced Vibration

From the different types of vibrations studied, one of particular interest is the so-called vortex-induced vibration (VIV). These are self-excited vibrations caused due to vortex shedding (see sec. 2.1.2) normally in long slender bodies. This type of vibrations occur in a specific region known as ‘lock-in’. The classical definition of lock-in is: the regime where the body oscillation frequency ( $f$ ) and the vortex shedding frequency ( $f_v$ ) are close to the natural frequency of the structure ( $f_n$ ), that is  $f \approx f_v \approx f_n$  (see Blevins 1990 and Sumer & Fredse 1997). However, on recent studies a lock-in regime was found at several times the natural frequency (see Moe & Wu 1990, and Khalak & Williamson 1997). One of the most accepted definitions, and the one used as a reference in this thesis, is the one proposed by Sarpkaya (1995). Synchronization, or lock-in, might be defined as the regime where the fluid force frequency must match the shedding frequency. Or as proposed by Khalak & Williamson (1999), synchronization is the matching of the frequency of the periodic wake vortex mode with the body oscillation frequency.

In order to study the lock-in region, and therefore the VIV phenomenon, there are different configurations of experimental apparatus used in the literature. These different configurations have unique features that allow different responses and behaviors. Despite the configuration, some data are almost identical and can be used in a broader way. However, that does not always happen and the chosen configuration will affect the equations and assumptions made, and therefore the results.

### 1.2.1 Types of experimental apparatus

#### 1.2.1.1 Rigid and flexible cylinders

There are two different types of cylinders: the rigid cylinder and the flexible cylinder (see Fig. 1.1). A rigid cylinder has the characteristic of not being deformed by the effect of external forces. In other words, if an axis is plotted along the cylinder, the relative position of any particle to this axis will not change despite the external forces applied to the cylinder. Although a real body is never totally rigid, this kind of cylinders are useful to describe movement (usually considering a continuous mass distribution). Moreover, in a flexible cylinder, the external forces cause deformation. This deformation appears as an opposition to the external force and therefore, when the force is removed the cylinder returns to its original state. What a flexible body experiences is what actually happens, hence, is a more accurate model but also a



more complex one. Due to its proximity to the reality, the chosen cylinder for this research was a flexible one.

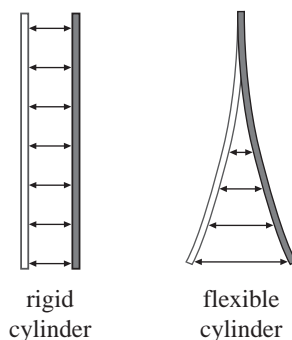


**Figure 1.1:** Rigid and flexible cylinders.

### 1.2.1.2 Elastic, pivoted and cantilevered cylinders

In the literature, there are different systems or apparatus to study VIV. Three of those systems are: elastic base system, pivoted rod or pendulum system and cantilevered bar system (see Fig. 1.2). Each has a different mathematical treatment.

The elastic base system consists of a rigid cylinder mounted on an elastic base. Normally this base allows the cylinder to move only in one degree-of-freedom. And due to the configuration it has always a two-dimensional phenomenon. Important research concerning this system are those of Jauvtis & Williamson (2004), Stappenbelt & Lalji (2008) and Blevins & Coughran (2009).

The pivoted pendulum system consists of a rigid cylinder mounted in a pivoted pendulum base. It can have one or two degrees-of-freedom, namely, oscillations in the cross-flow and in the in-line directions. This configuration allows the base to have the same natural frequency in both directions. Also the base allows the model to rotate around the Cardan-joint axis at the top of the rigid bar. Some interesting research using this system were carried out by Freire & Meneghini (2010) and Gonçalves et al. (2011).

The cantilevered bar system consists of a flexible cylinder attached to a rigid base. This configuration can have two degrees-of-freedom. Normally, this system has a very low structural damping coefficient and its stiffness directly depends on the length of the cylinder. Usually for this kind of system, the amplitude of the in-line oscillations are less than 10% of the amplitude of the cross-flow oscillations. Some researchers that used this system are: Pesce & Fujarra (2000) and Fujarra et al. (1998). This kind of system is the one used in the present work due to its resemblance to reality.

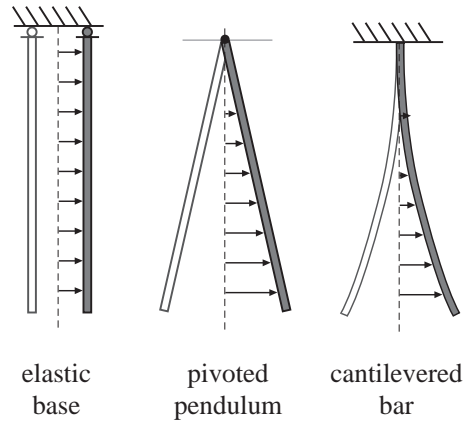


**Figure 1.2:** Different systems to study VIV.

### 1.2.1.3 Tapered and uniform

In the literature, different types of cylinders are used (see Fig. 1.3). Tapered cylinders are used to study three-dimensional vortex patterns and/or the spanwise variation of the amplitude of the oscillations. According to Techet et al (1998) using tapered cylinders one may get different hydrodynamic responses along the cylinder. On the other hand, uniform cylinders are most commonly used. They are easier to construct and to model mathematically. Because of this, a uniform cylinder is used in this work.

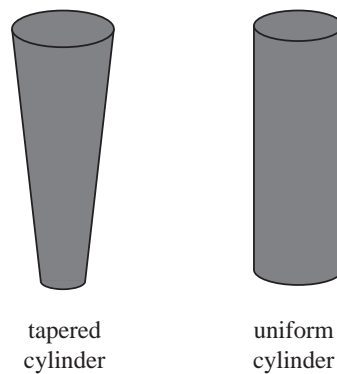


**Figure 1.3:** Tapered and uniform cylinders.

Stated the entire configuration of the experimental apparatus, *a cantilevered uniform flexible circular cylinder*, the mathematical model of the system can be established.

Next section indicates some important points about passing from actual problem to differential equations capable of describe the main variables.

### 1.2.2 Mathematical model

In engineering problems is not always possible to obtain mathematical solutions. Only in a few simple cases an analytic solution is found. When the problem exceeds the complexity of the equations or the methods to solve these equations, simplifications must be made. In spite of the simplifications, results must be capable of achieving certain goals.

The key to pass from a real problem to a mathematical solution is to obtain a mathematical model and, if it is possible, a discretized model. A discretized model includes a symbolic representation of the idealized system and all the simplifications and assumptions made.

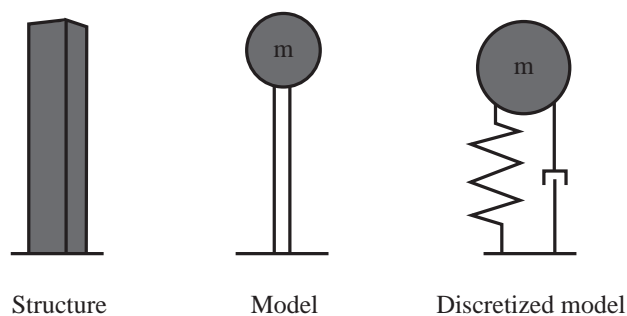


**Figure 1.4:** Converting a real problem to a mathematical model.

When the structure approaches to a model in which real mass (the one that a weight scale would measure) is replaced by an equivalent mass, the new system is called discretized model. An equivalent mass is a punctual mass connected by springs and dampers with no mass. If the real mass is represented in a distributed form (distributed in physical space), it is said that the system is now a model with distributed parameters.

In this work, the experimental apparatus is a cantilevered uniform flexible circular cylinder under VIV. The mathematical model is a discretized model, and the equation of motion generally used to represent the displacement in the cross-flow direction under this configuration is:

$$m\ddot{y}(t) + c\dot{y}(t) + ky(t) = F(t) \quad (1.1)$$

where  $m$  is the total mass of the system,  $c$  is the structural damping,  $k$  is the spring constant, and  $F$  is the fluid force in the transverse direction. When the body oscillation frequency is synchronized with the periodic wake mode,  $F(t)$  can be approximated to:

$$F(t) = F \sin(\omega t + \phi) \quad (1.2)$$

where

$$y(t) = A \sin(\omega t) \quad (1.3)$$

in which  $\omega = 2\pi f$ , and  $f$  is the oscillation frequency. The phase angle  $\phi$ , represents the offset between the fluid force and the body displacement. Sarpkaya (1979) and Bearman (1984) pointed out that this phase angle is related to the energy transfer from the fluid to the body, and therefore it influences the amplitude of oscillation.

### 1.2.2.1 Parameters

As it can be seen from the last section, there are three main parameters in the equation of motion: mass, spring constant, and structural damping coefficient. Each parameter has different features. Here the three elements are ideal, which implies the following facts:

Ideal mass:

- The ideal mass is totally rigid.
- The motion of an ideal mass is not affected by any damping force or friction.

Ideal spring:

- The ideal spring has no mass or internal damping.
- A positive value of  $y$  produces a negative restoring force, the spring force represents an opposition to original movement.

Ideal damper (mechanical resistance):

- The ideal damper has no mass and it does not causes a restoring force.
- Force due to viscosity is typically approximated as being proportional to velocity.

### 1.2.2.2 Forces

As an important part of the mathematical model, forces must be stated and decomposed to deeply understand some concepts, like the vortex formation. Lighthill (1986) shows that the total fluid force,  $F_{total}$ , expressed in Eq. 1.4 can be decomposed into a ‘potential force’,  $F_{potential}$ , and a ‘vortex force’,  $F_{vortex}$ . He also stated that the vortex force is caused by the dynamics of the ‘additional vorticity’, where additional vorticity is the entire vorticity in the flow field minus “part of the distribution of vorticity attached to the boundary in the form of a vortex sheet allowing exactly the tangential velocity associated with the potential flow” (Lighthill, 1986). The vortex force is directly related to vortex dynamics, and any change in the vortex force would lead to a change in the vortex formation mode.

$$F_{total} = F_{vortex} - F_{potential} \quad (1.4)$$

where the potential force is due to the added-mass (see sec.2.3.1.1 for detailed information about added also known as hydrodynamic mass):

$$F_{potential}(t) = m'\ddot{y}(t) \quad (1.5)$$

The equation of motion using the vortex force is given by

$$(m + m')\ddot{y}(t) + c\dot{y}(t) + ky(t) = F_v \sin(\omega t + \phi_{vortex}) \quad (1.6)$$

and the equation of motion using the total force is given by

$$m\ddot{y}(t) + c\dot{y}(t) + ky(t) = F_t \sin(\omega t + \phi_{total}) \quad (1.7)$$

These equations will be used later, in sec. 3.4.3, to explain the dynamics of the cylinder and the vortex shedding pattern observed. Meanwhile, once the configuration and equations used to study VIV were stated, in the next sections the different dynamic and hydrodynamic responses found in literature will be briefly explained.

### 1.2.3 Types of dynamic response in vortex-induced vibrations

According to Khalak & Williamson (1999), two different types of responses exist for an elastically mounted system depending on the mass-damping parameter ( $m^*\zeta$ ),

see Fig. 1.5. For a high  $m^*\zeta$ , experiments like the ones conducted by Feng (1968) and Brika & Laneville (1993) show two different branches of amplitude response with hysteresis in the transition between them. Khalak & Williamson described them as the ‘initial’ branch, which corresponds to the highest amplitudes reached, and the ‘lower’ branch. For a low  $m^*\zeta$ , experiments conducted by Khalak & Williamson (1996, 1997, 1999) show the existence of an additional branch. They find the so-called ‘upper’ branch and an hysteretic transition from initial to upper branch. On the other hand, transition from upper to lower branch turn out to be an intermittent switching of modes.

Despite the fact that this classification was intended for elastically mounted cylinders, the classification seems to fit with the flexible mounted cylinders as well. For such reason, this classification is used in this thesis. According to it and in order to get more information on the lock-in regime, in this research, it was decided to study the low  $m^*\zeta$  case.

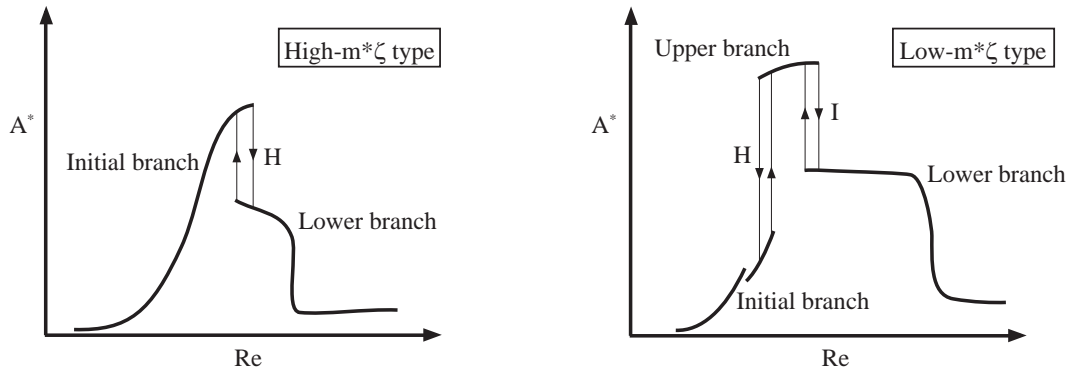


**Figure 1.5:** Sketches of the two different types of dynamic response. **H** means an hysteretic transition and **I** means an intermittent switching of modes. Based on Govardhan & Williamson (2000).

### 1.2.4 Types of hydrodynamic response in vortex-induced vibrations

A number of researches have reported different patterns of vortex formation as  $Re$  and  $A^*$  vary along the lock-in regime (see Fig. 1.6). Griffin & Ramberg (1974) were the first showing, in forced-vibrations experiments, that an asymmetric mode occurs where three vortices are formed per cycle. Also in forced-vibration studies, Williamson & Roshko (1988), show different vortex formation modes. These modes were defined as ‘2S’, ‘2P’ and ‘P+S’. ‘2S’ indicates two single vortices formed per cycle, ‘2P’ indicates two pair of vortices formed per cycle and ‘P+S’ indicates a pair of vortices and a single vortex per cycle.

It is important to note that the existence of the ‘2P’ mode in forced transverse vibrations was confirmed by Sheridan et al. (1998) using experimental measurements. Even a hybrid mode where the ‘2P’ and ‘2S’ modes occur at the same time at different spanwise locations along a tapered cylinder was found by Hover & Triantafyllou (1998), also in forced-vibration. However, some two-dimensional numerical simulations, carried out by Meneghini & Bearman (1995) and Blackburn & Henderson (1995), and experiments, by Jeon, Shan & Gharib (1995) and Atsavapranee et al. (1998), do not find the ‘2P’ mode.

Despite the fact that there are works where the ‘2P’ mode does not exist, Williamson & Roshko (1988) suggested that a phase jump,  $\phi$ , corresponds with a change of mode from ‘2S’ to ‘2P’ in forced-vibration experiments. Even more, Brika & Laneville (1993) and Khalak & Williamson (1999) show independently, in free-vibration experiments, that the jump from the initial branch to the lower branch is directly related to the mode change from ‘2S’ to ‘2P’. In a similar way, Govardhan & Williamson (2000) confirmed that a large jump in the ‘vortex phase’,  $\phi_{vortex}$ , in the initial-upper branch transition is associated with a jump between the ‘2S’ to ‘2P’ vortex wake modes. They also conclude that there is no jump in  $\phi_{vortex}$  at the upper-lower branch transition since both branches are associated with the ‘2P’ mode. However, interestingly, Evangelinos & Karniadakis (1999) conclude that the ‘P+S’ pattern may be associated with the upper branch.

Besides the vortex formation modes mentioned above, others have been found. The ‘P’ mode indicates a pair of vortices formed per cycle. Although it may be mistaken as a ‘2S’ mode, the ‘P’ mode have the vortices of a pair closer and on the same horizontal axis. Other vortex formation mode, the ‘C’ mode, is defined as a vortex coalescence and is rarely seen.

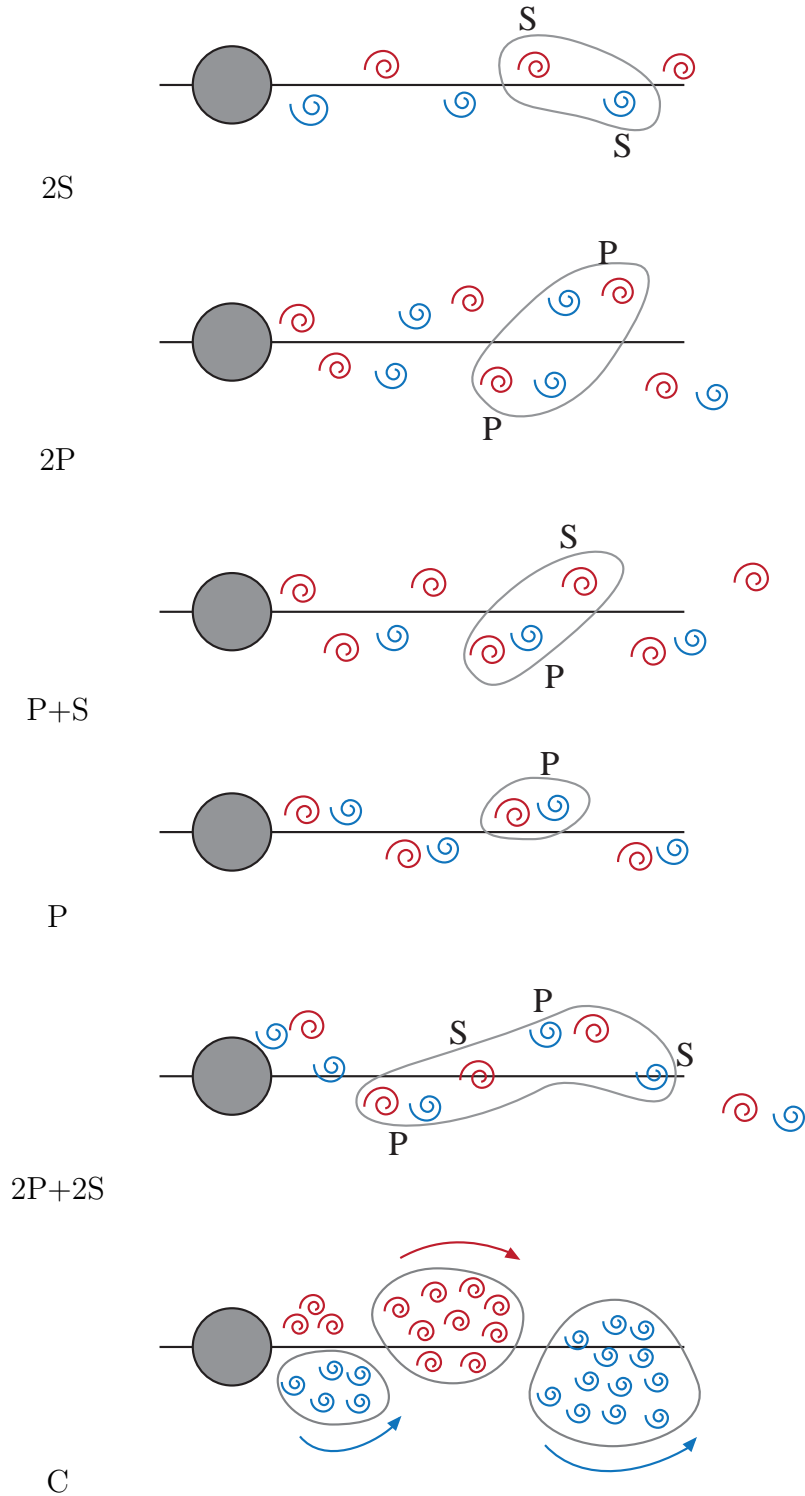


**Figure 1.6:** Sketches of the vortex shedding patterns founded in Vortex-Induced Vibrations. **S** means a single vortex and **P** means a vortex pair, each pattern is defined by the number of pairs and single vortices formed per cycle. Gray lines encircles the vortices shed in one complete cycle. Based on Williamson & Roshko (1988).



# 2 Flow around a circular cylinder in steady and oscillatory currents

In this chapter, some theory of flow around circular cylinders is explained. It starts from the simplest case, a cylinder in steady current, and moves to more complicated cases, like a cylinder in oscillatory current. Even though the first cases are not under VIV, along these sections some phenomena, like vortex shedding and the appearance of hydrodynamic mass, that also happens in VIV are explained. Finally, in the last part of the chapter, circular cylinders in VIV are studied. A wide explanation about vibrating systems, and its solutions to motion equations, is offered.

## 2.1 Flow around a cylinder in steady current

### 2.1.1 Regimes of flow around a smooth circular cylinder

The Reynolds number ( $Re$ ), is a non-dimensional quantity used to describe similar flow patterns in fluid flows under different circumstances. It is defined as the ratio between the inertial and the viscous forces, so it can be noticed the importance of each force for a given flow conditions. In the case of flow around a smooth circular cylinder, it is defined as:

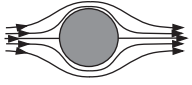
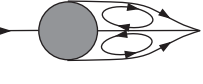
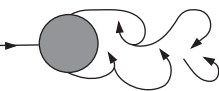
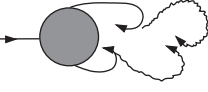
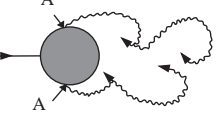
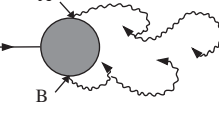
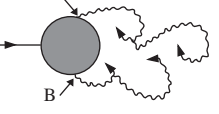
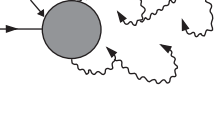
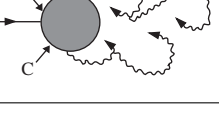
$$Re = \frac{\textit{inertial forces}}{\textit{viscous forces}} = \frac{\rho DU}{\mu} = \frac{DU}{\nu} \quad (2.1)$$

where  $D$  is the diameter of the cylinder,  $U$  is the main flow velocity, and  $\nu$  is the kinematic viscosity.

The flow is subjected to enormous changes as the  $Re$  increase from zero. Fig. 2.1 shows the different regimes of flow classified according to the Reynolds number. As it can be seen (Fig. 2.1a), for very small  $Re$  there are no separation, it only occurs when  $Re > 5$ . For  $5 < Re < 40$ , a fixed pair of vortices appear in the wake of the cylinder (Fig. 2.1b), which length, according to Batchelor (1967), increases with the  $Re$ .

When  $Re$  exceeds a value of 40, the flow is no longer stable and a phenomenon called vortex shedding shows up. This event consists in the shedding of vortices

alternately to either side of the cylinder, normally with a very specific frequency. This is normally known as a “vortex street” (Fig. 2.1d-f). In the range  $40 < Re < 200$ , the vortex street is fully laminar and it does not vary along the cylinder (is a 2-D phenomenon).

a)		No separation / Creeping flow	$Re < 5$
b)		A fixed pair of symmetric vortices	$5 < Re < 40$
c)		Laminar vortex street	$40 < Re < 200$
d)		Transition to turbulence in the wake	$200 < Re < 300$
e)		Wake completely turbulent	$300 < Re < 3 \times 10^5$ Subcritical
f)		One side with a laminar and the other with turbulent boundary layer separation (still both sides with a laminar boundary layer)	$3 \times 10^5 < Re < 3.5 \times 10^5$ Critical (Lower transition)
g)		Both sides with turbulent boundary layer separation (both sides with partly laminar partly turbulent boundary layer)	$3.5 \times 10^5 < Re < 1.5 \times 10^6$ Supercritical
h)		Boundary layer completely turbulent at one side	$1.5 \times 10^6 < Re < 4 \times 10^6$ Upper transition
i)		Boundary layer completely turbulent at both sides	$4 \times 10^6 < Re$ Transcritical

**Figure 2.1:** Regimes of flow around a smooth circular cylinder in steady current. **A:** laminar boundary layer separation; **B:** turbulent boundary layer separation; and **C:** turbulent boundary layer separation with boundary layer completely turbulent.

When  $Re$  increases, the flow starts a transition from laminar to turbulent. As stated by Bloor (1964), in the range  $200 < Re < 300$  this transition moves towards the cylinder, and once  $Re = 400$  the vortices formed are turbulent. According to the work of Gerrard (1978) and Williamson (1988) in the range  $200 < Re < 300$  the vortices are shed in different cells along the cylinder, so the phenomena is now 3-D. It is important to notice that although the wake can be partially turbulent, the boundary layer over the cylinder remains still laminar.

Even for the subcritical range,  $300 < Re < 3 \times 10^5$ , the boundary layer stays laminar despite the fact that the wake is now completely turbulent (Fig. 2.1e). Beyond this point,  $3 \times 10^5 < Re < 3.5 \times 10^5$ , the range is known as the critical flow regime. Here the boundary layer starts to become turbulent at the separation point but only in one side of the cylinder (Fig. 2.1f). This turbulence in the boundary layer causes a non-zero mean lift on the cylinder. In accordance with Schewe (1983), the side of the cylinder at which the turbulent separation occurs may switch and consequently the lift changes its direction.

In  $3 \times 10^5 < Re < 3.5 \times 10^5$  the regime is known as the supercritical flow regime. Here the boundary layer separation is turbulent on both sides of the cylinder, but the transition to turbulent flow in the boundary layer is not complete. The transition from laminar to turbulent is somewhere between the stagnation point and the separation point (Fig. 2.1g). Beyond  $Re = 1.5 \times 10^6$ , the boundary layer is totally turbulent on one side of the cylinder. The other side is partially laminar and partially turbulent. This type of response corresponds to the so-called upper transition flow regime,  $1.5 \times 10^6 < Re < 4 \times 10^6$ . Further this last value,  $Re = 4 \times 10^6$ , the boundary layer is turbulent everywhere and is known as the transcritical flow regime (Fig. 2.1i).

The preceding regimes are based mainly in the work of Roshko (1961) and Schewe (1983). However, there is no general classification well accepted by the entire scientific community.

### 2.1.2 Vortex shedding

As mentioned in the last section, for  $Re > 40$  the vortex shedding phenomenon appears. For those cases, the boundary layer separates from the cylinder surface due to the adverse pressure gradient, which is imposed by the divergent geometry of the flow environment at the rear side of the cylinder. This event forms a shear layer (Fig. 2.2).

The boundary layer formed contains a certain vorticity. This vorticity feeds the shear layer (that is formed downstream the separation point) and yields the shear layer to roll up into a vortex with the same sign of the incoming vorticity (say vortex A in Fig. 2.2). In like manner on the other side of the cylinder occurs the same phenomenon but with a lag time, forming another vortex (say vortex B in Fig. 2.2).

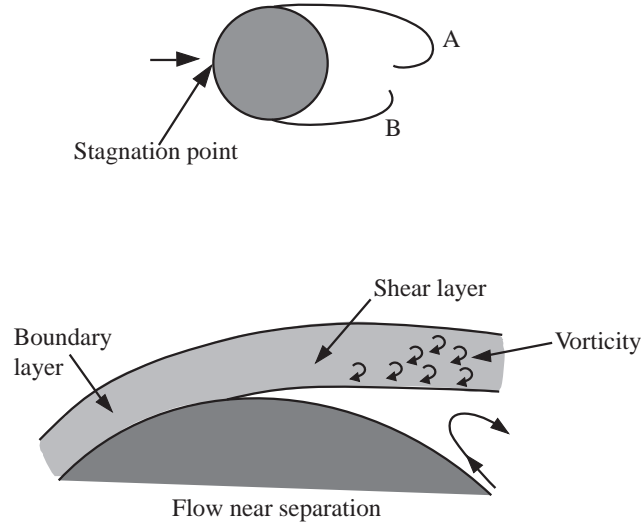


**Figure 2.2:** The shear layer. The shear layer roll up to form a vortex, one for each side of the cylinder. Based on Sumer & Fredsøe (1997).

The pair of vortices formed due to the shear layer is unstable when is exposed to small disturbances. This leads one vortex to grow larger than the other. The larger vortex throws the other vortex toward the wake due to the asymmetric flow (see Fig. 2.3). One vortex spins in the clockwise direction while the other spins in the anticlockwise direction. This difference will cut off the supply of vorticity from the boundary layer to one vortex and will cause the shedding of it. As a free vortex, it will be drawn downstream by the main flow.

The vortex shedding only happens when the two shear layers (one at each side of the cylinder) interact with each other. If this interaction between the layers is affected somehow, no vortex shedding will occur. Some ways to prevent the interaction are to place a horizontal plate at the rear side of the cylinder, or to place the cylinder close enough to a wall, among others.



**Figure 2.3:** Vortex shedding mechanism. In the first scheme, the vortex **A** is larger and throws the vortex **B** across the wake. In the second scheme, the vortex **B** has grown enough to throw the vortex **C** across the wake. This mechanism is repeated in an alternate manner at each side of the cylinder to form the “vortex street”. Based on Sumer & Fredsøe (1997).

### 2.1.2.1 Vortex-shedding frequency

As the Reynolds number is used to describe flows, there is a dimensionless number that helps to describe an oscillatory flow. This number depends on the normalization of the vortex shedding frequency:

$$St = St(Re) = \frac{f_v D}{U} \quad (2.2)$$

where  $f_v$  is the vortex shedding frequency,  $D$  is the diameter of the cylinder and  $U$  is the main flow velocity. This normalized vortex shedding frequency is known as the Strouhal number ( $St$ ).

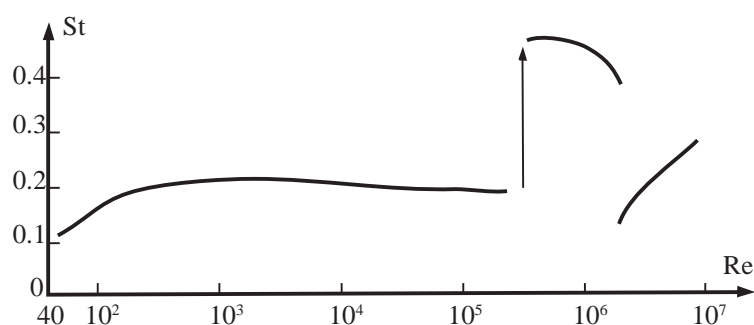


**Figure 2.4:** Sketch of the Strouhal number for a smooth circular cylinder. Based on experimental data from: Williamson (1989), Roshko (1961), and Schewe (1983).

When the vortex shedding first appears, the  $St$  number takes a value of approximately 0.1 (see Fig. 2.4). It increases until  $Re \simeq 300$ , from this value onwards the  $St$  number stays practically at a constant value of 0.2. The  $St$  number change its value again when  $Re = 3 \times 10^5$ , suddenly it jumps from 0.2 to 0.45. At this same point,  $Re = 3 \times 10^5$ , the boundary layer is turbulent at the separation point on both sides of the cylinder. The outcome is a delay in the boundary layer separation where the separation point moves downstream (see Fig. 2.5). Now that the vortices are closer to each other, the interaction is faster than before and the shedding vortex increases drastically, the same as the  $St$  number.

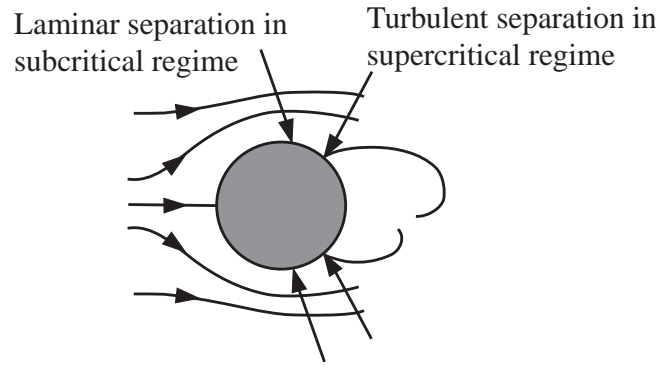


**Figure 2.5:** Sketch of the separation points. Based on Sumer & Fredsøe (1997).

At  $Re = 1.5 \times 10^6$ , the  $St$  number jumps again, but this time its value decreases. At this point, the boundary layer at one side of the cylinder is turbulent and laminar on the other side. This asymmetry inhibits the vortex interaction partially and the vortex shedding becomes irregular. This behavior changes when  $Re$  overpass the value of  $4.5 \times 10^6$ ; there, the  $St$  number takes a value of 0.25-0.30.

## 2.2 Forces on a cylinder in steady current

Because of the flow around a circular cylinder two forces will appear, one due to the pressure and one due to the friction. The total mean resultant force due to pressure per unit length is:

$$\bar{F}_p = \int \bar{p} \cdot r_0 d\phi \quad (2.3)$$

While the total resultant force due to friction is:

$$\bar{F}_f = \int \bar{\tau}_0 \cdot r_0 d\phi \quad (2.4)$$

in which  $\bar{p}$  is the time averaged pressure and  $\bar{\tau}_0$  is the time averaged wall shear stress on the cylinder surface. The geometry of these integrals is shown in Fig. 2.6.

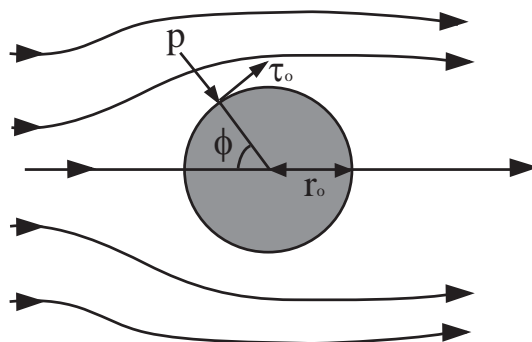


**Figure 2.6:** Definition sketch.

Besides the above method, there are other way to classify these forces depending on the direction in which they are applied. The total in-line force, known as the mean drag, is the sum of the corresponding component of the Eq. 2.3 and 2.4:

$$\bar{F}_D = \int \bar{p} \cdot \cos(\phi) \cdot r_0 d\phi + \int \bar{\tau}_0 \cdot \sin(\phi) \cdot r_0 d\phi \quad (2.5)$$

While the total cross-flow force, known as the mean lift, is:

$$\bar{F}_L = \int \bar{p} \cdot \sin(\phi) \cdot r_0 d\phi + \int \bar{\tau}_0 \cdot \cos(\phi) \cdot r_0 d\phi \quad (2.6)$$

In this case this last force,  $\bar{F}_L$ , will be null due to symmetry in the flow. Nevertheless, the instantaneous cross-flow component is non-zero and its value can be large.

### 2.2.1 Drag and lift

The forces, as well as the flow itself, vary as the  $Re$  number is changed, but also when the surface roughness, the cross-sectional shape and the incoming turbulence change. Independently of these changes, the vortex shedding phenomenon is always present.

Due to the vortex shedding, the pressure distribution is different as the vortex shedding process goes on. This changes are periodic and they will result in the variation of the force components on the cylinder.

As Fig. 2.7 shows, the drag force acting on the cylinder will oscillate around the mean value and will always be positive or in the same direction. The lift force, on the other hand, change its direction and it may have a zero value in a specific time. However, both forces vary periodically along with the vortex shedding process.

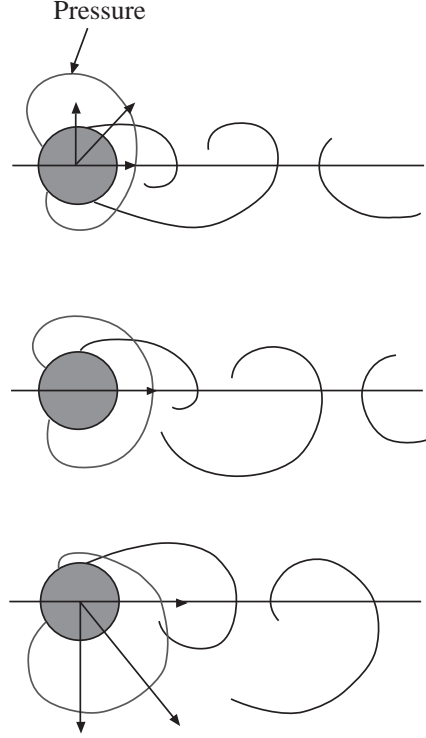


**Figure 2.7:** Sketch of time development of pressure distribution at different moments of the vortex shedding process. Based on Drescher (1956).

### 2.2.1.1 Mean drag

**Form drag and friction drag** For  $Re > 10^4$ , Achenbach (1968) proved that the form drag (or in-line pressure force) represents the 97-98% of the total drag force. For practical purposes, the friction drag can be omitted in most of the cases.

Following this idea, Fig. 2.8 shows the pressure distribution obtained from the potential flow theory, which is given by:

$$\bar{p} - p_0 = \frac{1}{2}\rho U^2 (1 - 4 \sin^2 \phi) \quad (2.7)$$

where  $p_0$  is the hydrostatic pressure. As it can be seen, the measured pressure distribution is negative at the rear side of the cylinder. In contrast, the potential



flow theory gives a significantly different result. One may think that as a result of separation. The pressure on the cylinder remains constant at the rear side because the flow in the wake is very weak compared to the outer-flow. This result is important because it shows that sometimes the potential flow theory is not close to reality, and the outcomes obtained with it cannot always be applied to certain problems.

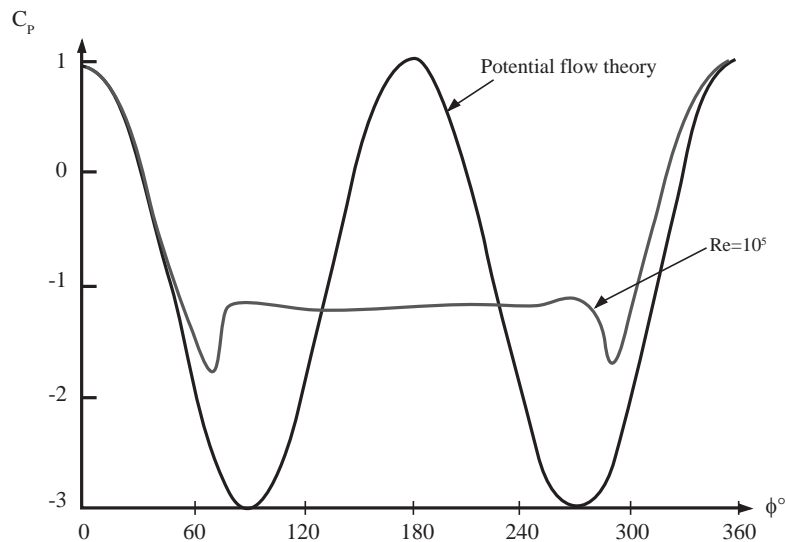


**Figure 2.8:** Sketch of pressure distributions, potential flow theory and  $Re = 10^5$ . Based on Achenbach (1968).

**Drag coefficient** The drag force can be calculated as

$$\bar{F}_D = \int (\bar{p} \cos(\phi) + \bar{\tau}_0 \sin(\phi)) r_0 d\phi \quad (2.8)$$

manipulating the equation, it can be written as

$$\frac{\bar{F}_D}{\frac{1}{2}\rho DU^2} = \int \left[ \left( \frac{\bar{p} - p_0}{\rho U^2} \right) \cos(\phi) + \left( \frac{\bar{\tau}_0}{\rho U^2} \right) \sin(\phi) \right] d\phi \quad (2.9)$$

where  $D = 2r_0$ , is the cylinder diameter. The right-hand of the Eq. 2.9 is a function of  $Re$ . Consequently, it can be written in the form

$$\frac{\bar{F}_D}{\frac{1}{2}\rho DU^2} = \bar{C}_D \quad (2.10)$$

where  $C_D$  is known as the mean drag coefficient or drag coefficient.

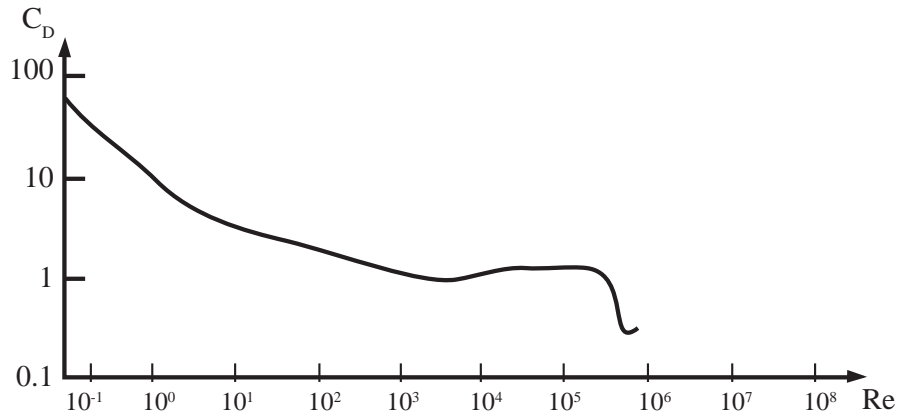


**Figure 2.9:** Drag coefficient for a smooth circular cylinder as function of the  $Re$  number. Based on data from: Schewe (1983) and Schlichting (1979).

Fig. 2.9 present the behavior of the drag coefficient when  $Re$  varies. A critical point occurs when  $Re = 3 \times 10^5$ , here the drag coefficient drops drastically. This is known as the drag crisis and it can be explained with the pressure diagrams (see Fig. 2.10).

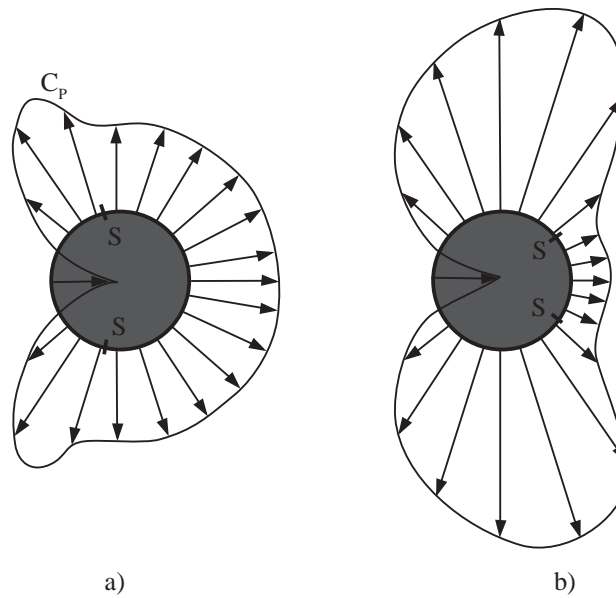


**Figure 2.10:** Pressure distributions. **S** denotes the separation points. a) Circular cylinder in the subcritical regime, and b) Circular cylinder in the supercritical regime. Based on Achenbach (1968).

The separation points moves from  $\phi = 78^\circ$  in a laminar separation, to  $\phi = 140^\circ$  in turbulent separation. This results in a narrow wake with a smaller negative pressure, which will lead to a smaller drag coefficient.

## 2.3 Forces on a cylinder in oscillatory flows

Now that the forces and its origin were explained. Forces in oscillatory flows, which are more like those on VIV, will be explained in detail in this section.

### 2.3.1 Drag force in oscillatory flow

The drag force in a steady current is given by:

$$F_D = \frac{1}{2}\rho C_D D U |U| \quad (2.11)$$

in which  $F_D$  is the in-line force per unit length of the cylinder and  $C_D$  is the drag force coefficient. Here instead of write  $U^2$  the expression is  $U |U|$ , so the force can conserve the sign (direction) of the velocity. For oscillatory flows, where  $U = U_m \sin(\omega t)$ , the drag force has two more components, namely:

$$F_D = \frac{1}{2}\rho C_D D U |U| + m' \dot{U} + \rho V \dot{U} \quad (2.12)$$

in which the second term of the right hand is the hydrodynamic mass force and the third term is the Froude-Krylov force; here  $m'$  denotes the hydrodynamic mass and  $V$  is the volume of the cylinder.

#### 2.3.1.1 Hydrodynamic mass force

In order to understand the hydrodynamic mass, one might think in a plate submerged into still water. When the plate moves from rest in the horizontal position (see Fig. 2.11a), it undergoes practically no resistance. When the plate moves from rest in the vertical position, Fig. 2.11b, not only the plate but also the fluid surrounding is moving along. This phenomenon occurs due to the pressure from the plate. This mass of fluid that is accelerated with the plate due to the pressure is known as the hydrodynamic mass. The existence of the hydrodynamic mass means that the total force to move the body is not  $F = ma$  but  $F = (m + m')a$ , where  $m$  is the mass of the solid object and  $a$  is the acceleration.

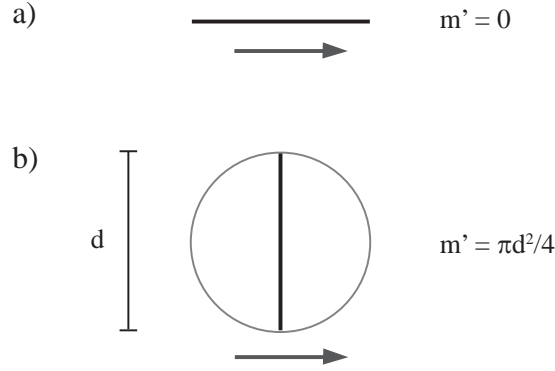


**Figure 2.11:** Movement of a plate in a still fluid; a) horizontal plate, and b) vertical plate. Based on Sumer & Fredsøe (1997).

The hydrodynamic mass is normally calculated excluding the frictional effects. That is to say that the flow is calculated using only the pressure forces and the inertia forces. As a result, the hydrodynamic mass may be calculated using potential flow theory.

In order to know  $m'$  for a body in still water first the body needs to be accelerated, later the flow field around the body needs to be calculated (if it is possible using potential flow theory). With the flow field the pressure on the surface of the body can be known, and finally the force on the body due to pressure may be determined.

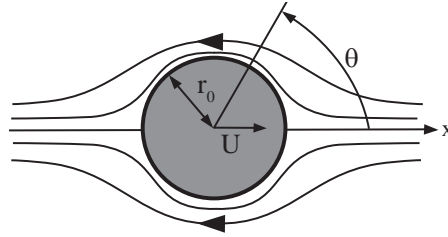


**Figure 2.12:** Sketch of potential flow around an accelerated cylinder moving in the  $x$  axis at  $U$  velocity in otherwise still fluid.

Considering the case sketched in Fig. 2.12, the velocity potential is given by (Milne-Thomson, 1962)

$$\phi = U \frac{r_0^2}{r} \cos(\theta) \quad (2.13)$$

from which the velocity components can be obtained:

$$v_\theta = -\frac{1}{r} \frac{\partial \phi}{\partial \theta} = U \frac{r_0^2}{r^2} \sin(\theta) \quad (2.14)$$

$$v_r = -\frac{\partial\phi}{\partial r} = U\frac{r_0^2}{r^2}\cos(\theta) \quad (2.15)$$

Now the pressure around the cylinder can be calculated using the Bernoulli equation

$$\frac{p}{\rho} + \frac{1}{2}v^2 - \frac{\partial\phi}{\partial t} = cte \quad (2.16)$$

in which  $v^2 = v_r^2 + v_\theta^2 = U^2(\sin^2(\theta) + \cos^2(\theta)) = U^2$  on the cylinder surface. Since  $v^2$  does not vary with  $r$  or  $\theta$ , the pressure can be written as

$$\frac{p}{\rho} = \frac{\partial\phi}{\partial t} + cte \quad (2.17)$$

Now the pressure can be calculated neglecting the constant term

$$p = \rho\frac{\partial\phi}{\partial t} = \rho\frac{\partial}{\partial t}\left(U\frac{r_0^2}{r}\cos(\theta)\right) = \rho r_0\cos(\theta)\frac{\partial U}{\partial t} = \rho r_0 a\cos(\theta) \quad (2.18)$$

Integrating around the cylinder, the total force due to pressure is

$$F_{p,s} = -\int \rho r_0 a\cos(\theta) d\theta = -\rho r_0^2 a\pi \quad (2.19)$$

The force required to accelerate a cylinder in an otherwise still fluid is

$$F = ma + \rho r_0^2 \pi a = (m + m')a \quad (2.20)$$

from where  $m' = \rho r_0^2 \pi$ . Usually the hydrodynamic mass is written as

$$m' = \rho C_m A \quad (2.21)$$

in which  $A$  is the cross-sectional area, for a circular cylinder  $A = \pi r_0^2$ , and  $C_m$  is the hydrodynamic coefficient. For a circular cylinder:

$$C_m = 1 \quad (2.22)$$

*It is important to notice that this result is based on several assumptions and simplifications. For example, a circular cylinder with velocity  $U$  in otherwise still fluid; frictional effects equal to zero; namely, this calculation implies that the fluid can be described using the potential flow theory. If these requirements are not well accomplished, the  $C_m$  needs to be calculated using other techniques.*

### 2.3.1.2 The Froude-Krylov force

As seen in the previous section, the hydrodynamic mass force is caused due to the acceleration of the fluid in the nearby surroundings. However the accelerated motion of the fluid in the not so close surroundings, outer flow region, will also generate a pressure gradient:

$$\frac{\partial p}{\partial x} = -\rho \frac{dU}{dt} = -\rho a \quad (2.23)$$

where  $U$  is the velocity in the main flow, far away from the cylinder. This force will produce an extra force, known as the Froude-Krylov force. This force is also calculated using the pressure:

$$F_{p,f} = - \int p dS \quad (2.24)$$

where  $S$  is the surface of the body. Using the Gauss theorem, the equation now is

$$F_{p,f} = - \int \frac{\partial p}{\partial x} dV = \rho V a \quad (2.25)$$

If the body moves in an otherwise still water, there will be no pressure gradient in the outer flow, and therefore there will be no Froude-Krylov force.

### 2.3.1.3 The Morison equation

The total in-line (drag) force for an accelerated fluid environment where the cylinder is held stationary can be calculated using the in-line force in steady current, the hydrodynamic mass force and the Froude-Krylov force. The  $F_D$  force is now:

$$F_D = \frac{1}{2} \rho C_D \overline{DU} |U| + \rho C_m A \dot{U} + \rho A \dot{U} \quad (2.26)$$

Manipulating the equation, it can be written as

$$F_D = \frac{1}{2} \rho C_D \overline{DU} |U| + \rho (C_m + 1) A \dot{U} \quad (2.27)$$

$$F_D = \frac{1}{2}\rho C_D D U |U| + \rho C_M A \dot{U} \quad (2.28)$$

where  $C_M = C_m + 1$ , and it is called the inertia coefficient. Eq. 2.28 is known as the Morison equation. And in the case of a body that moves relative to the flow in the in-line direction, the Morison equation can be written as:

$$F_D = \frac{1}{2}\rho C_D D (U - U_b) |U - U_b| + \rho C_m A (\dot{U} - \dot{U}_b) + \rho A \dot{U} \quad (2.29)$$

where  $U_b$  is the body velocity. The last term in Eq. 2.29 only depends only on  $U$  because this force is associated with the motion of the fluid and not with the motion relative to the body.

**Measurements of the  $C_D$  and  $C_M$  coefficients** Nowadays, there are several numerical codes to calculate the flow around and the forces on a circular cylinder in oscillatory flows but they are under development and are not fully able to describe the variation of the force coefficients. Despite technological advances in the numerical field, experiments are still the best source of information at the present time.

### 2.3.2 Lift force in oscillatory flow

Under an oscillatory flow, a cylinder may experience a lift force. This lift force oscillates at a fundamental frequency different from the one of the flow. The frequency in the lift force depends on the frequency of vortex shedding. That is why if the flow around the cylinder is a creeping flow, no lift will be generated.

For oscillatory flow, a helpful parameter is the so-called Keulegan-Carpenter number ( $KC$ ). This quantity is equal to:

$$KC = \frac{2\pi a}{D} \quad (2.30)$$

where  $a$  is the amplitude of the motion and  $D$  is the diameter of the cylinder. Small  $KC$  numbers mean that the motion of the water particles is small compared to the total width of the cylinder, therefore separation may not even occur. On the other hand, large  $KC$  numbers mean that water particles travel large distances compared to the width of the cylinder, causing separation and vortex shedding. For the vortex street to exist,  $KC$  is approximately 4. Therefore, at this point the lift force starts to grow. In order to have a well-established lift force  $KC$  need to be around 6 or 7.

The lift force undergoes two maxima values (see Fig. 2.13), the first and the biggest one at  $KC = 10$  and the second when  $KC = 16$ . Williamson (1989) poses that these peaks may reflect an increase in the repeatability of the shedding patterns. Each peak corresponds to a certain pattern of shedding. The first peak corresponds to a single-pair regime and the second peak corresponds to a double-pair regime.

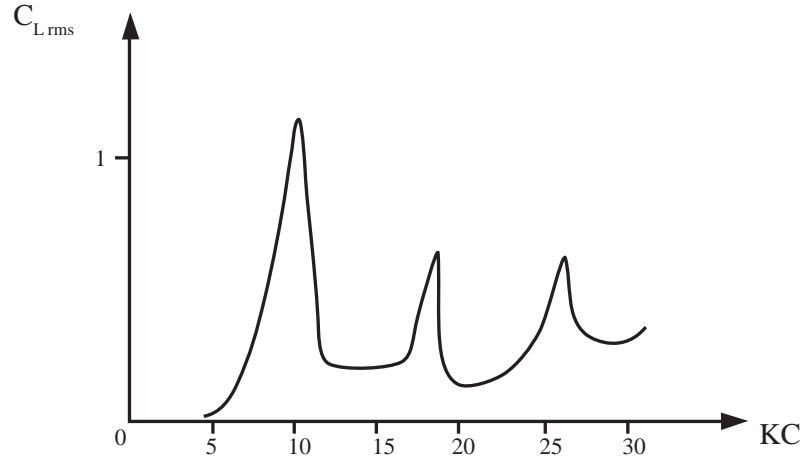


**Figure 2.13:** Sketch of the lift force coefficient (RMS) as function of  $KC$  number. Based on Williamson (1985).

The lift force (and also the drag force) has a sinusoidal behavior, so the force can be described using the maximum value or its corresponding RMS (root-mean-square) value:

$$F_{Lmax} = \frac{1}{2} \rho C_{Lmax} D U_m^2 \quad (2.31)$$

$$F_{Lrms} = \frac{1}{2} \rho C_{Lrms} D U_m^2 \quad (2.32)$$

in which  $U_m$  is the maximum velocity. Both lift coefficients are related by the equation:

$$C_{Lmax} = \sqrt{2} \cdot C_{Lrms} \quad (2.33)$$



## 2.4 Circular cylinders in Vortex-Induced Vibration

### 2.4.1 Solutions to vibration equation

A vibrating structure, sketched in Fig. 2.14, has three forces acting on it: a spring force, a damping force and a force on the structure. The spring force, namely  $-ky$ , is based on  $k$  the spring constant and  $y$  the displacement of the structure from the equilibrium position. The damping force,  $c\dot{y}$ , is due to  $c$  the viscous damping coefficient and the velocity of the system. Finally the force on the structure,  $F(t)$ , depends on external factors acting on the system.

The differential equation that governs the motion of the structure is:

$$F(t) = m\ddot{y}(t) + c\dot{y}(t) + ky(t) \quad (2.34)$$

where  $m$  is the total mass of the system. Remembering that the three elements are ideal, see sec. 1.2.2.1 for more detailed information.

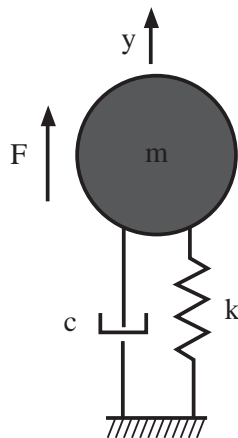


**Figure 2.14:** Sketch of a flexibly-mounted system vibrating in  $y$  direction.

#### 2.4.1.1 Free vibrations without viscous damping

In this case no external forces are acting on the structure  $F(t) = 0$  (free vibrations) and the damping is null,  $c = 0$ . The equation is now

$$m\ddot{y} + ky = 0 \quad (2.35)$$

The solution to this equation is

$$y = A \cos(\omega_v t) + B \sin(\omega_v t) \quad (2.36)$$

where  $\omega_v$  is the angular frequency of the motion, namely

$$\omega_v = \sqrt{\frac{k}{m}} \quad (2.37)$$

#### 2.4.1.2 Free vibrations with viscous damping

In this case the damping must be considered, but the external forces are still zero. The equation can be written as

$$m\ddot{y}(t) + c\dot{y}(t) + ky(t) = 0 \quad (2.38)$$

Here the solution is of the form

$$y = C_1 \exp(r_1 t) + C_2 \exp(r_2 t) \quad (2.39)$$

where  $r_1 = \frac{1}{2m}(-c + \sqrt{c^2 - 4mk})$  and  $r_2 = \frac{1}{2m}(-c - \sqrt{c^2 - 4mk})$ . Depending on the value of  $m$ ,  $c$  and  $k$  three different cases may occur. Only two are of interest for the present work (both responses are shown in Fig. 2.15):

**Over-damped case ( $c^2 > 4mk$ )** For this case,  $r_1$  and  $r_2$  have real values. Considering  $y(0) = A_y$  and  $\dot{y} = 0$ , the solution will be:

$$y = \frac{A_y}{r_1 - r_2} (r_1 \exp(r_2 t) - r_2 \exp(r_1 t)) \quad (2.40)$$

This type of motion is called 'aperiodic' motion.

**Under-damped case ( $c^2 < 4mk$ )** For this case,  $r_1$  and  $r_2$  are complex. The real part of the solution, considering the same initial conditions as in the over-damped case, may be written as:

$$y = A_y \exp\left(-\frac{c}{2m}t\right) \cos(\omega_{dv}t) \quad (2.41)$$

where  $A$  is the amplitude of vibrations at time  $t = 0$ , and the angular frequency is given by

$$\omega_{dv} = \sqrt{\frac{k}{m} - \left(\frac{c}{2m}\right)^2} \quad (2.42)$$

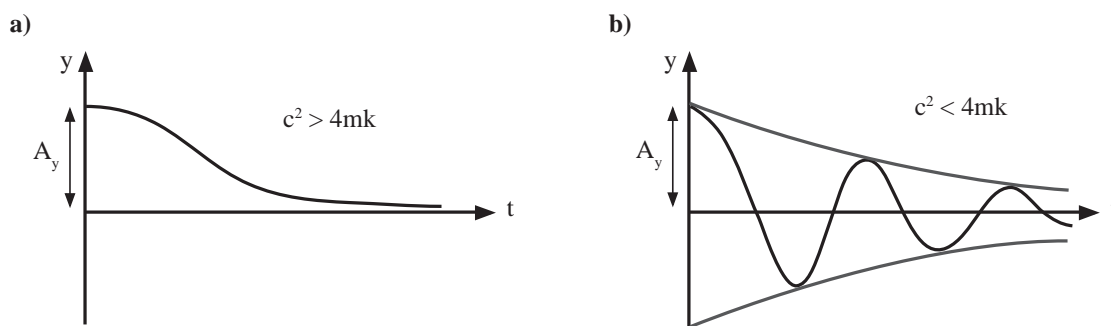


**Figure 2.15:** Free vibrations with viscous damping. a) over-damped case with no vibration, and b) underdamped case the oscillations decrease with time.

### 2.4.1.3 Forced vibrations with viscous damping

In this case, there is an external force acting on the system,  $F(t)$ . Now the equation is in its full form, Eq. 2.29. If the external force takes the form  $F = F_0 \cos(\omega t)$ , where  $\omega$  is the angular frequency associated with the force, the general solution would be:

$$y = A_y \exp\left(-\frac{c}{2m}t\right) \cos(\omega_{dv}t) + C_1 \cos(\omega t) + C_2 \sin(\omega t) \quad (2.43)$$

The first term in this equation represents the case when  $F = 0$ , and with the time its contribution to the movement of the system will be zero. Therefore, the other two terms will govern the movement and the system will have the same angular frequency as the force,  $\omega$ .

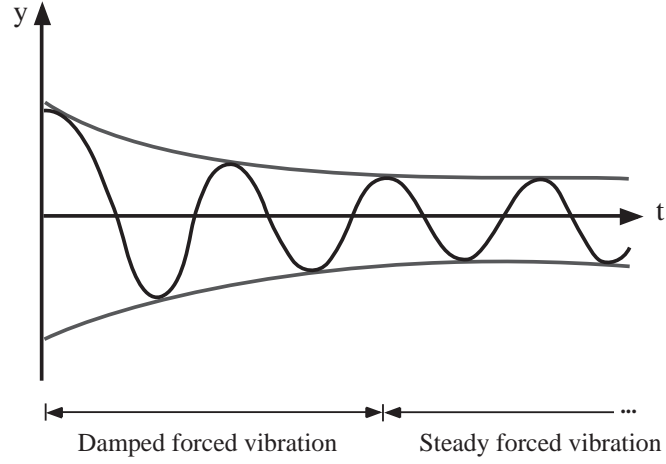


**Figure 2.16:** Forced vibrations with viscous damping.

The case when only the two last terms of the Eq. 2.43 affect the structure is known as steady forced vibrations. The solution will be then may written as

$$y = A \cos(\omega t - \phi) \quad (2.44)$$

where

$$A = \sqrt{C_1^2 + C_2^2} = \frac{F_0}{k} \left[ \frac{1}{\sqrt{\left(1 - \frac{\omega^2}{\omega_v^2}\right)^2 + \left(\frac{c}{m\omega_v}\right)^2 \left(\frac{\omega}{\omega_v}\right)^2}} \right] \quad (2.45)$$

and

$$\phi = \tan^{-1} \left( \frac{C_1}{C_2} \right) = \tan^{-1} \left[ \frac{\left(\frac{c}{m\omega_v}\right) \left(\frac{\omega}{\omega_v}\right)}{1 - \left(\frac{\omega}{\omega_v}\right)^2} \right] \quad (2.46)$$

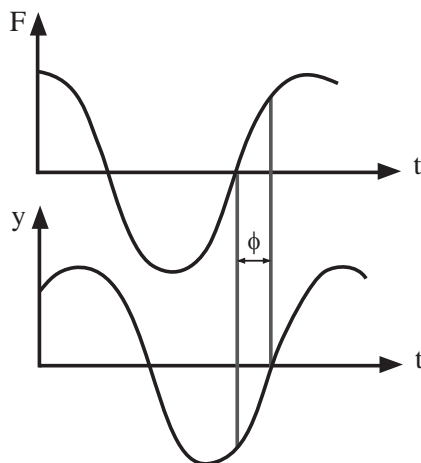


**Figure 2.17:** Phase delay ( $\phi$ ) illustration.

## 2.4.2 Damping

A vibrating structure has the ability to dissipate energy into heat or other type of energy. This ability is known as damping and its role in the flow induced vibrations is to limit the vibrations. There are three types of damping: the structural damping, the material damping and the fluid damping. Structural damping is generated by friction. Material damping is generated by the dissipation of internal energy inside the material. Fluid damping is generated by the dissipation of energy due to the fluid that moves along with the vibrating structure (hydrodynamic mass). Usually the most important types of energy dissipation are the structural and the fluid damping.

### 2.4.2.1 Structural damping

If a rigid cylinder is suspended with springs in still water and displaced from its equilibrium position and then released, the cylinder would start to oscillate. These oscillations will eventually disappear due to damping (structural plus fluid damping). To separate the structural damping the structure should be placed in vacuum. Only in this case the damping will be caused merely by the structural damping.

For the simplest case, consider a structure in vacuum with free vibrations and with no damping. The equation will be

$$m\ddot{y} + ky = 0 \quad (2.47)$$

and the solution will be written as

$$y = A_y \cos(\omega_v t) \quad (2.48)$$

where  $\omega_v = \sqrt{k/m}$ , will be the angular frequency of an undamped free vibrations system in vacuum.

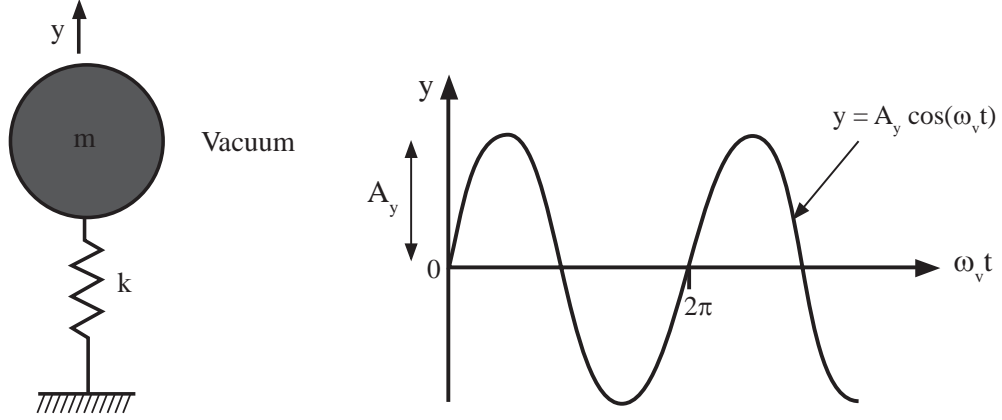


**Figure 2.18:** Free vibrations in vacuum without damping.

Now consider the last system with damping. Since the structure is placed in vacuum, the damping force will only correspond to the structural damping. The equation to solve will be

$$m\ddot{y} + c\dot{y} + ky = 0 \quad (2.49)$$

and its solution

$$y = A_y \exp\left(-\frac{c}{2m}t\right) \cos(\omega_{dv}t) \quad (2.50)$$

where  $\omega_{dv}$  corresponds to Eq. 2.42. For convenience, the damping coefficient may be written as

$$\zeta_s = \frac{c}{2m\omega_{dv}} \quad (2.51)$$

Eq. 2.51 is the definition of the structural damping factor. Re-writing the solution:

$$y = A_y \exp(-\zeta_s \omega_{dv} t) \cos(\omega_{dv} t) \quad (2.52)$$

in which

$$\omega_{dv} = \omega_v \sqrt{\frac{1}{1 + \zeta_s^2}} \quad (2.53)$$

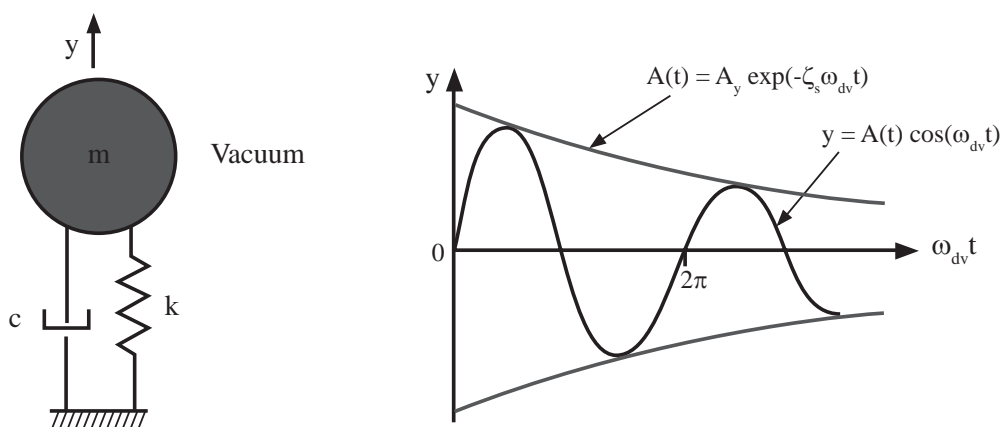


**Figure 2.19:** Free vibrations in vacuum with damping.

### 2.4.2.2 Fluid damping in still fluid

Finally, consider a damped and free vibrations system in otherwise still fluid. The difference with the last system is that the vibrations will decay faster in a fluid than in vacuum. This is due to the fluid damping is added to the structural damping.

When the cylinder is oscillating, the Morison force acts and the mass is no longer  $m$  but rather  $m + m'$ . An additional hydrodynamic resistance force is present, which can be observed as an increment in the total damping.

The equation for this case will be

$$(m + m')\ddot{y} + c\dot{y} + \frac{1}{2}\rho C_D D |\dot{y}| \dot{y} + ky = 0 \quad (2.54)$$

and its solution will be written as

$$y = A_y \exp(-\zeta \omega_d t) \cos(\omega_d t) \quad (2.55)$$

where the angular frequency,  $\omega_d$ , is given by

$$\omega_d = \omega_n \sqrt{1 - \zeta^2} \tag{2.56}$$

reminding that

$$\omega_n = \sqrt{\frac{k}{m + m'}} \tag{2.57}$$

and  $\zeta$  is the total damping (considering both structural and fluid damping)

$$\zeta = \zeta_s + \zeta_f \tag{2.58}$$

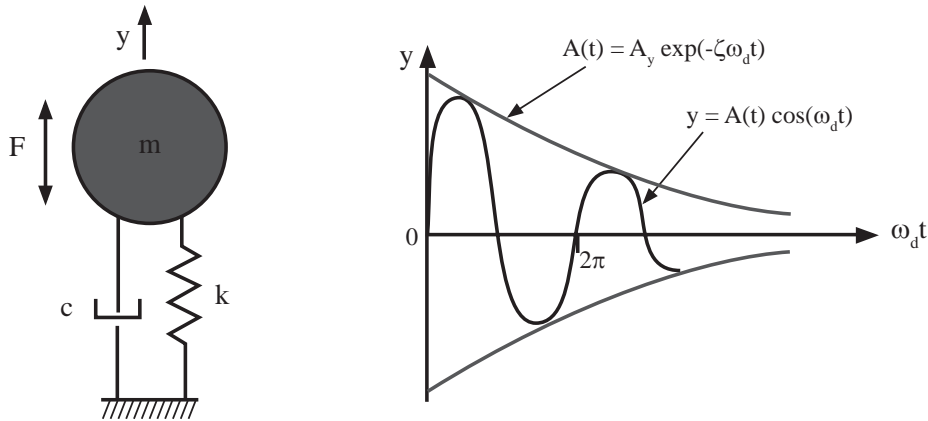


**Figure 2.20:** Free vibrations in still fluid with damping.

### 2.4.2.3 Measurement of damping

Testing is the ‘easiest’ way to determine the damping of a system. This is usually done in air and/or in water. One of the main techniques used for measuring of damping is the free decay. It consists in apply a known excitation to the structure (move the system from its equilibrium point), record the response of the structure and find the damping by matching the theoretically predicted response with the recorded results.



If  $y_n$  and  $y_{n+1}$  were two consecutive amplitudes recorded in the experiment (see Fig. 2.21), the ratio of both will be

$$\frac{y_n}{y_{n+1}} = \frac{A_y \exp(-\zeta\omega_d t)}{A_y \exp(-\zeta\omega_d (t + T))} = \exp(\zeta\omega_d T) \quad (2.59)$$

in which  $T$  is the period of the vibration

$$T = \frac{2\pi}{\omega_d} \quad (2.60)$$

From the Eq. 2.59,  $\zeta$  is obtained as:

$$\zeta = \frac{1}{2\pi} \ln \left( \frac{y_n}{y_{n+1}} \right) \quad (2.61)$$

The quantity  $\delta = \ln(y_n/y_{n+1})$  is known as logarithmic decrement, so the damping may be written as  $\zeta = \delta/(2\pi)$ .

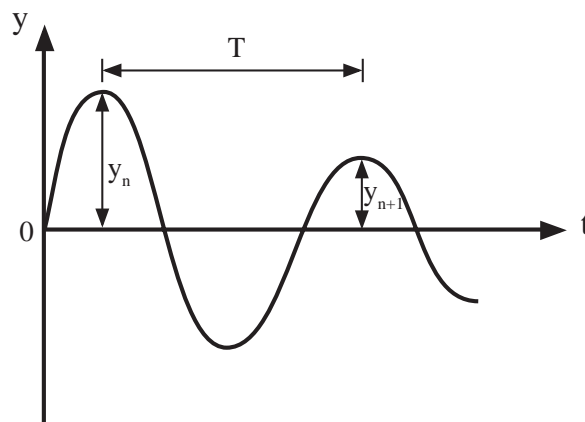


**Figure 2.21:** Recorded response of the structure in a free decay experiment.

### 2.4.3 Cross-flow vortex-induced vibrations

As mentioned before, for  $Re > 40$  a cylinder in a steady current will experience vortex shedding. Due to the vortex shedding, the lift and drag forces will oscillate. Now considering a flexibly-mounted cylinder, these forces may induce vibrations of

the cylinder. The lift force causes cross-flow vibrations and the drag produces in-line vibrations (see Fig. 2.22).

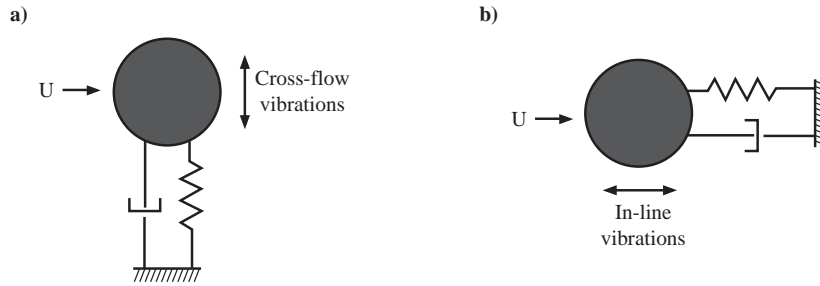


**Figure 2.22:** Different type of oscillations.

In 1968, Feng carried out an experiment where a circular cylinder with one degree of freedom were exposed to air flow. He noticed that at a certain air velocity, the cylinder experienced small vibrations. At that point the natural frequency and the vibration frequency of the system coincided. He also noted that before that particular point, the vortex-shedding frequency were identical to the stationary-cylinder frequency. However after that point the vortex shedding frequency ( $f_v$ ), the vibration frequency ( $f$ ) and the natural frequency ( $f_n$ ) of the system were the same despite the air velocity. This phenomenon was known as ‘lock-in’, ‘synchronization’, ‘resonance’, among others. As a note, recent studies have proven that this phenomenon is shown even when the frequencies are not equals, synchronization can be achieved at hundreds of times the natural frequency.

It can be concluded that at that specific point, the lift force and the movement of the cylinder occur at the same frequency and therefore the amplitude of the cylinder oscillations will be large (which in fact happens). When the air flow velocity overpassed some value Feng noticed that the shedding frequency unlocked from the natural frequency and jumped to follow the stationary-cylinder frequency again; that means that the large amplitudes stopped.

For small vibrations in still fluid,  $A/D < 0.8$ ,  $C_m$  is close to 1. When the cylinder is subject to a current the value of  $C_m$  will be different (see Fig. 2.23). In fact the new hydrodynamic mass coefficient will be denoted as  $C_{mc}$ , therefore the hydrodynamic mass will be defined as

$$m'_c = \rho C_{mc} \frac{\pi D^2}{4} \quad (2.62)$$

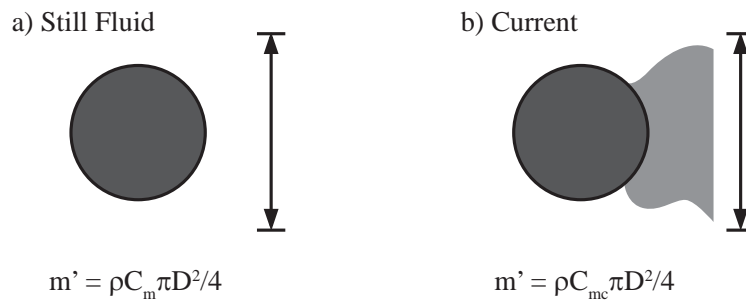


**Figure 2.23:** Hydrodynamic mass in still fluid and in current.

$C_{mc}$  values have been measured by Sarpkaya (1978) for a circular cylinder subject to a steady current and oscillating in the cross-flow direction (forced oscillations), see Fig. 2.24. These results will be used in sec. 4.2.2 for comparison with the ones obtained in this work.

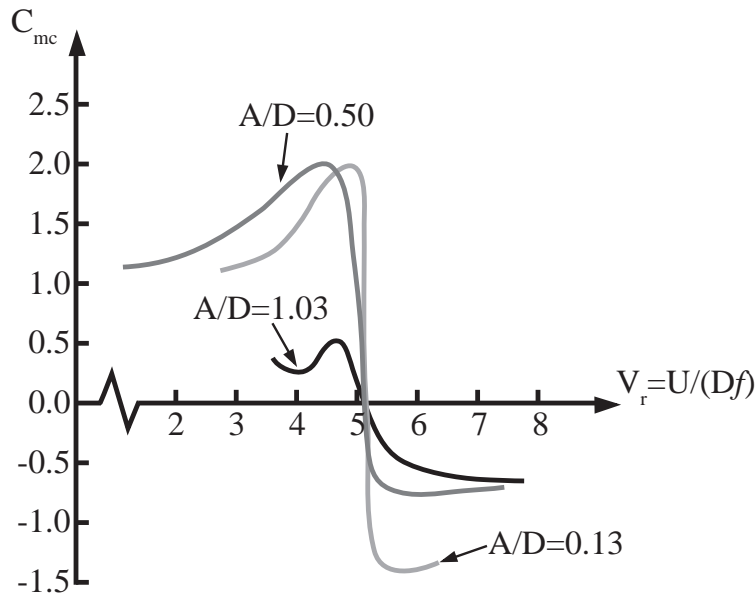


**Figure 2.24:** Sketch of the hydrodynamic mass coefficient for a circular cylinder vibrating in the cross-flow direction (forced oscillations) and subject to a current.  $V_r$  is the reduced velocity, where  $U$  is the velocity of the main flow,  $D$  is the diameter of the cylinder and  $f$  is the frequency of the forced vibrations. Based on Sarpkaya (1978)



# 3 Dynamic and hydrodynamic analysis of a circular cylinder in Vortex-Induced Vibration

In this chapter the experimental setup is explained. With the experimental apparatus, the dynamic response in free vibration is processed in order to get the parameters for the discretized model. Knowing the coefficients  $m$  (total mass of the system),  $c$  (structural damping), and  $k$  (spring constant) and the dynamic response, useful data are calculated along the synchronization regime. Some of these important data are: maximum amplitude in the cross-flow direction, frequency of the cylinder, phase angles  $\phi_{total}$  and  $\phi_{vortex}$ , and added mass. Besides that, at the end of the chapter, the hydrodynamic response is shown in the three different branches of the lock-in region.

## 3.1 Experimental setup

In order to study the VIV phenomenon, an experimental apparatus was built. The complete model scheme is shown in Fig. 3.1. The experimental apparatus consists of a metallic solid circular cylinder. Its diameter is about 2.4 millimeters and its height is 400 millimeters, so the entire synchronization regime can be studied. The cylinder is fixed to an acrylic plate of 9 millimeters thickness, which is beveled in the inlet region to avoid unwanted disturbances to the main flow.

An external lighting was used so the high-speed video camera could record the tip of the cylinder. The lighting consisted of two 180-lumen rechargeable LED lanterns. The lanterns were facing each other, both pointing to the tip of the cylinder.

The high-speed video camera used to record the cylinder was an “Edgertronic®”. It is engineered with a specialized  $1280 \times 1024$  CMOS Image Sensor, ultra high-speed electronics, memory, and image processing electronics. This camera allows up to 17,791 fps at  $192 \times 96$  pixels resolution.

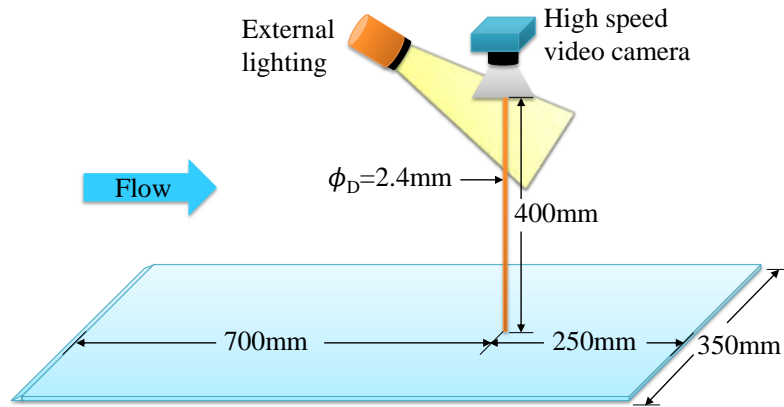


**Figure 3.1:** Experimental model scheme.

## 3.2 Testing materials

In order to find the best material to perform the experiments, several different materials were tested: stainless steel, silver steel, aluminum, bronze and iron. Two distinct tests were developed:

1. The experimental apparatus is placed on a flat surface having still *air* as surrounding fluid. Then a small impulse perturbation is given to the metallic cylinder and the response is recorded at 240 frames per second (fps).
2. The experimental apparatus is placed on a flat surface having still *water* as surrounding fluid. Then a small impulse perturbation is given to the metallic cylinder and the response is recorded at 240 fps.

Then the images were processed using Matlab® R2011a to obtain the path and the frequency of the tip of the cylinder. To achieve this, a special code was developed using the Particle Tracking Velocimetry (PTV) technique.

The PTV technique consists of giving a template figure of the region of interest (in this case the tip of the cylinder, see Fig. 3.2). The code computes the  $(x, y)$  location coordinates of the best match between the obtained images and the template image. This allows to get the path of the cylinder over time in both axes separately.

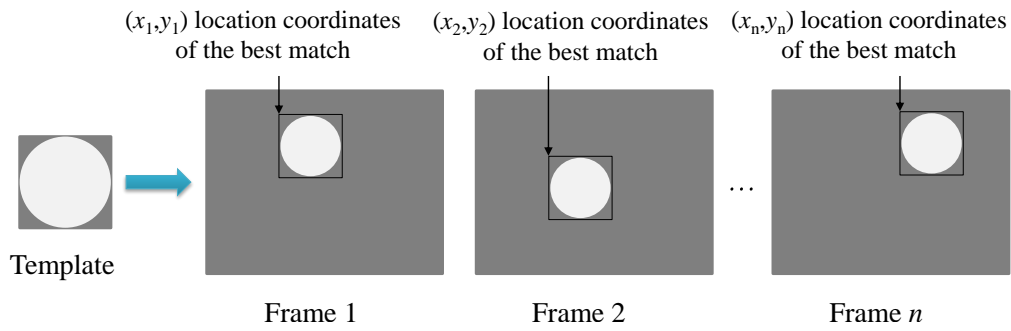


**Figure 3.2:** PTV technique in the tip of the cylinder.

The path can be processed by the discrete Fourier transform. The Fourier analysis converts time into frequency by decomposing a sequence of values into components of different frequencies. By doing this, the natural frequency of the system can be known. In Tab. 3.1 the different paths and their respective frequency histograms in air are shown. Tab. 3.2 presents the corresponding results in water.

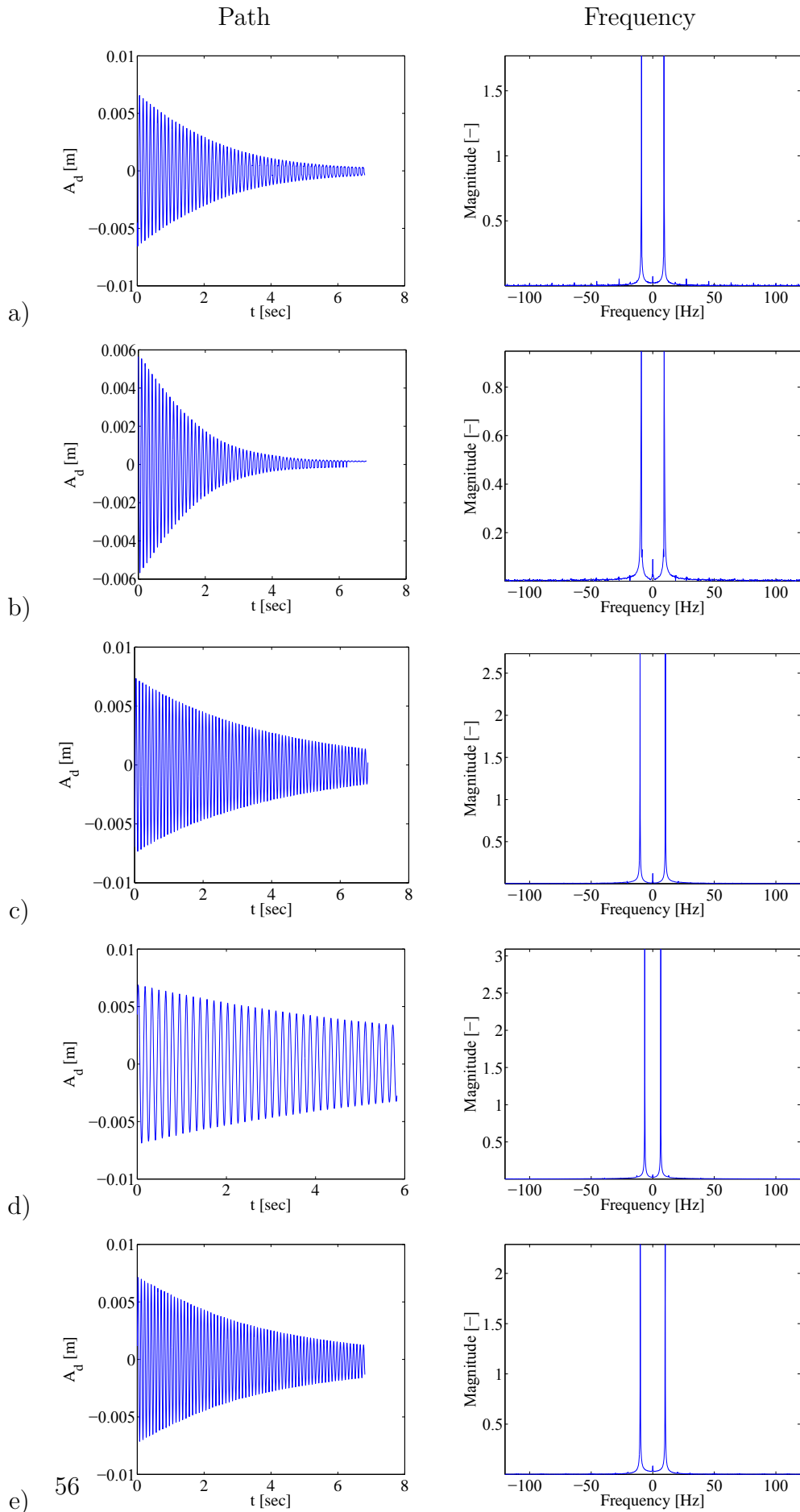


**Table 3.1:** Impulse response of the different materials in still air. a)Stainless steel, b)Silver steel, c)Aluminum, d)Bronze, and e)Iron



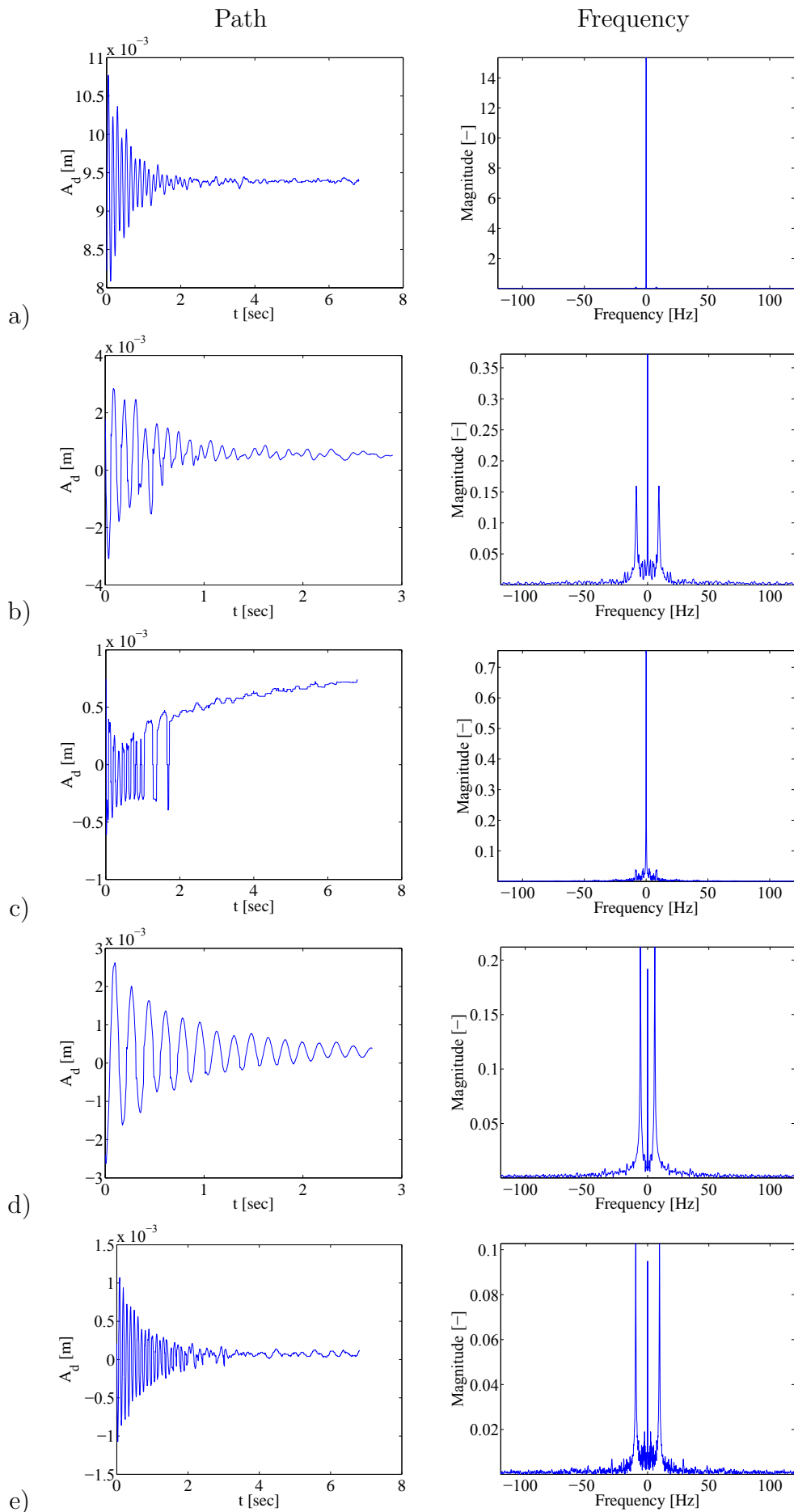


**Table 3.2:** Impulse response of the different materials in still water. a)Stainless steel, b)Silver steel, c)Aluminum, d)Bronze, and e)Iron

The aim of these experiments was to find the material with the biggest change in the frequency,  $\Delta f = f_{air} - f_{water}$ , and a regular behavior in the dynamic response. With these two characteristics in mind it was decided to use bronze,  $\Delta f \approx 0.5$ , as the only test material hereinafter. This specific cylinder had a diameter of 2.391mm.

### 3.3 Obtaining parameters

#### 3.3.1 Stiffness of the cylinder ( $k$ )

Once the cylinder was chosen, the specific mass, spring and damper coefficients need to be determined. The first step was to find the stiffness ( $k$ ). In order to accomplish this, a picture of the top view of the cylinder in the equilibrium position was taken. Then using a set of weights and pulleys, a known perpendicular force was applied (Fig. 3.3), and a picture with the same camera position was taken. This procedure was repeated with several weights to obtain different measurements, so they can be compared. With the acquired photos, the displacement of the center of the cylinder relative to the equilibrium point was calculated (Fig. 3.4). Finally Eq. 3.1 was used:

$$k = \frac{F}{x} \tag{3.1}$$

where  $F$  represents the known force applied to the cylinder and  $x$  is the displacement of the center of the cylinder.

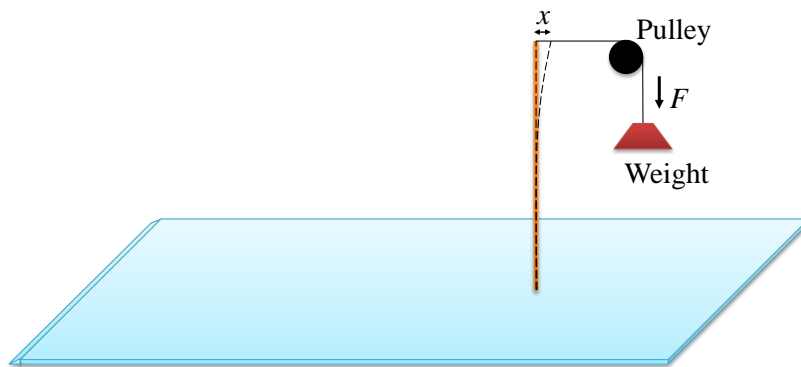


**Figure 3.3:** Schematic diagram: experimental procedure for the estimation of stiffness of the cylinder.

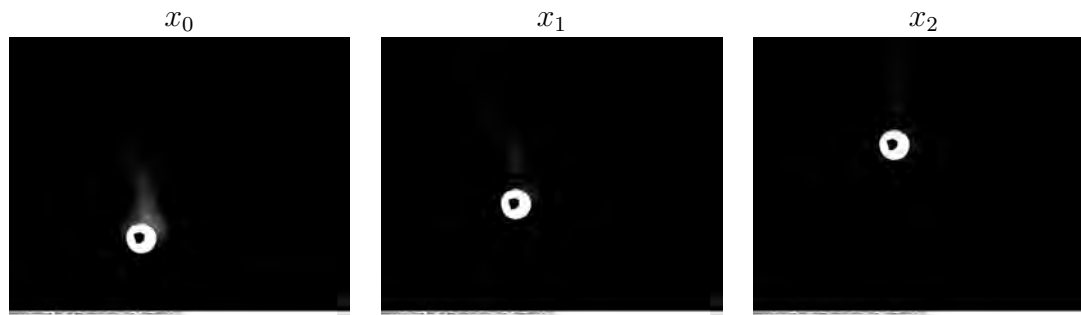


**Figure 3.4:** Actual photos of the stiffness experiment. a) equilibrium position, b) displacement  $x_1$  with a force applied  $F_1$ , c) displacement  $x_2$  with a force applied  $F_2$ .

### 3.3.2 Free vibration with viscous damping ( $\zeta$ )

The next step was to find the damping of the cylinder. To achieve this, the experimental apparatus was subjected to a small impulse perturbation and the dynamic response was recorded. These images were processed using the PTV technique, see Fig. 3.5. The recorded answer was adjusted to the mathematical model:

$$y(t) = A_0 \exp(-\zeta\omega_d t) \sin(\omega_d t + \varphi) \quad (3.2)$$

where  $A_0$  is the maximum amplitude,  $\omega_d$  is the damped angular frequency, and  $\varphi$  is the phase that determines the behavior needed to match the initial conditions. Here the damping ratio,  $\zeta$ , consists of the structural damping,  $\zeta_s$ , and the damping due to the surrounding fluid,  $\zeta_f$ . For detailed information about the solutions to vibration equation, and structural and fluid damping see sec. 2.4.

$$\zeta = \zeta_s + \zeta_f = \frac{1}{2\pi} \ln \left( \frac{y_n}{y_{n+1}} \right) \quad (3.3)$$

**Free vibration with air as surrounding fluid** In this case, the assumption that the response in air is practically equal to the response in vacuum was made. This means that the damping ratio corresponds only to the structure damping, namely  $\zeta = \zeta_s$ . Using the response in air to fit Eq. 3.2, the coefficients  $\zeta$  and  $\omega_d$  were known. And with Eq. 3.4 the value of  $\omega_n$  was calculated.

$$\omega_d = \omega_n \sqrt{\frac{1}{1 + \zeta^2}} \quad (3.4)$$

Knowing  $\omega_n$  and using Eq. 3.5, the value of  $m$  was known. Here  $m$  represents the equivalent mass coefficient needed for the discretized model, see Fig. 3.6a.

$$\omega_n = \sqrt{\frac{k}{m}} \tag{3.5}$$

Strictly speaking, Eq. 3.5 should have not only  $m$  but  $m + m'$  in the right hand of the equation. However, the assumption that the response in air is practically equal to the response in vacuum allows to neglect the hydrodynamic mass,  $m'$  (see sec. 2.3.1.1 for detailed information about  $m'$ ).

Finally, the only unknown parameter was the viscous damping coefficient,  $c$ . Using Eq. 3.6, this last parameter could be calculated.

$$\omega_d = \sqrt{\frac{k}{m} - \left(\frac{c}{2m}\right)^2} \tag{3.6}$$

*It is important to highlight that all three parameters ( $m$ ,  $c$  and  $k$ ) calculated here are assumed to be calculated in vacuum, and their values will be used on the discretized model.*

**Free vibration with water as surrounding fluid** As can be seen from Fig. 3.5, the response in water is different from the response in air. In water, the frequency is lower and the damping of oscillations is bigger. This is because here the damping ratio,  $\zeta$ , corresponds to both structural and fluid damping, namely  $\zeta = \zeta_s + \zeta_f$ . The viscosity of water is bigger than air viscosity, and this leads to an increased energy dissipation. In this case the value of  $\zeta_f$  is so big that it dominates the total damping,  $\zeta$ .

The same method to know the parameters used in free vibration with air as surrounding fluid was applied. Using Eq. 3.2 to fit the response in water, the coefficients  $\zeta$  and  $\omega_d$  were known; and using Eq. 3.4 the value of  $\omega_n$  was calculated.

Then in order to calculate the mass coefficient, Eq. 3.5 becomes

$$\omega_n = \sqrt{\frac{k}{m + m'}} \tag{3.7}$$

Here the mass involves not only the mass due to the structure,  $m$ , but also the hydrodynamic mass,  $m'$ , which is the mass of fluid accompanying the displacement

of the cylinder due to the inherent viscosity of the fluid (see Fig. 3.6 b). From the free vibration with air as surrounding fluid, the value of  $m$  is known and  $m'$  can be calculated.

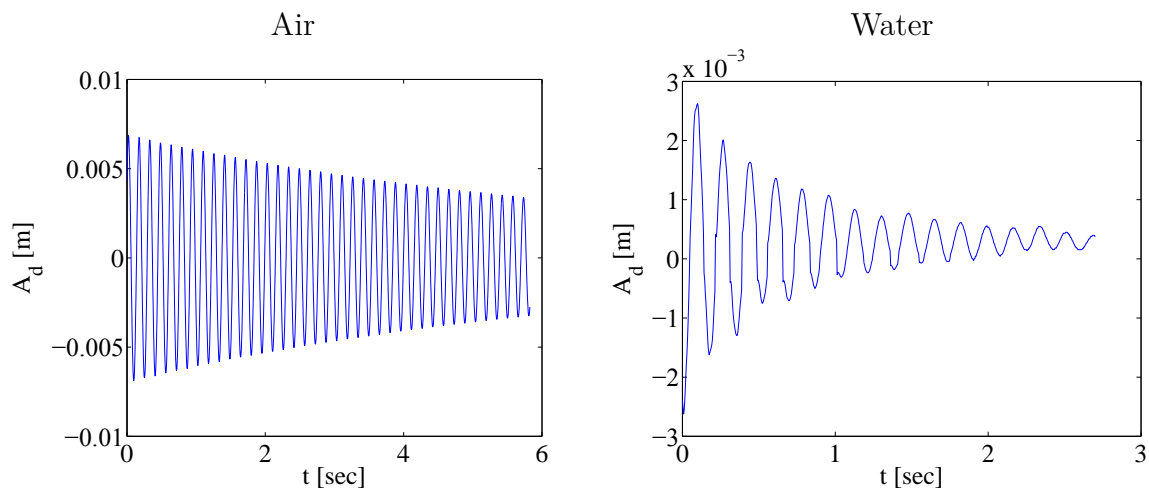


**Figure 3.5:** Response of the bronze cylinder in free vibration.

### 3.3.3 Discretized model: Results

The parameters obtained for the experimental model in free vibration with air as surrounding fluid are:

Parameter	Value
$m_{punctual}$	6.41 g
$c$	$6.51 \times 10^{-4}$ N·s/m
$k$	10.54 N/m

**Table 3.3:** Parameters obtained for the experimental model.<sup>(1)</sup>

(1) The parameters are calculated in air (considered like vacuum).

It is important to note that the ‘real’ mass of the cylinder, that is to say the mass obtained by weighing the metallic cylinder in a scale, is  $m_{scale} = 14.58$ g. That is more than twice as heavy as the equivalent mass coefficient,  $m_{punctual} = 6.41$ g.

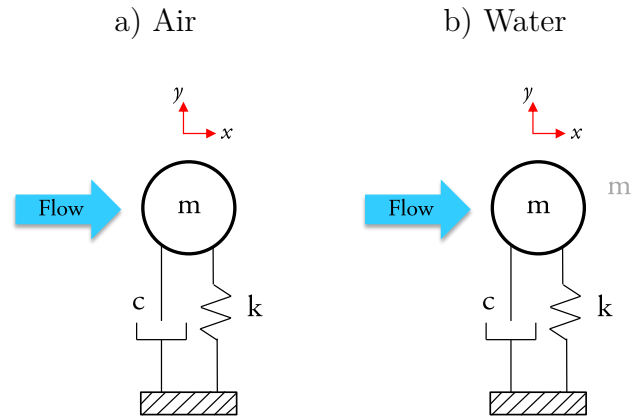


**Figure 3.6:** Discretized model. a) In air the equations only include the mass due to the structure, b) in water the equations include the mass due to the structure and the hydrodynamic mass.

### 3.4 Dynamic response

For tracking the tip of the cylinder in the synchronization regime, a water tunnel was used. The tunnel has a test section of  $0.381 \text{ m} \times 0.508 \text{ m} \times 1.5 \text{ m}$ . The operating velocity range varies between 0.01 and 0.3 m/s. Levels of turbulence in the test section are less than 1% RMS.

The experimental apparatus with the bronze cylinder was placed on the tunnel test section to get the dynamic response of the cylinder in the in-line direction (axis  $x$ ) and cross-flow direction (axis  $y$ ) to the flow at different Reynolds numbers,  $Re$ . The experiments cover the entire synchronization regime, with  $Re$  ranging from 97 to 320. A variable  $\Delta Re$  was used depending on the different branches (initial, upper or lower).

#### 3.4.1 Test 1

In this test, the most significant result was the maximum amplitude in the cross-flow direction against  $Re$ . This is illustrated in Fig. 3.7. These results are qualitatively similar to the data reported in Oviedo et al (2014), see Fig. 3.8.

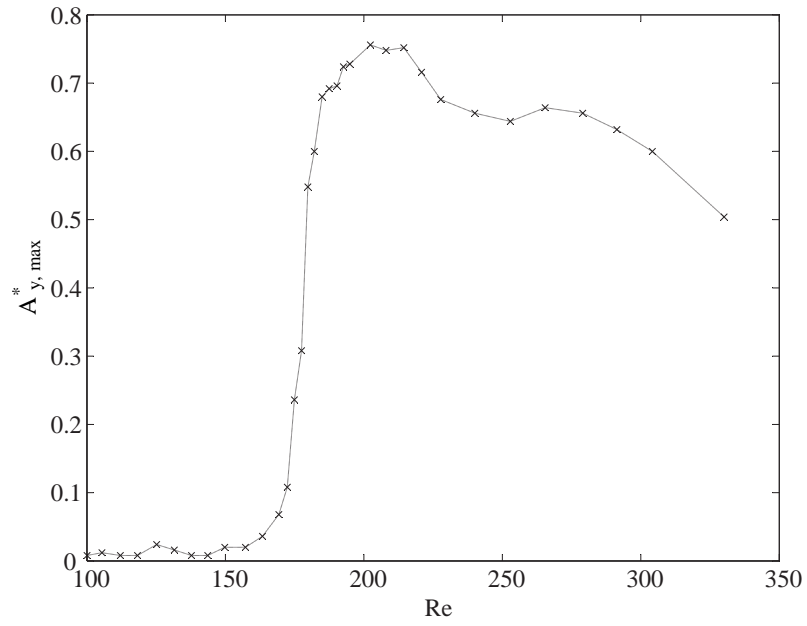


**Figure 3.7:** Maximum amplitude in the transverse direction vs Reynolds number.

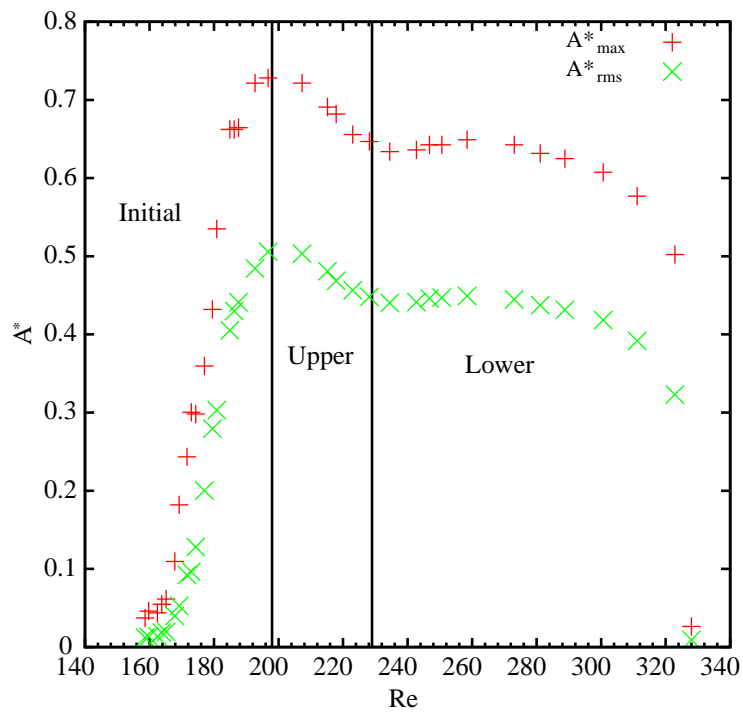


**Figure 3.8:** Maximum amplitude in the transverse direction vs Reynolds number from Oviedo et al. (2014).

### 3.4.2 Test 2

Once the Test 1 was finished, the methodology was polished and sought to shorten the Reynolds intervals in order to get more detailed data. Also, in Test 2, three repetitions were performed, results are shown in Fig. 3.9.

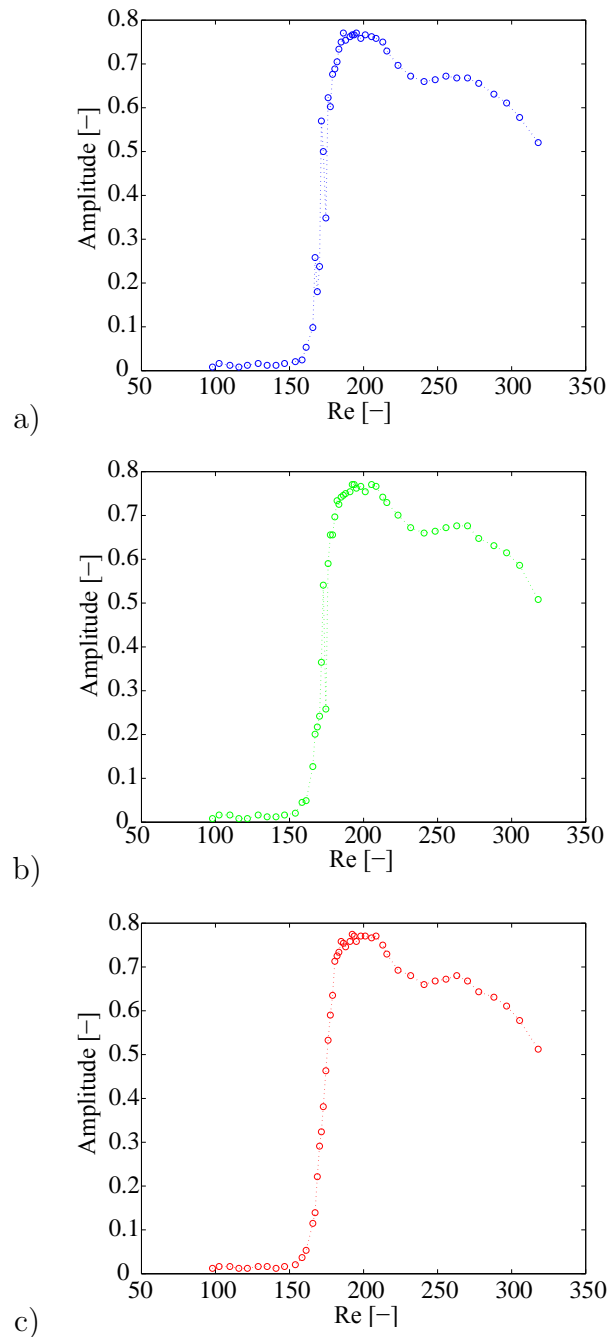


**Figure 3.9:** Maximum amplitude in the transverse direction vs Reynolds number.



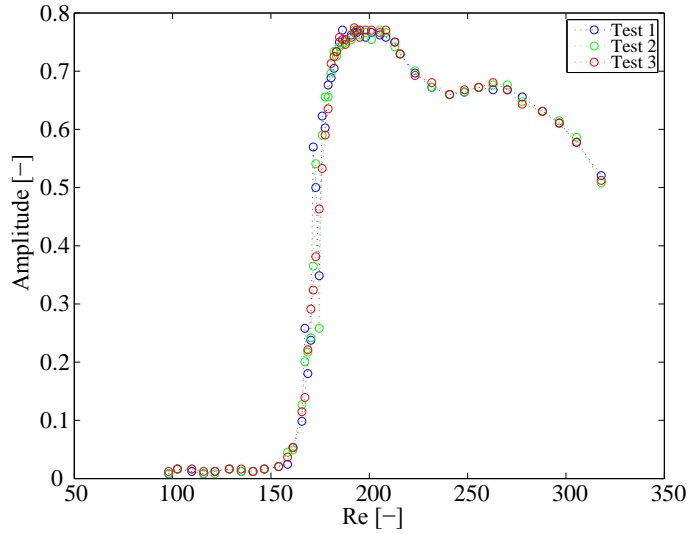


**Figure 3.10:** The three tests vs Reynolds number.

With the three replicates, the average maximum amplitude for each Reynolds number was obtained. Using these results the standard deviation were calculated and normalized according to the number of elements used in the sample (in this case 3). Finally, a chart of each data with their respective error line were plotted, see Fig. 3.11.

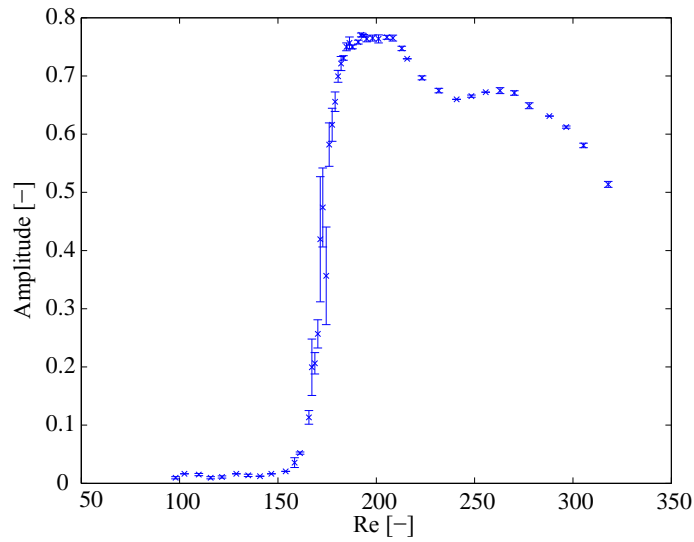


**Figure 3.11:** Error lines of the average maximum amplitude.

Fig. 3.12 represents an example of the behavior of the tip of the cylinder in the three different branches of the synchronization regime.

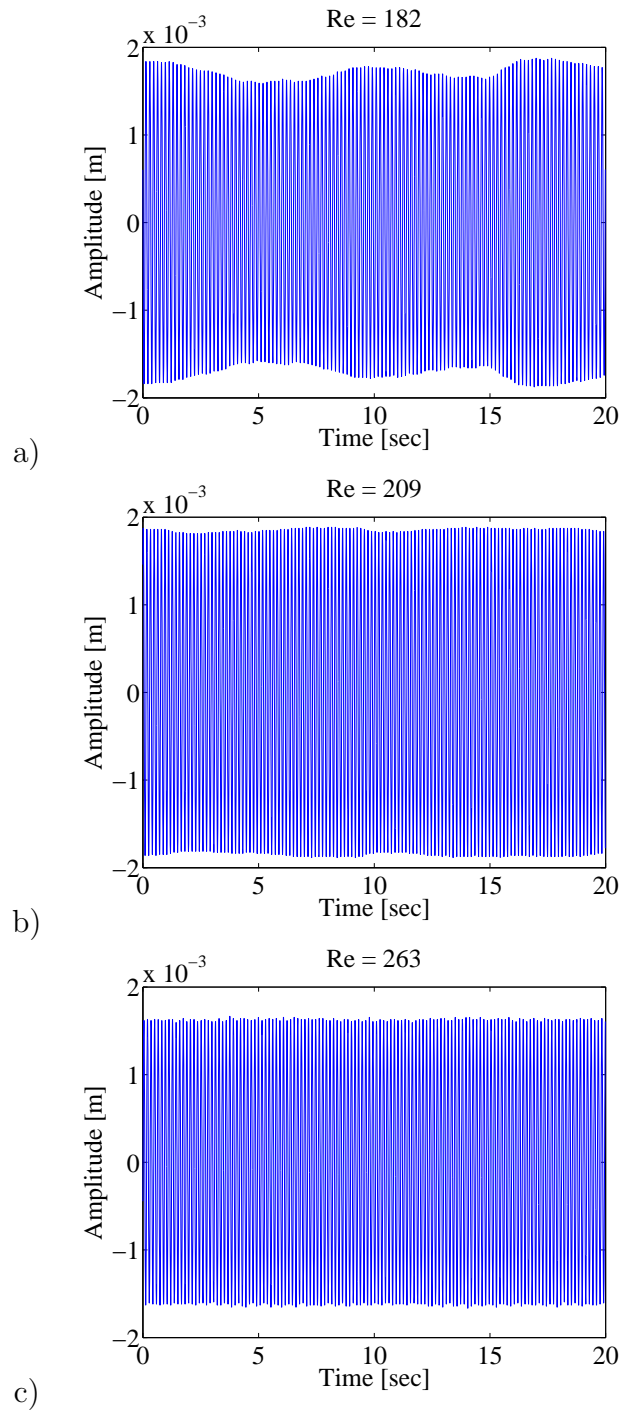


**Figure 3.12:** Path of the tip of the cylinder. a) initial @  $Re=182$ , b) upper @  $Re=209$  and c) lower @  $Re=263$ .

The results of tests 1 and 2 proved that the dynamic of the cylinder is consistent with that described in several scientific articles presented by Oviedo (2014) and Khalak & Williamson (1999). In Fig. 3.13, the left column the orbits of the free-end

of the cylinder are shown. In the right column the cylinder displacements over time are shown in both axes, blue line for the x axis and green line for the y axis. Both columns show the three branches of the lock-in region.

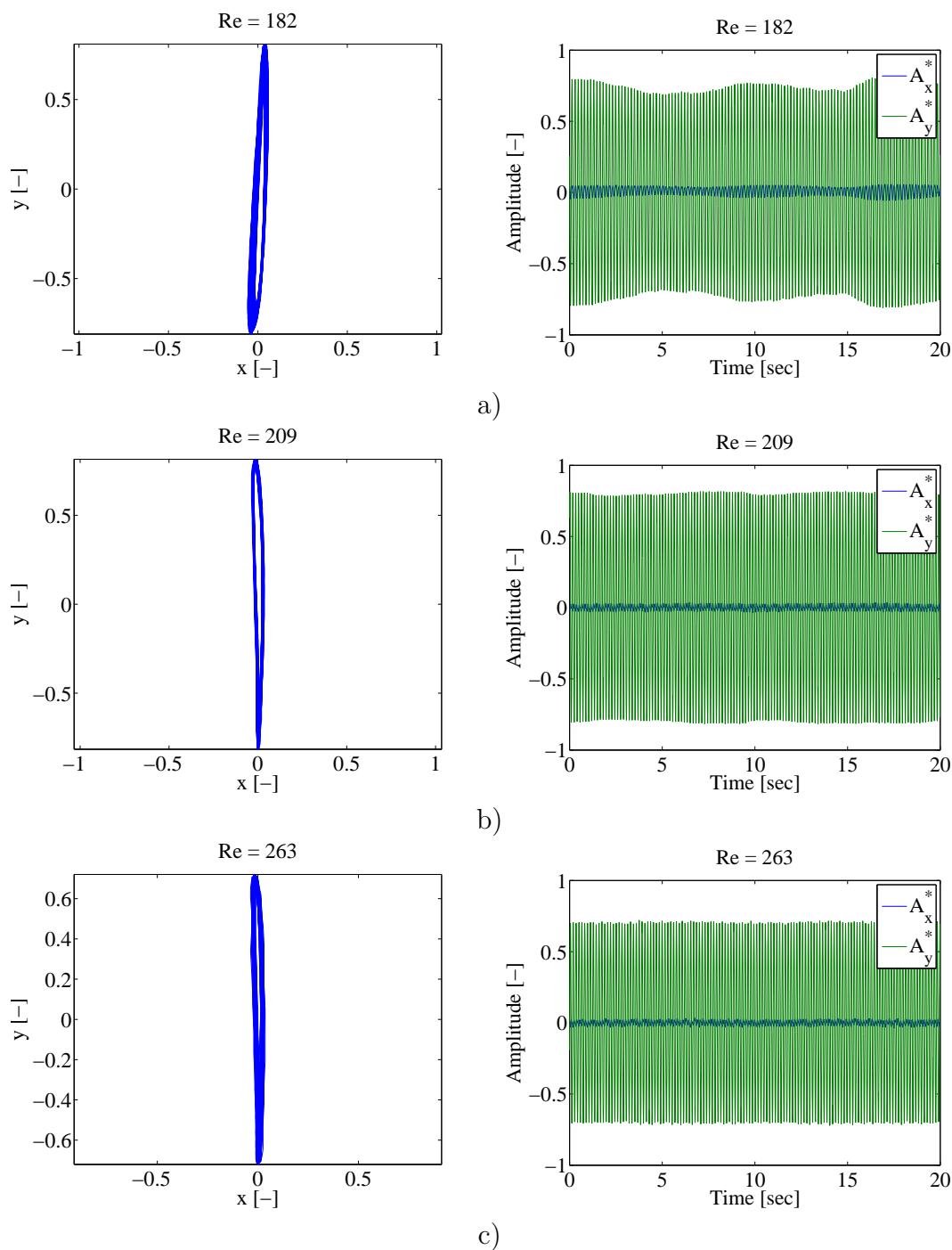


**Figure 3.13:** Orbits of the free-end of the cylinder and cylinder displacements over time in both axes. Both columns show the three branches of the lock-in region: a) initial @  $Re=182$ , b) upper @  $Re=209$  and c) lower @  $Re=263$ .

### 3.4.3 Results in the synchronization regime

To get the forces involved in the dynamic of the cylinder, the following equations were used (see sec. 1.2.2.2 for detailed information):

$$F_{total} = F_{vortex} - F_{inertial} \quad (3.8)$$

where:

$$F_{total} = F_t \sin(\omega t + \phi_{total}) = m\ddot{y} + c\dot{y} + ky \quad (3.9)$$

$$F_{vortex} = F_v \sin(\omega t + \phi_{vortex}) = (m + m')\ddot{y} + c\dot{y} + ky \quad (3.10)$$

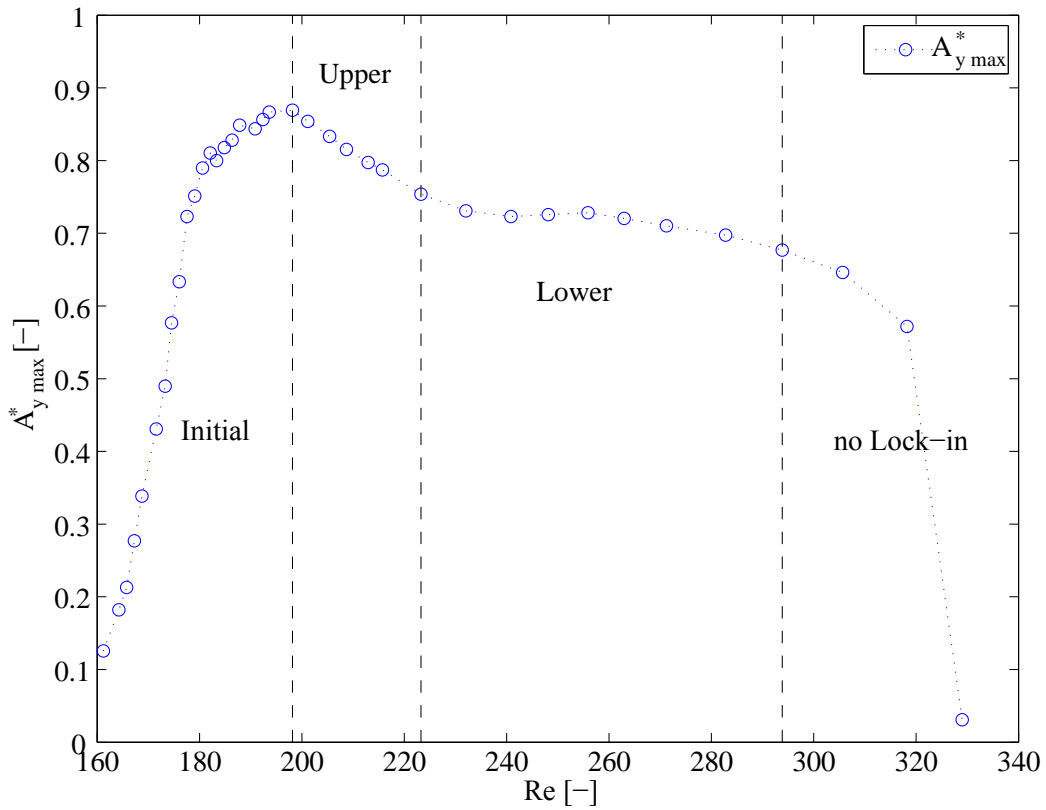


**Figure 3.14:** Maximum amplitude in the cross-flow direction vs Reynolds number.

In Fig. 3.14, the maximum amplitude in the cross-flow direction in the entire synchronization regime is shown. The initial branch begins when the cylinder starts vibrating and ends when the maximum amplitude is reached. At this same point the frequency of the cylinder is equal to the natural frequency in water (Fig. 3.15). Here the upper branch begins and ends when the frequency of the cylinder is equal to the natural frequency in the vacuum. From this point, and till the end of the synchronization regime, the frequency of the cylinder stays constant. This last branch is known as the lower branch. Henceforth a fast decay in the amplitude is observed. It is no longer the lock-in region and the frequency of the cylinder is no longer the frequency in vacuum.

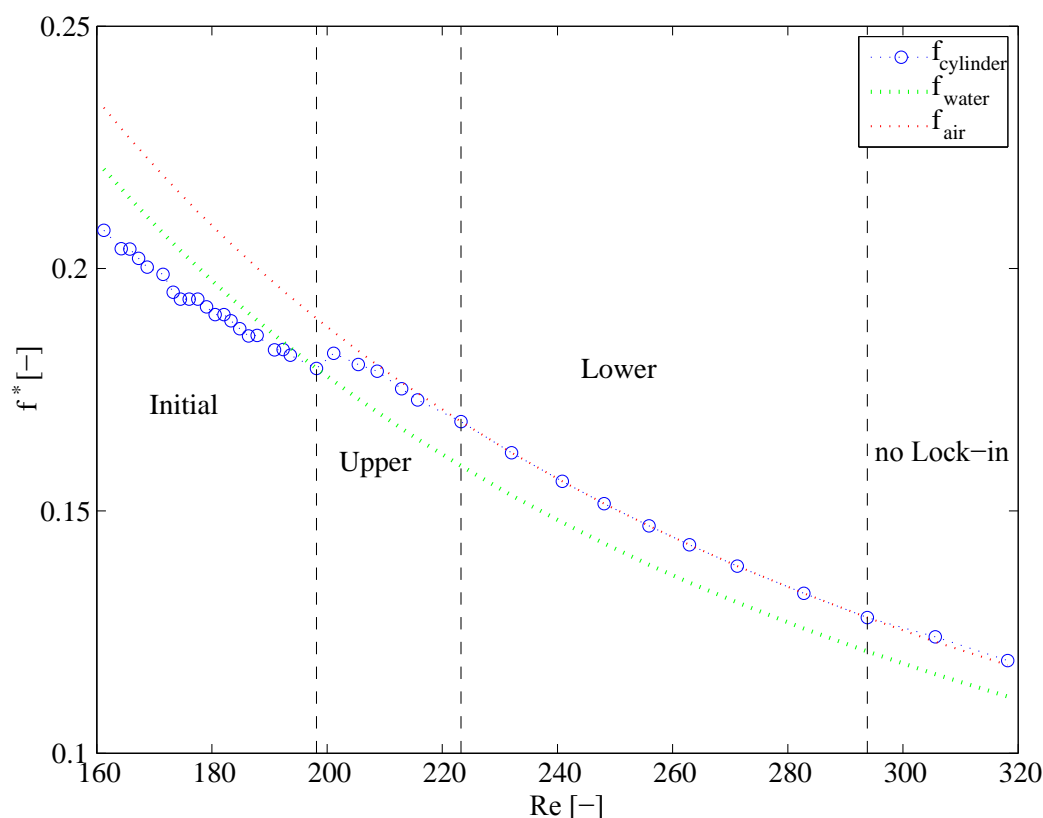


**Figure 3.15:** Frequency of the cylinder vs Reynolds number.

In Fig. 3.16, the total phase angle,  $\phi_{total}$ , in the entire synchronization regime is shown. In the initial branch  $\phi_{total}$  is practically zero, it corresponds to a perfect synchronization between the total fluid force,  $F_{total}$ , and the cylinder displacement,  $y$ . This coupling explains the fast increment in the cylinder amplitude. Throughout the cycle the fluid propels the cylinder, namely the fluid inserts energy on the cylinder. In the upper branch,  $\phi_{total}$  increase, that implies a loss of synchronization between the force and the displacement. This is reflected in the decrease of the amplitude

of the cylinder. In the lower branch,  $\phi_{total}$  jumps till reach practically 90 degrees. This implies that in half the cycle the fluid propels the cylinder and in the other half the fluid stops the cylinder. This behavior is consistent with the fact that the maximum amplitude remains relatively constant along the lower branch. Finally, out of the synchronization regime the  $\phi_{total}$  is equal to 180 degrees (see Fig. 3.18). In this case, the force of the fluid and the displacement of the cylinder are always in opposite directions. This explains the fast decline in the amplitude of the cylinder, the fluid is always stopping the movement of the cylinder.

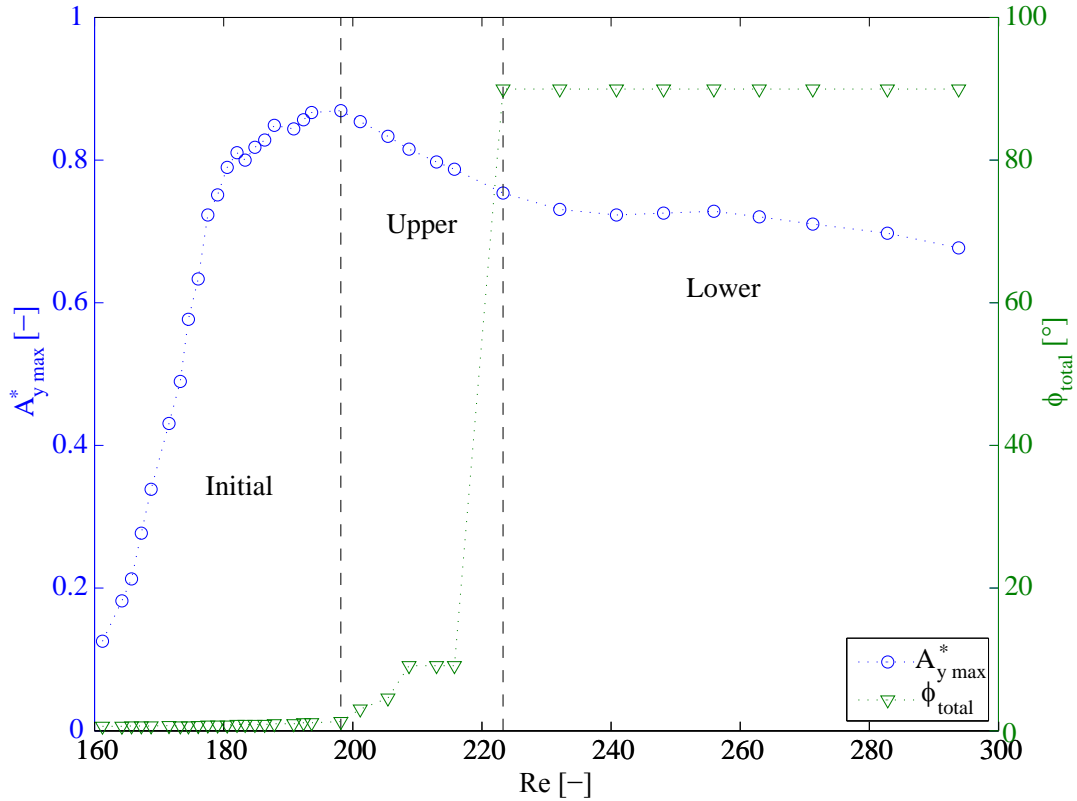


**Figure 3.16:** Maximum amplitude in the cross-flow direction and total phase angle vs Reynolds number.

Fig. 3.17 shows the behavior of the added mass in the synchronization regime. The added mass or hydrodynamic mass, as mentioned earlier, is the mass of the fluid accompanying the displacement of the cylinder due to the inherent viscosity of the fluid. The added mass reaches its maximum value at the beginning of the initial branch. From there the added mass has a lineal decay in its value until it arrives to the upper branch. In the upper branch, the behavior changes and the decay is exponential. Finally, the added mass reaches zero in the entire lower branch. This zero value is consistent with the fact that in this branch the frequency of the

cylinder is equal to the frequency in vacuum, and it means no friction between the environment and the moving bodies.

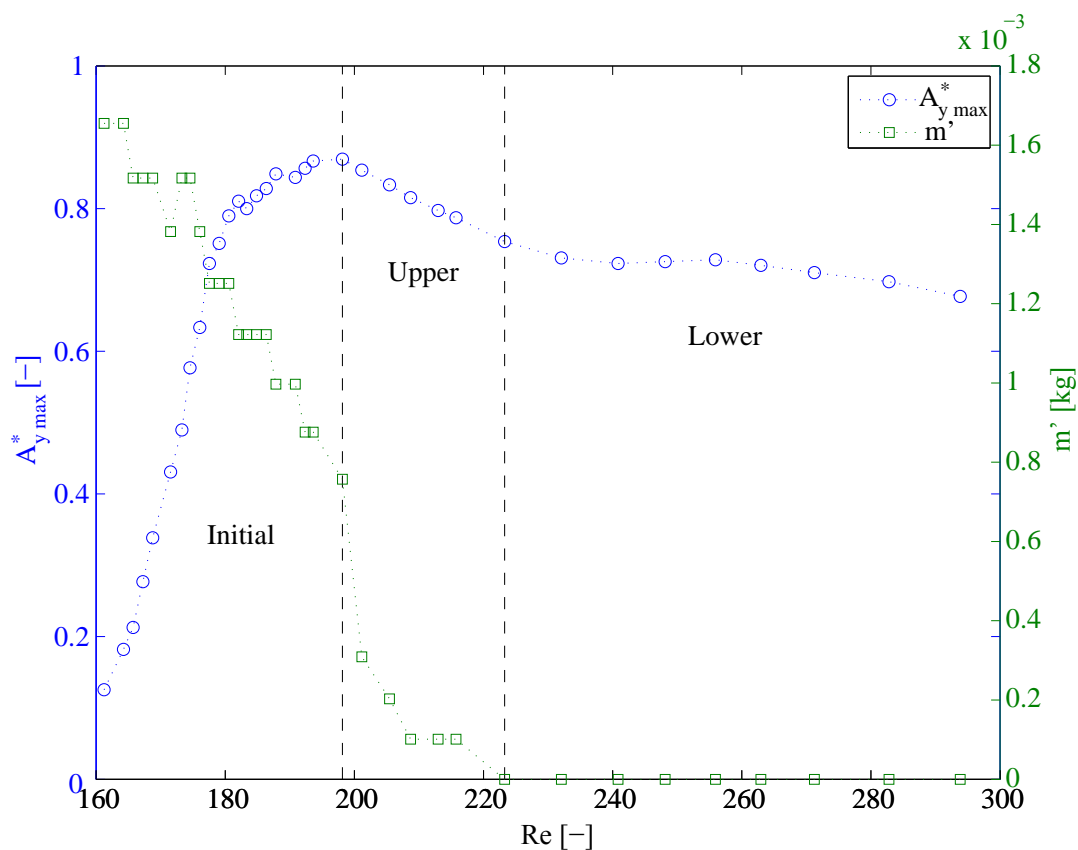


**Figure 3.17:** Maximum amplitude in the cross-flow direction and added mass vs Reynolds number.

Fig. 3.18 shows the phase angles  $\phi_{total}$  and  $\phi_{vortex}$ . The  $\phi_{vortex}$  is normally associated with the hydrodynamic response. In this case, it can be seen that the vortex phase angle is practically constant along the entire synchronization regime, which can be interpreted as having the same configuration in the hydrodynamic formed after the cylinder (see sec. 3.5.2).

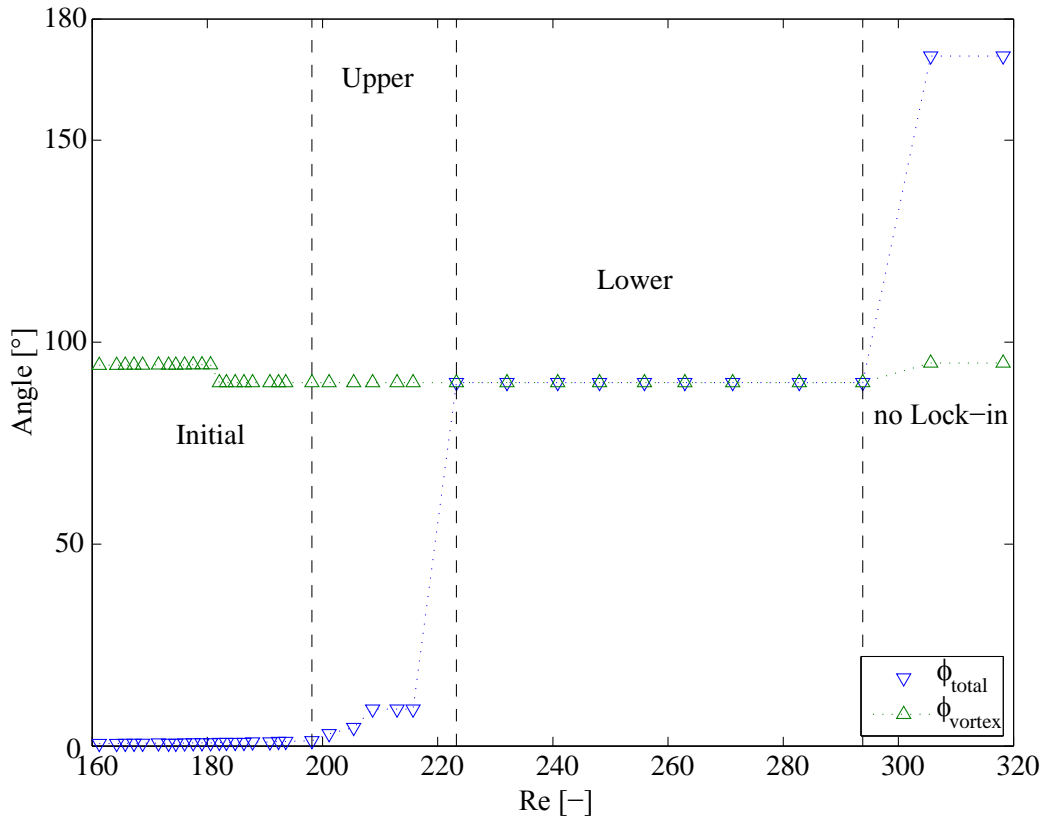


Figure 3.18: Phase angles vs Reynolds number.

## 3.5 Hydrodynamic response

### 3.5.1 Particle Image Velocimetry

In order to study the hydrodynamics around the circular cylinder, the Particle Image Velocimetry (PIV) technique was used. The scheme used to perform the experiments is shown in Fig. 3.19. For this technique the fluid was seeded with tracer particles. In this case, the particles were hollow glass spheres (about  $14\mu\text{m}$  of diameter), with the quality of being neutrally buoyant, which outer surface is coated silver to achieve optimal light reflection.

When the fluid is seeded correctly, a spatial plane is illuminated with a high-power laser. This allows the particles to shine and be visible for the camera.



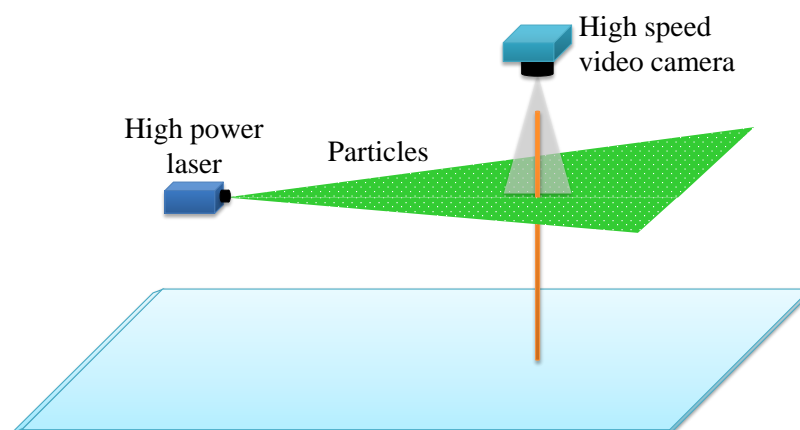


**Figure 3.19:** Experimental model with the laser.

The high-speed video camera used to record the cylinder was an “Edgetronic®”. The motion of the seeding particles was used to calculate speed and direction (the velocity field) of the flow being studied, see Fig. 3.20. In order to perform the PIV, the images were processed using the “PIVlab” software.

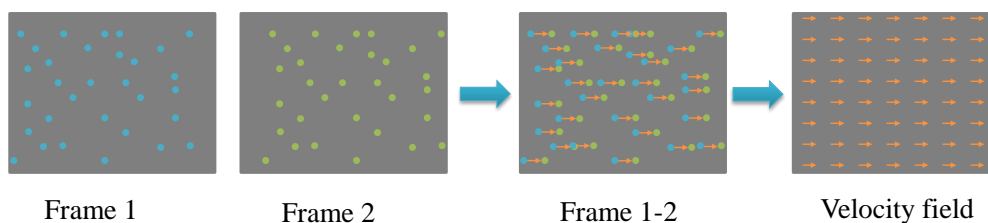


**Figure 3.20:** PIV technique.

### 3.5.2 Vortex shedding pattern

The hydrodynamic response is expected to be the same in the three branches. In this case, it can be observed that the hydrodynamic is 2S mode (two-pair of single vortex), as can be observed in Fig. 3.21. This means two pairs of vortices are shed per period, one vortex spins clockwise and the other spins counter-clockwise.

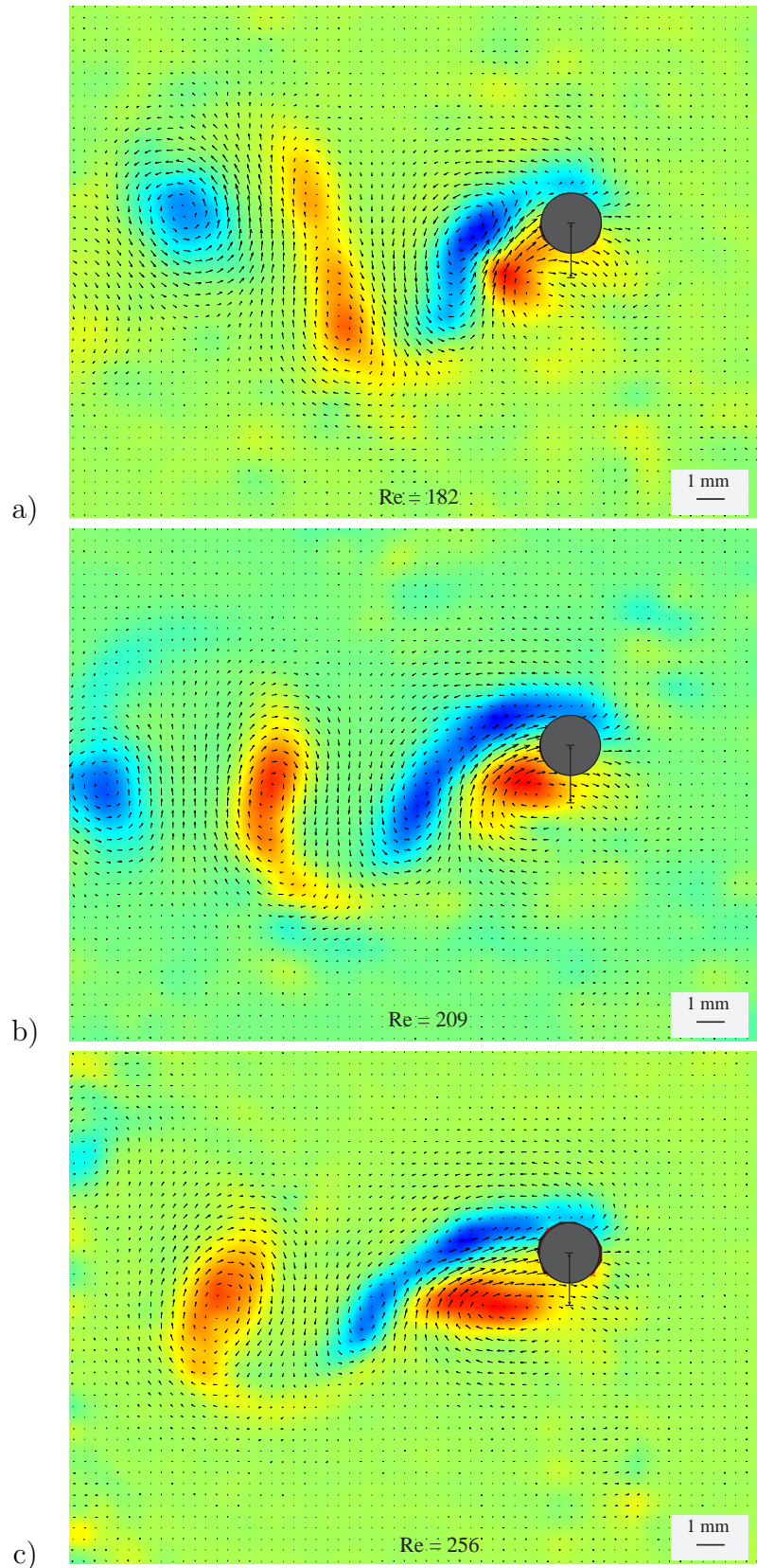


**Figure 3.21:** Vorticity in the three branches of the synchronization regime. All the images were taken when the cylinder was in its maximum amplitude. a) initial @  $Re=182$ , b) upper @  $Re=209$  and c) lower @  $Re=256$ .

It is important to notice that in all the experiments developed in this thesis, a 1millimeter Mitutoyo® calibration pattern was used. This pattern allows to calculate the uncertainty of the experiments, as well as having traceability and accurate values in the measurements and calculations.

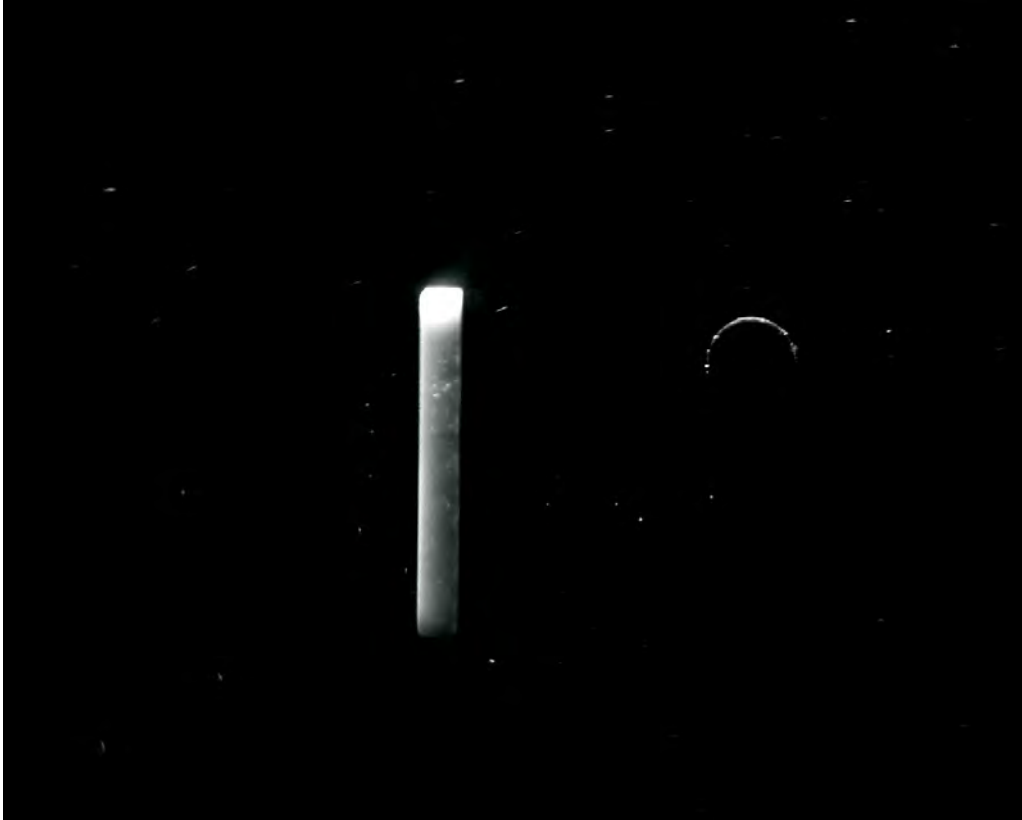


**Figure 3.22:** 1mm Mitutoyo® calibration pattern.



# 4 The usage of equivalent parameters and its implications

The first part of this chapter, shows the difference between using equivalent parameters (those used in a discretized model) and ‘real’ parameters (for example, the mass obtained by weighing the cylinder directly in a scale). The results shown are based on the same dynamic responses, the only change is the value of parameters. In the second part of the chapter, the results obtained in the present work and those available in literature are compared. Some differences, as well as resemblances, are compared and discussed, and an explanation is given for such results.

## 4.1 Equivalent parameters vs real parameters

As mentioned before, this thesis is an effort to propose a standard method to identify the parameters. sec. 3.3 presents a methodology to determine them:

1. Stiffness,  $k$ . Using a set of weights and pulleys to apply a known force on the free-end of the cylinder and calculating its displacement from the equilibrium point, the spring constant was known by Eq. 3.1,  $k = F/x$ .
2. Structural damping,  $\zeta_s$ , and damped angular frequency,  $\omega_d$ . The dynamic response of the cylinder in free vibration with air as surrounding fluid was recorded.
  - a) Eq. 3.3,  $\zeta_s = \ln(y_n/y_{n+1})/(2\pi)$ , was used to estimate the damping.
  - b) The dynamic response was adjusted to Eq. 3.2,  $y(t) = A_0 \exp(-\zeta\omega_d t) \sin(\omega_d t + \varphi)$ , from where it can be determined the damped angular frequency.
3. Natural angular frequency,  $\omega_n$ . Using Eq. 3.4,  $\omega_d = \omega_n/\sqrt{1 + \zeta^2}$ , the natural angular frequency was calculated.
4. Total mass of the cylinder (without added mass),  $m$ . Using Eq. 3.5,  $\omega_n = \sqrt{k/m}$  the value of the equivalent mass coefficient was obtained.
5. Viscous damping coefficient,  $c$ . Using Eq. 3.6,  $\omega_d = \sqrt{\frac{k}{m} - \left(\frac{c}{2m}\right)^2}$ , this last parameter was calculated.

These parameters are shown in Tab. 4.1.

On the other hand, the real parameters were obtained following the same methodology described previously for steps 1, 2. Then (step 3) the mass of the cylinder is measured using a weight scale. Finally, the viscous damping coefficient is calculated using 3.6. These parameters are shown in the right part of Tab. 4.1.

	Equivalent parameters	Real parameters
$m$	6.41 g	14.58 g
$c$	$6.51 \times 10^{-4}$ N·s/m	$1.47 \times 10^{-3}$ N·s/m
$k$	10.54 N/m	10.54 N/m

**Table 4.1:** Parameters obtained for the mathematical model.

#### 4.1.1 Phase angle ( $\phi_{total}$ )

As seen in sec. 3.4.3, the total phase angle depends on the parameters:  $F_{total} = F_t \sin(\omega t + \phi_{total}) = m\ddot{y} + c\dot{y} + ky$ . Fig. 4.1 shows  $\phi_{total}$ , blue circles for results using equivalent parameters and green squares for results using the real parameters. Blue line shows a variation in the phase angle consistent with the maximum amplitude of the cylinder, see Fig. 3.16. On the other hand, the green line shows no variation along the entire lock-in region,  $\phi_{total} \approx 360^\circ$ . This would mean that the total force is always synchronized with the displacement of the cylinder, and therefore the fluid gives energy into the cylinder permanently. If this would be the case, one might expect the amplitude of the cylinder to grow larger and larger across the three branches (initial, upper and lower), which in fact does not happen.

#### 4.1.2 Phase angle ( $\phi_{vortex}$ )

Similar to  $\phi_{total}$ , the vortex phase angle depends on the parameters:  $F_{vortex} = F_v \sin(\omega t + \phi_{vortex}) = (m + m')\ddot{y} + c\dot{y} + ky$ . And therefore one might expect  $\phi_{vortex}$  to vary from using equivalent or real parameters. Although Fig. 4.2 seems to indicate that there is a large jump in  $\phi_{vortex}$ , in fact this jump is from  $94^\circ$  to  $90^\circ$ , namely  $\phi_{vortex}$  changes only four degrees. As stated in sec. 3.4.3, this phase angle is normally associated with the hydrodynamic response. In both cases,  $\phi_{vortex}$  is practically constant along the entire synchronization regime, which can be interpreted as having the same configuration in the hydrodynamic response.

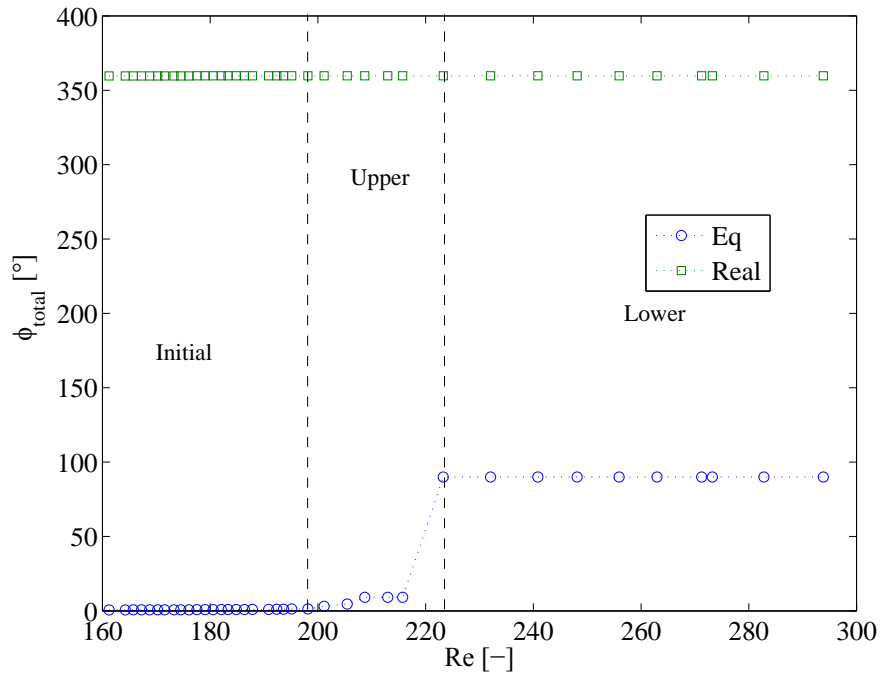


**Figure 4.1:** Comparison of  $\phi_{total}$  using equivalent and real parameters.

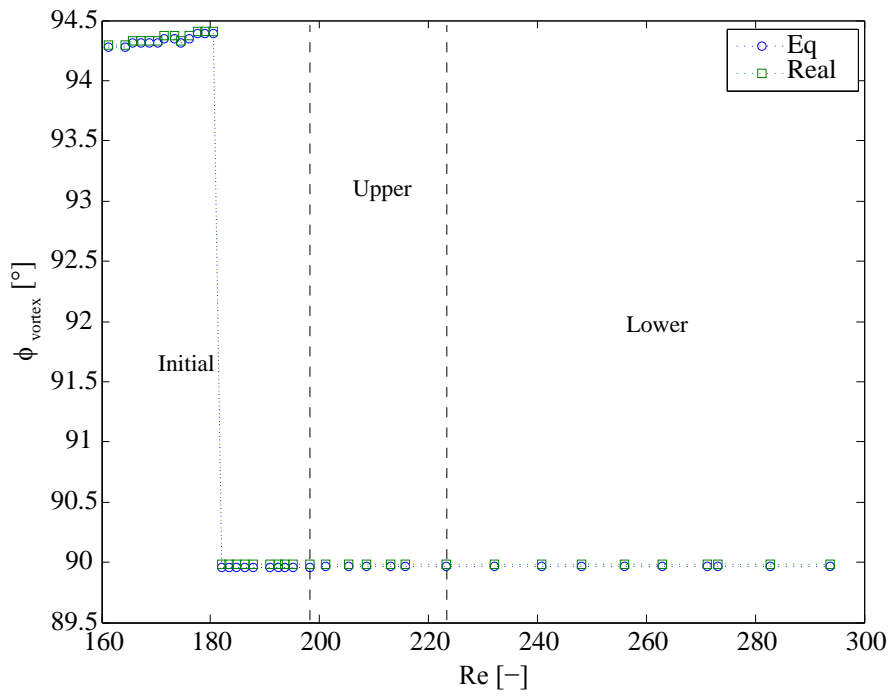


**Figure 4.2:** Comparison of  $\phi_{vortex}$  using equivalent and real parameters.

### 4.1.3 Added mass

As it can be noted in Fig. 4.3, the hydrodynamic (or added) mass shows the same behavior using equivalent or real parameters. The only difference is that data is moved vertically due to the difference between  $m_{punctual}$  and  $m_{scale}$ . As explained in sec. 3.4.3, for the blue line the zero value in the lower branch is consistent with the fact that in this branch the frequency of the cylinder is equal to the frequency in vacuum. This means that there is no friction between the environment and the moving bodies, and therefore no hydrodynamic mass exists in such circumstances. On the other hand, green line, there is no satisfactory explanation for negative mass values. Mass should never be negative because it represents the quantity of matter in a body.

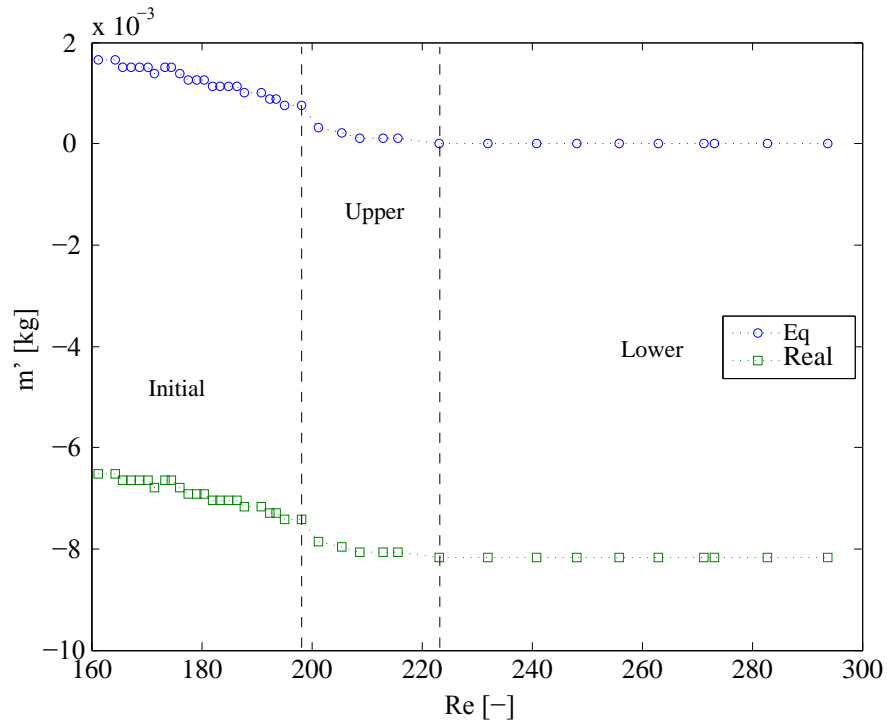


Figure 4.3: Comparison of  $m'$  using equivalent and real parameters.

## 4.2 Comparing actual results with literature

### 4.2.1 Phase angle

Govardhan & Williamson (2000) concluded that "there are two distinctly different jumps between modes. In essence, the mode change initial  $\rightarrow$  upper is associated with a jump in vortex phase  $\phi_{vortex}$ . This is associated with a jump between 2S and



2P vortex wake modes (as defined in Williamson & Roshko 1988). The second mode change upper→lower corresponds with a jump in total phase  $\phi_{total}$ , see Fig. 4.4. In both cases, the jump is calculated of around  $\pi$ . Despite these results, in this work, there is no evidence of those jumps between modes. Instead, a constant  $\phi_{vortex}$  value was observed, which is consistent with the fact that the hydrodynamic response of the cylinder is the same across the synchronization regime. Also, instead of a jump in  $\phi_{total}$ , this phase angle vary from  $0^\circ$  in the initial branch to approximately  $90^\circ$  in the lower branch, with a rapid transition along the upper branch. Although this variation does not indicate a jump between modes, it agrees with the maximum amplitude of the cylinder, see Fig. 3.16. These important discrepancies may be due to the use of real parameters instead of equivalent parameters.

In the same investigation, Govardhan & Williamson (2000) observed that the initial branch is associated with the 2S mode and the upper and lower branches are associated with the 2P mode, while Evangelinos & Karniadakis (1999) concluded that the ‘P+S’ pattern may be associated with the upper branch. However, in the present work, PIV technique clearly proved that the three branches are associated with the 2S mode.

In agreement with Govardhan & Williamson (2000), the frequency of oscillation of the cylinder passes through the natural frequency of the cylinder in water in the transition from initial to upper branch. In like manner, the frequency of oscillation of the cylinder passes through the natural frequency of the cylinder in vacuum in the transition from upper to lower branch.

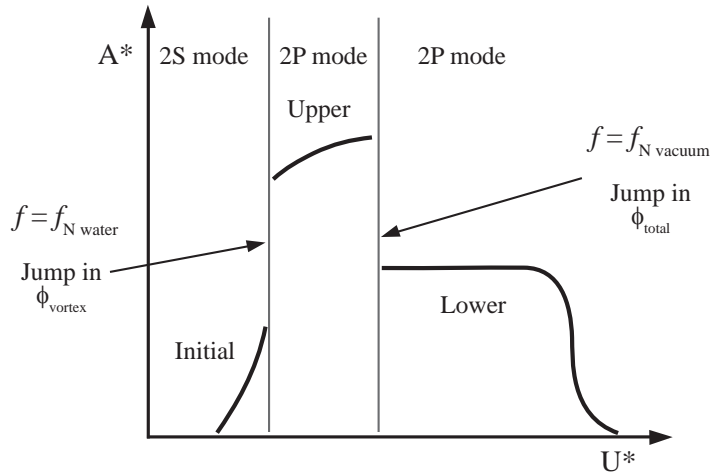


**Figure 4.4:** Schematic diagram of the low ( $m * \zeta$ ) type of response showing the two jump phenomena (free vibration). Based on Govardhan & Williamson (2000).

## 4.2.2 Hydrodynamic mass coefficient

As mentioned in sec. 2.4.3, when a cylinder is subject to a current the hydrodynamic mass coefficient will be denoted as  $C_{mc}$ , and therefore the hydrodynamic mass will be defined as

$$m'_c = \rho C_{mc} \frac{\pi D^2}{4} \quad (4.1)$$

Fig. 4.5 shows, in gray, the hydrodynamic mass coefficient for a cylinder in forced vibrations in the cross-flow direction. The results obtained in this work are shown in red. There are notable differences between the data. However, an important highlight is that data in red are never negative. One might think that this is due to the usage of punctual parameters instead of real ones. As seen in sec. 4.1.3, the use of real parameters may lead to negative added mass values.

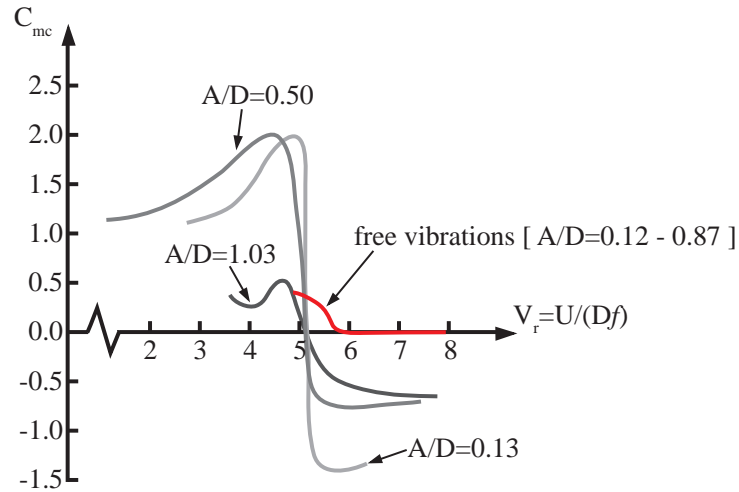


**Figure 4.5:** Comparison of the hydrodynamic mass coefficient: in gray, cross-flow forced vibrations (Sarpkaya, 1978); and in red, cross-flow free oscillations.

# Conclusions

In this work, an experimental apparatus was built to investigate the vortex-induced vibrations (free oscillations) of a *cantilevered uniform flexible circular cylinder* in a steady current along the entire lock-in region. A Matlab® code was developed to determine the dynamic response of the cylinder using the PTV technique. For the hydrodynamic response, in order to use the PIV technique, a customized system to seed the fluid was constructed. Conclusions derived from this study are:

Both responses, dynamic and hydrodynamic, agree with the types of responses found in the literature.

A standard method to identify the parameters was proposed. By using this methodology, all three parameters ( $m$ ,  $c$  and  $k$ ) calculated are ‘equivalent parameters’. These parameters are ideal and punctual, and can be used in a discretized model. Results obtained in this work suggest that the use of equivalent parameters in the motion equation,  $m\ddot{y} + c\dot{y} + ky = F$ , can explain in a better way the behavior of the cylinder.

Using equivalent parameters a variation in the total phase angle consistent with the maximum amplitude of the cylinder was found. In the initial branch the force  $F_{total}$ , and the displacement  $y$ , are totally synchronized. The fluid propels the cylinder throughout the cycle. This is the reason why the amplitude increases so fast until it reaches its maximum. In the upper branch the force and the displacement have a slightly offset, which causes a small decrease in the maximum amplitude. In the lower branch the force and the displacement are shifted 90 degrees. That causes that in half cycle the force stops the cylinder movement, while in the other half the force impulses it. This behavior is consistent with the fact that the maximum amplitude remains relatively constant along this branch. Finally, in the no lock-in region,  $\phi_{total} \approx 180^\circ$ . This means that the force is always stopping the cylinder, and therefore the maximum amplitude decreases dramatically to almost zero.

On the other hand, using real parameters and following the same argument, it was found that the cylinder would have an unrealistic behavior. In this case, the total force and the displacement are always synchronized,  $\phi_{total} \approx 360^\circ$ . This would mean that the fluid gives energy to the cylinder permanently, and therefore, one might expect the amplitude of the cylinder to grow larger and larger across the synchronization regime, which in fact does not happen.

Using equivalent parameters to determine the added mass,  $m'$ , it was found a behavior that is consistent with the frequency of the cylinder. The added mass reaches its maximum value at the beginning of the initial branch, and from this point it has

a lineal decay until it arrives to the upper branch. In the upper branch its behavior changes and the decay is now exponential. In the entire lower branch, the added mass has a zero value, which is consistent with the fact that in this branch the frequency of the cylinder is equal to the frequency in vacuum.

Using the real parameters,  $m'$  has negative values. Data is moved vertically due to the difference between  $m_{punctual}$  and  $m_{scale}$ . There is no satisfactory explanation for these negative values due to mass should never be negative because it represents the quantity of matter in a body.

Regarding comparison between actual results and the ones available in the literature, conclusions derived are:

In this work there is no evidence of two distinctly different jumps between modes as stated by Govardhan & Williamson (2000). Results show a constant  $\phi_{vortex}$  value, which is consistent with the fact that the hydrodynamic response of the cylinder is the same across the synchronization regime. For  $\phi_{total}$ , it varies from  $0^\circ$  in the initial branch to approximately  $90^\circ$  in the lower branch, with a rapid transition along the upper branch. It does not represent a jump between modes but it is consistent with the maximum amplitude of the cylinder.

PIV technique clearly proved that the three branches are associated with the 2S mode. In contrast with Govardhan & Williamson (2000), who observed that the initial branch is associated with the 2S mode and the upper and lower branches are associated with the 2P mode, and Evangelinos & Karniadakis (1999), who concluded that the ‘P+S’ pattern may be associated with the upper branch.

It is a possibility that these important discrepancies may be due to the use of real parameters instead of equivalent parameters. Results shown here are based in a single experimental apparatus, therefore, further work is needed to clarify if these discrepancies are also due to other circumstances.

## Contributions

The main contribution of this work is a standard method to identify the ‘equivalent parameters’ that can be used in a discretized model. As far as is known, there is no such method, or use of the equivalent mass parameter, reported in the literature. Using equivalent parameters, the results show that:

- The variation in the total phase angle,  $\phi_{total}$ , is consistent with the maximum amplitude of the cylinder.
- The behavior of the added mass,  $m'$ , is consistent with the frequency of the cylinder.
- The constant value of the vortex phase angle,  $\phi_{vortex}$ , is consistent with the fact that the hydrodynamic response of the cylinder is the same across the synchronization regime.

- There is no evidence of two distinctly different jumps between modes as stated by Govardhan & Williamson (2000).
- In contrast to what was observed by Govardhan & Williamson (2000) and Evangelinos & Karniadakis (1999), the three branches are associated with the 2S mode in the hydrodynamic response.

### **Future Work**

Considering the results of this work and what is available in the literature, it is suggested to perform further experiments using the standard method proposed. These experiments would have to vary the size and/or the material of the cylinder. The ideal scenario would be to change one variable at a time, that is, change only the height of the cylinder, or only its diameter, or just the material. That would allow to see the effect of each variable separately. Data obtained not only would clarify if the discrepancies found in this work are due to the use of real parameters instead of equivalent parameters, but also would help to find if there is any factor that causes a change in the  $\phi_{total}$ ,  $\phi_{vortex}$ ,  $m'$ , and the vortex shedding patterns. This information could help to predict the dynamic and hydrodynamic responses of the cylinder.



# Acknowledgments

I would like to express my gratitude to the National Council for Science and Technology (CONACYT) for the scholarship given to obtain my master's degree. Also I would like to thank to the Center for Research and Graduate Studies of the Faculty of Engineering (CIEP-FI) of the Autonomous University of San Luis Potosi (UASLP) for their support for the development of this project. Particularly to my dean Dr. Francisco Oviedo Tolentino for his support and assistance throughout the investigation process, to Dra. Geydy Luz Gutiérrez Urueta for her comments and improvements to this thesis, and to Dr. Ricardo Romero Méndez for the facilities and laboratory equipment provided to the project.





# Bibliography

- [1] ACHENBACH, E. Distribution of local pressure and skin friction around a circular cylinder in cross-flow up to  $re = 5 \times 10^6$ . *Journal of Fluid Mechanics* 34, 04 (1968), 625–639.
- [2] ACHENBACH, E., AND HEINECKE, E. On vortex shedding from smooth and rough cylinders in the range of reynolds numbers  $6 \times 10^3$  to  $5 \times 10^6$ . *Journal of fluid mechanics* 109 (1981), 239–251.
- [3] ATSAVAPRANEE, P., BENAROYA, H., AND WEI, T. Vortex dynamics in the near wake of a freely-oscillating cylinder. In *Proceedings of the FEDSM* (1998), vol. 98, pp. 1–6.
- [4] BATCHELOR, G. An introduction to fluid dynamics, 1967.
- [5] BEARMAN, P. W. Vortex shedding from oscillating bluff bodies. *Annual review of fluid mechanics* 16, 1 (1984), 195–222.
- [6] BLACKBURN, H. M., AND HENDERSON, R. D. A study of two-dimensional flow past an oscillating cylinder. *Journal of Fluid Mechanics* 385 (1999), 255–286.
- [7] BLEVINS, R. D. Flow-induced vibration.
- [8] BLEVINS, R. D., AND COUGHRAN, C. S. Experimental investigation of vortex-induced vibration in one and two dimensions with variable mass, damping, and reynolds number. *Journal of Fluids Engineering* 131, 10 (2009), 101202.
- [9] BLOOR, M. S. The transition to turbulence in the wake of a circular cylinder. *Journal of Fluid Mechanics* 19, 02 (1964), 290–304.
- [10] BRIKA, D., AND LANEVILLE, A. Vortex-induced vibrations of a long flexible circular cylinder. *Journal of Fluid Mechanics* 250 (1993), 481–508.
- [11] DRESCHER, H. *Messung der auf querangeströmte Zylinder ausgeübten zeitlich veränderten Drücke*. Verlag Friedr. Vieweg & Sohn, 1956.
- [12] EVANGELINOS, C., AND KARNIADAKIS, G. E. Dynamics and flow structures in the turbulent wake of rigid and flexible cylinders subject to vortex-induced vibrations. *Journal of Fluid Mechanics* 400 (1999), 91–124.
- [13] FENG, C. The measurement of vortex induced effects in flow past stationary and oscillating circular and d-section cylinders.

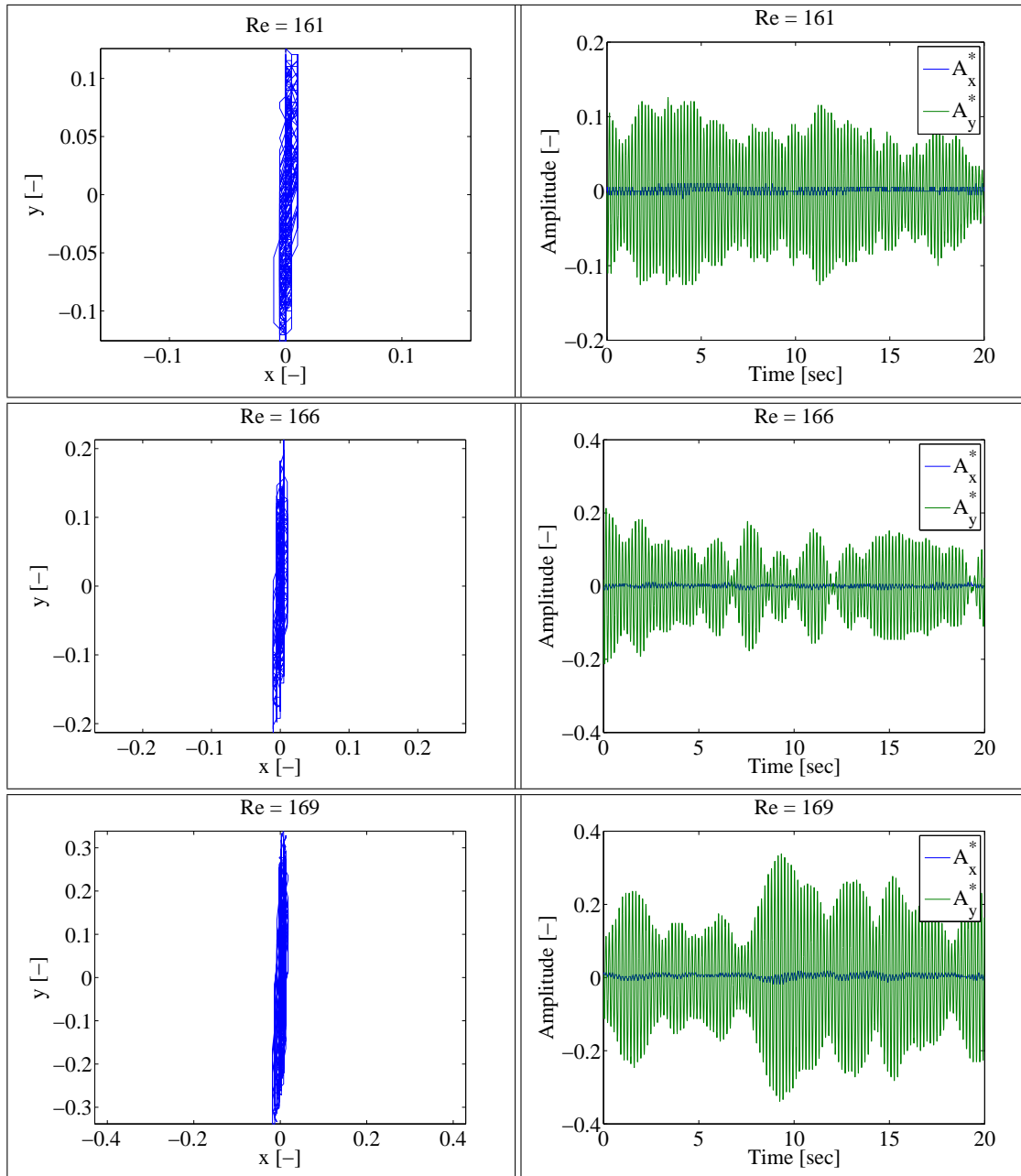
- 
- [14] FREIRE, C., AND MENEGHINI, J. Experimental investigation of viv on a circular cylinder mounted on an articulated elastic base with two degrees-of-freedom. In *Symposium on Bluff Body Wakes and Vortex-Induced Vibrations, BBVIV6, Capri Island, Italy* (2010).
- [15] FUJARRA, A., PESCE, C., FLEMMING, F., AND WILLIAMSON, C. Vortex-induced vibration of a flexible cantilever. *Journal of Fluids and Structures* 15, 3 (2001), 651–658.
- [16] GERRARD, J. The mechanics of the formation region of vortices behind bluff bodies. *Journal of Fluid Mechanics* 25, 02 (1966), 401–413.
- [17] GOVARDHAN, R., AND WILLIAMSON, C. Modes of vortex formation and frequency response of a freely vibrating cylinder. *Journal of Fluid Mechanics* 420 (2000), 85–130.
- [18] GRIFFIN, O., AND RAMBERG, S. Some recent studies of vortex shedding with application to marine tubulars and risers. *Journal of Energy Resources Technology* 104, 1 (1982), 2–13.
- [19] GRIFFIN, O. M., AND RAMBERG, S. E. The vortex-street wakes of vibrating cylinders. *Journal of Fluid Mechanics* 66, 03 (1974), 553–576.
- [20] HOVER, F., TECHET, A., AND TRIANTAFYLLOU, M. Forces on oscillating uniform and tapered cylinders in cross flow. *Journal of Fluid Mechanics* 363 (1998), 97–114.
- [21] JAUVTIS, N., AND WILLIAMSON, C. The effect of two degrees of freedom on vortex-induced vibration at low mass and damping. *Journal of Fluid Mechanics* 509 (2004), 23–62.
- [22] JEON, D., SHAN, J., AND GHARIB, M. Vorticity fields in the wake of an oscillating cylinder near the ‘critical curve’. *Bulletin of the American Physical Society* 40 (1996).
- [23] KHALAK, A., AND WILLIAMSON, C. Dynamics of a hydroelastic cylinder with very low mass and damping. *Journal of Fluids and Structures* 10, 5 (1996), 455–472.
- [24] KHALAK, A., AND WILLIAMSON, C. Fluid forces and dynamics of a hydroelastic structure with very low mass and damping. *Journal of Fluids and Structures* 11, 8 (1997), 973–982.
- [25] KHALAK, A., AND WILLIAMSON, C. Motions, forces and mode transitions in vortex-induced vibrations at low mass-damping. *Journal of fluids and Structures* 13, 7 (1999), 813–851.
- [26] LIGHTHILL, J. Fundamentals concerning wave loading on offshore structures. *Journal of Fluid Mechanics* 173 (1986), 667–681.
- [27] MENEGHINI, J., AND BEARMAN, P. Numerical simulation of high amplitude oscillatory flow about a circular cylinder. *Journal of Fluids and Structures* 9, 4 (1995), 435–455.

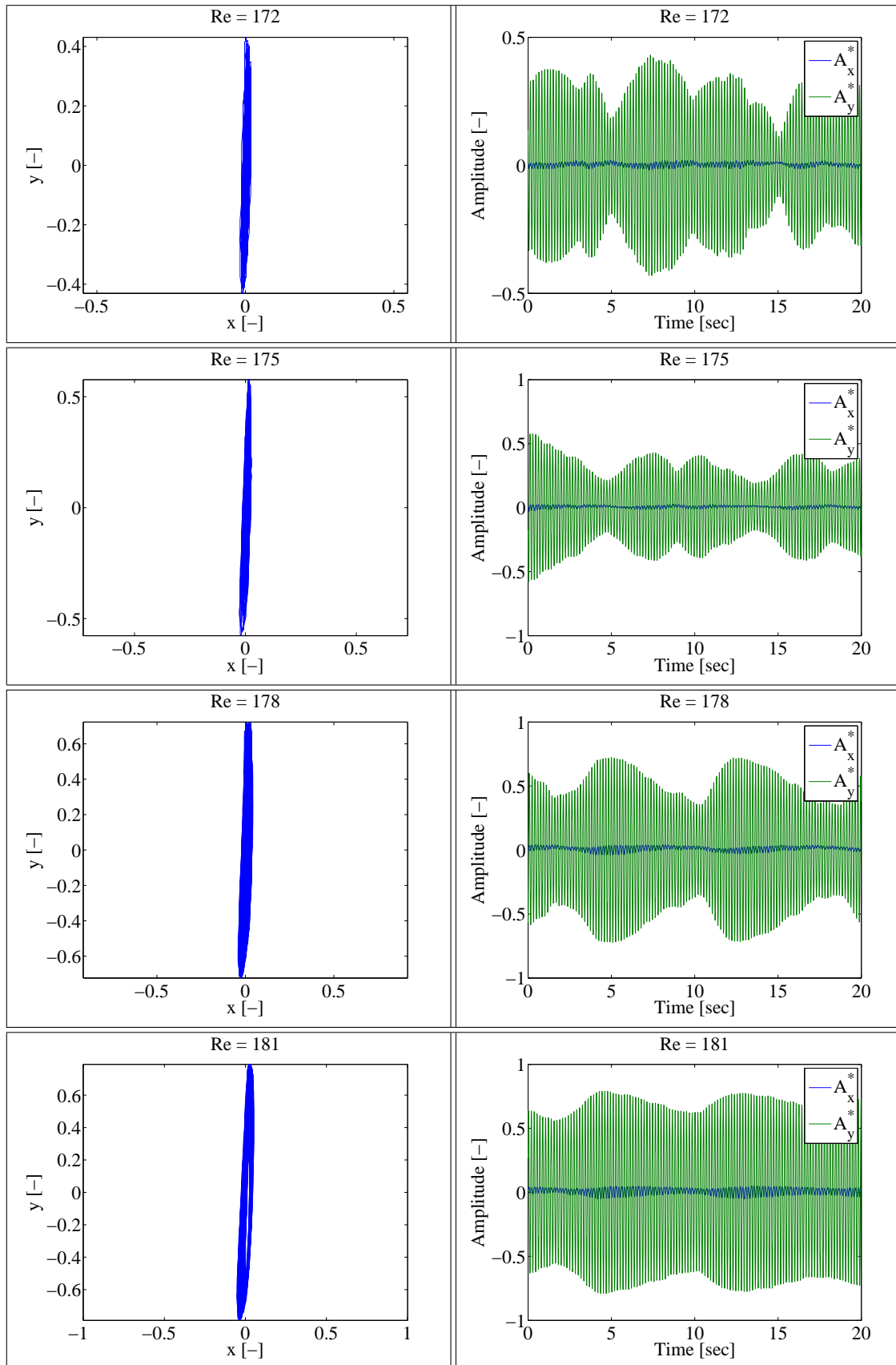
- [28] MILNE-THOMSON, L. M. *Theoretical Hydrodynamics*. Macmillan And Company, 1962.
- [29] MOE, G., AND WU, Z.-J. The lift force on a cylinder vibrating in a current. *Journal of Offshore Mechanics and Arctic Engineering* 112, 4 (1990), 297–303.
- [30] OVIEDO-TOLENTINO, F., PÉREZ-GUTIÉRREZ, F., ROMERO-MÉNDEZ, R., AND HERNÁNDEZ-GUERRERO, A. Vortex-induced vibration of a bottom fixed flexible circular beam. *Ocean Engineering* 88 (2014), 463–471.
- [31] PARKINSON, G. Phenomena and modelling of flow-induced vibrations of bluff bodies. *Progress in Aerospace Sciences* 26, 2 (1989), 169–224.
- [32] PESCE, C., FUJARRA, A., ET AL. Vortex-induced vibrations and jump phenomenon: experiments with a clamped flexible cylinder in water. *International Journal of Offshore and Polar Engineering* 10, 01 (2000).
- [33] ROSETTI, G. F., GONÇALVES, R. T., FUJARRA, A. L., AND NISHIMOTO, K. Parametric analysis of a phenomenological model for vortex-induced motions of monocolumn platforms. *Journal of the Brazilian Society of Mechanical Sciences and Engineering* 33, 2 (2011), 139–146.
- [34] ROSHKO, A. Experiments on the flow past a circular cylinder at very high reynolds number. *Journal of Fluid Mechanics* 10, 03 (1961), 345–356.
- [35] SARPKEYA, T. Vortex-induced oscillations: a selective review. *Journal of Applied Mechanics* 46, 2 (1979), 241–258.
- [36] SARPKEYA, T. Hydrodynamic damping, flow-induced oscillations, and biharmonic response. *Journal of offshore Mechanics and Arctic engineering* 117, 4 (1995), 232–238.
- [37] SCHEWE, G. On the force fluctuations acting on a circular cylinder in cross-flow from subcritical up to transcritical reynolds numbers. *Journal of fluid mechanics* 133 (1983), 265–285.
- [38] SCHLICHTING, H., GERSTEN, K., AND GERSTEN, K. *Boundary-layer theory*. Springer Science & Business Media, 2000.
- [39] SHERIDAN, J., CARBERRY, J., LIN, J.-C., AND ROCKWELL, D. On the near-wake topology of an oscillating cylinder. *Journal of fluids and structures* 12, 2 (1998), 215–220.
- [40] STAPPENBELT, B., LALJI, F., ET AL. Vortex-induced vibration super-upper response branch boundaries. *International Journal of Offshore and Polar Engineering* 18, 02 (2008).
- [41] SUMER, B., AND FREDSE, J. *Hydrodynamics around cylindrical structures*, 1997.
- [42] SUMER, B. M., AND FREDSØE, J. *Hydrodynamics around cylindrical structures*. No. 12. World Scientific, 1997.

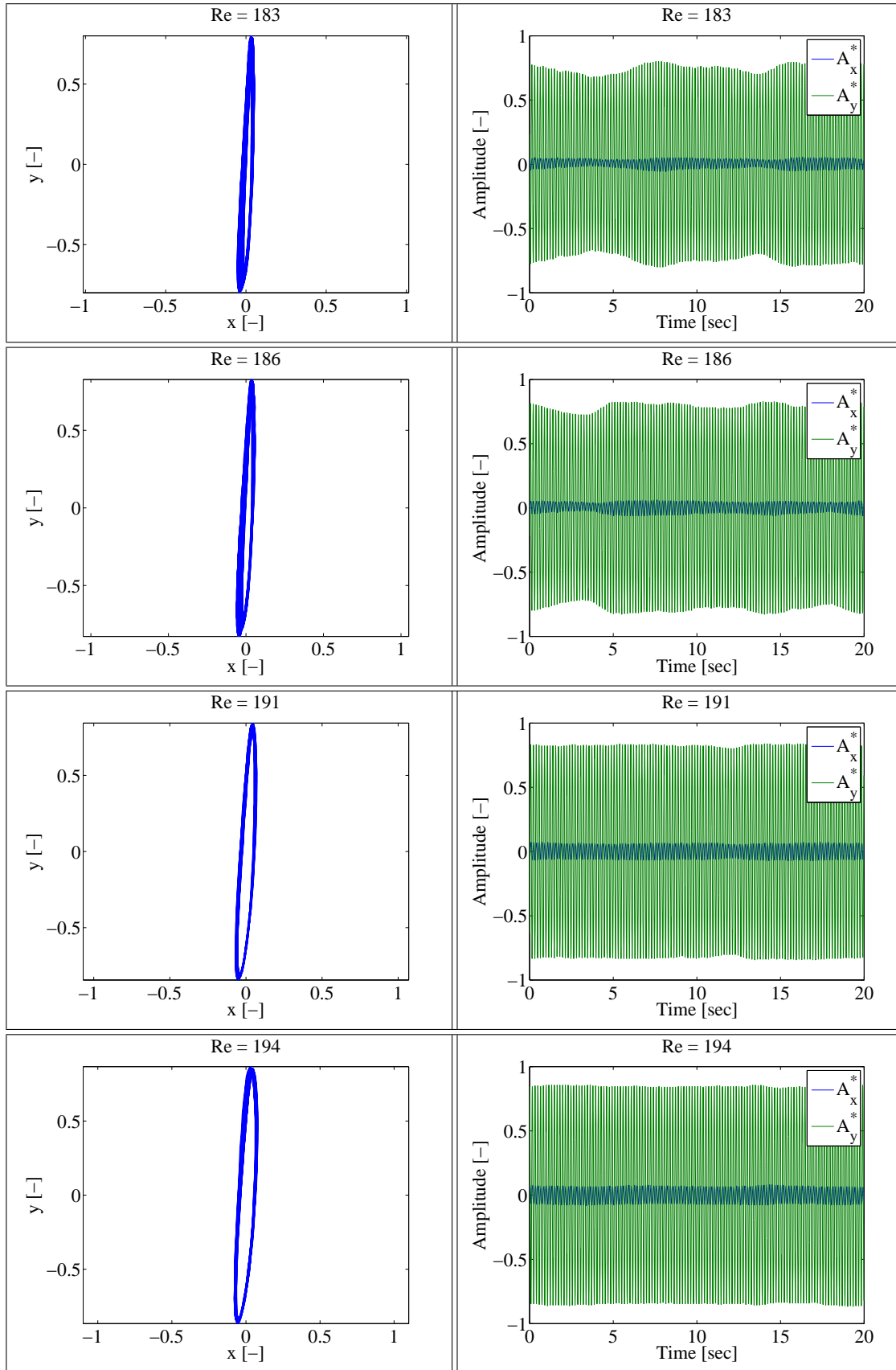
- [43] TECHET, A., HOVER, F., AND TRIANTAFYLLOU, M. Vortical patterns behind a tapered cylinder oscillating transversely to a uniform flow. *Journal of Fluid Mechanics* 363 (1998), 79–96.
- [44] WILLIAMSON, C. Sinusoidal flow relative to circular cylinders. *Journal of Fluid Mechanics* 155 (1985), 141–174.
- [45] WILLIAMSON, C. The existence of two stages in the transition to three-dimensionality of a cylinder wake. Tech. rep., DTIC Document, 1988.
- [46] WILLIAMSON, C. Oblique and parallel modes of vortex shedding in the wake of a circular cylinder at low reynolds numbers. *Journal of Fluid Mechanics* 206 (1989), 579–627.
- [47] WILLIAMSON, C., AND GOVARDHAN, R. Vortex-induced vibrations. *Annu. Rev. Fluid Mech.* 36 (2004), 413–455.
- [48] WILLIAMSON, C., AND GOVARDHAN, R. A brief review of recent results in vortex-induced vibrations. *Journal of Wind Engineering and Industrial Aerodynamics* 96, 6 (2008), 713–735.
- [49] WILLIAMSON, C., AND ROSHKO, A. Vortex formation in the wake of an oscillating cylinder. *Journal of fluids and structures* 2, 4 (1988), 355–381.

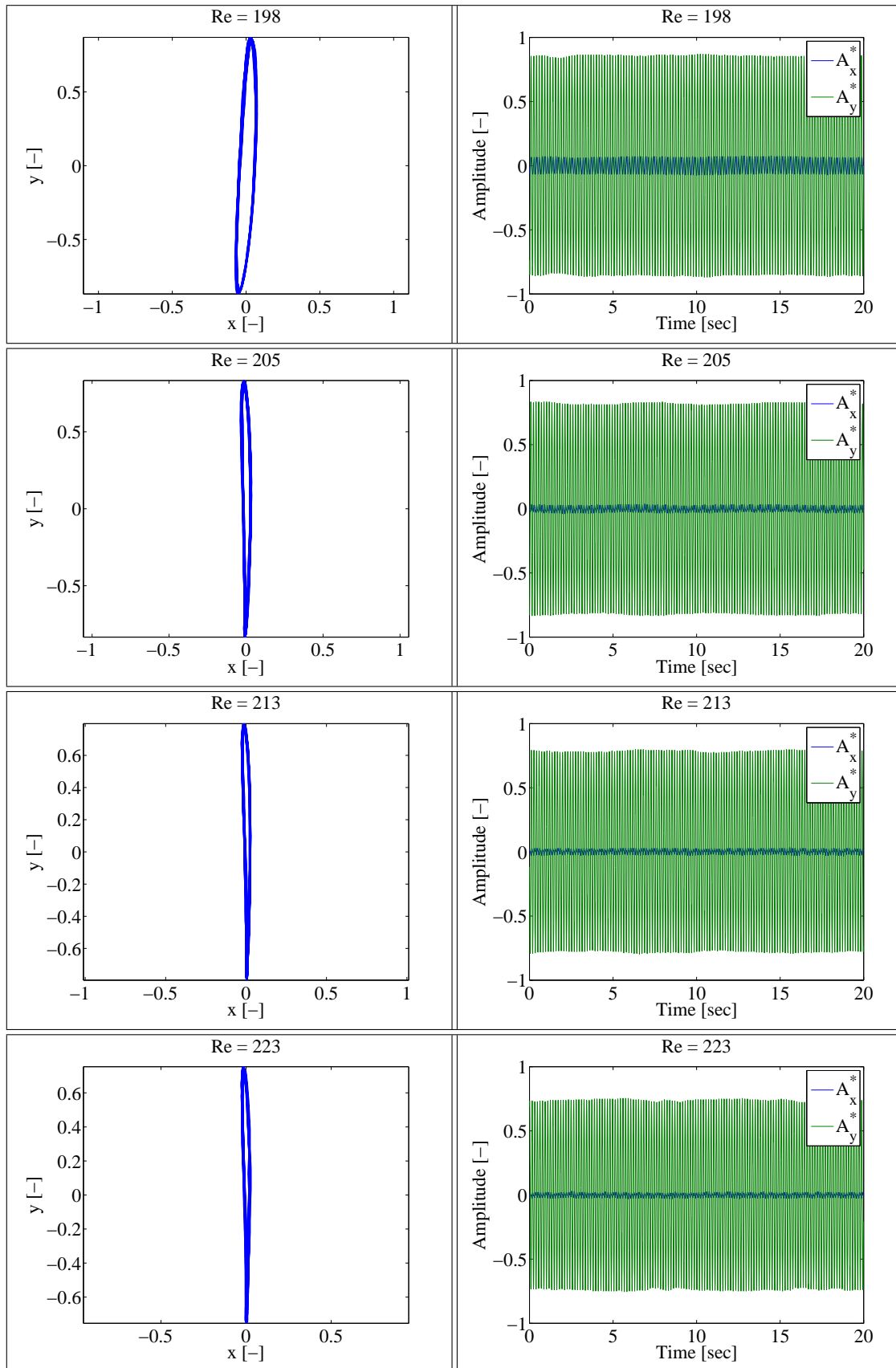
# Appendix

## Paths

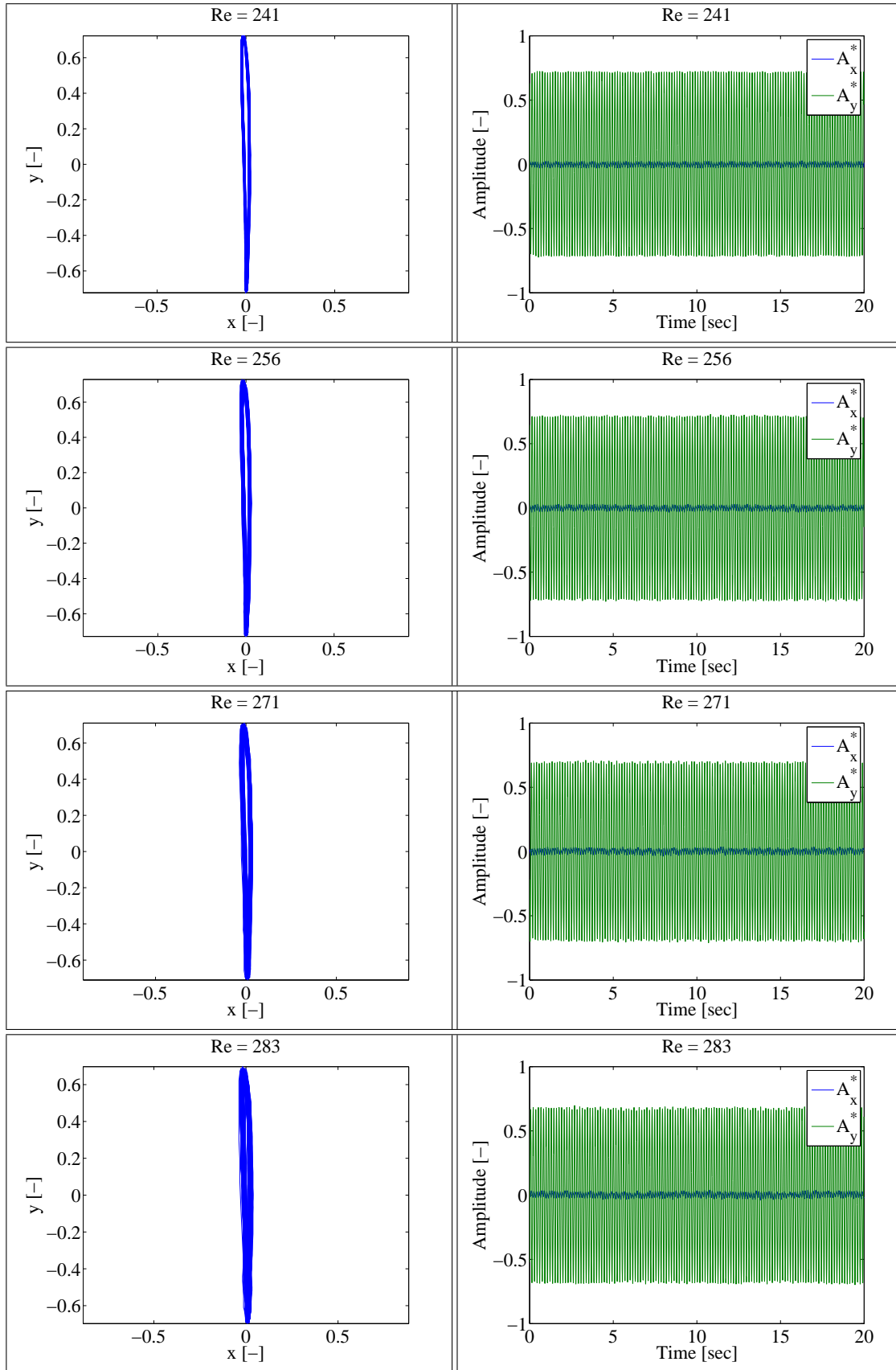


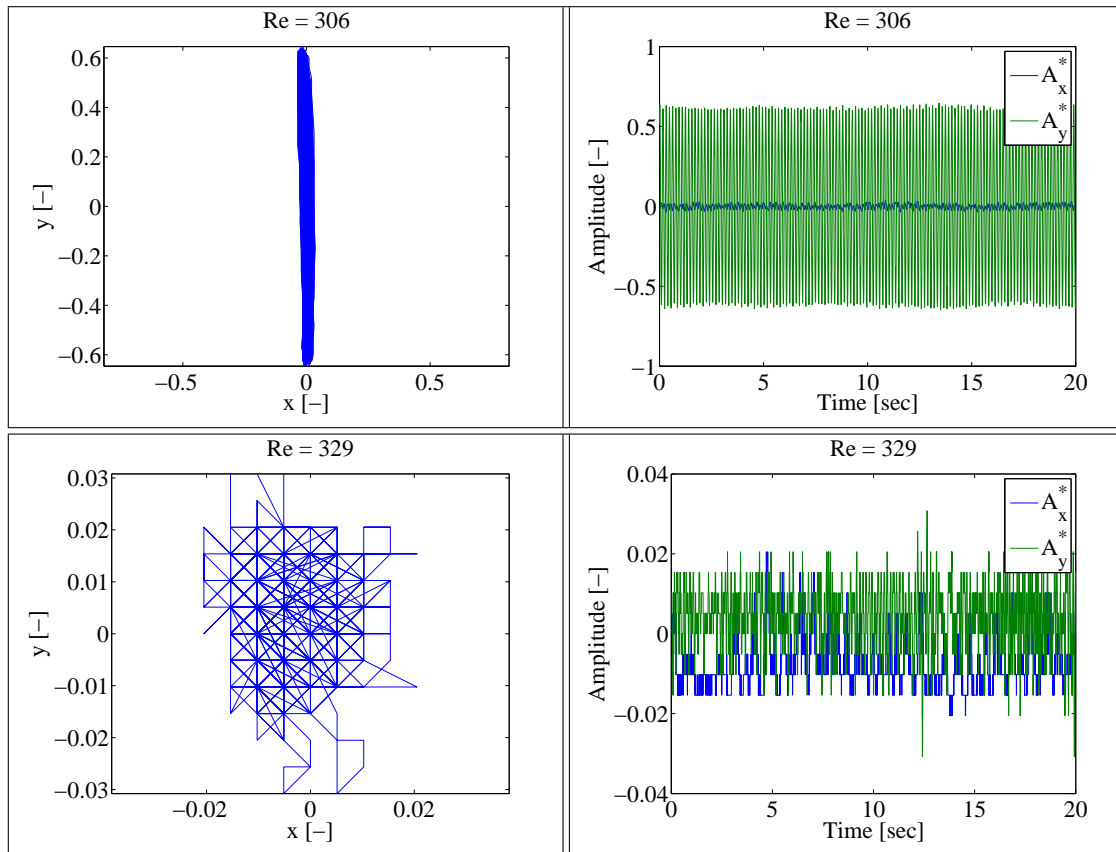












## Vortex shedding patterns

